UNIVERSITY OF CALIFORNIA,
IRVINE

Energy and Spectral Efficiency in Wireless Heterogeneous Networks

DISSERTATION

submitted in partial satisfaction of the requirements
for the degree of

DOCTOR OF PHILOSOPHY

in Electrical and Computer Engineering

by

Cemil Can Coskun

Dissertation Committee:
Professor Ender Ayanoglu, Chair
Professor Ahmed M. Eltawil
Professor A. Lee Swindlehurst

2017

DEDICATION

To the boy who lived . . .

TABLE OF CONTENTS

LIST OF FIGURES

Page

LIST OF TABLES

LIST OF ALGORITHMS

ACKNOWLEDGMENTS

My Ph.D. journey has started five years ago. I didn't know anybody in Irvine before I moved here. I have never expected that I will meet awesome people who made my life in Irvine full of joy and excitement. While I am finishing my Ph.D., I would like to express my thanks to all people who made these five years easier for me. I could not finish this dissertation without their help, guidance, and support.

First and foremost, I would like to thank my advisor, Professor Ayanoglu for all his expertise, understanding, guidance, and support. He made this dissertation possible by creating interest in me about this topic. It was always a great pleasure for me working with him.

Second, I would like to thank my committee members, Professor Swindlehurst and Professor Eltawil. I also would like to thank Professor Jafarkhani, Professor Ketseoglou, and Professor Venkatasubramanian who were in my qualifying exam committee. Their comments and suggestions helped me improve the quality of this dissertation.

Third, I would like express my thanks to Dr. Kemal Davaslioglu. I learned a lot from him. We have started collaborating in my second year in Ph.D. His knowledge and guidance always helped me finding the correct path in this journey. When I had a problem, he was always there to help. His help is not only limited to my academic life, but he also guided me in my personal life.

Fourth, I would like to thank all my friends in Irvine and U.S. whose company brought joy to my life. I would like to thank Dr. Erdem Koyuncu, Dr. Bahattin Tolga Oztan, Dr. Omer Nebil Yaveroglu, and Ecehan Uludag who joined me during the lunch hours, specifically at 12:45PM. I also want to thank them for not complaining a lot about 12:45PM choice. I would like to thank my friends Dr. Ilge Akkaya, Selin Dag, and Erdem Karaca for being my family in U.S although we live in different cities. I would like express my thanks to Dr. Caner Guclu, Dr. Fulya Ozcan, Kumru Arslan, Dr. Thania Muñoz Diaz who have been my family in Irvine. They brought joy and happiness to my life and helped me find the strength in me to get up every morning and work. I also would like to thank everyone I met during my Ph.D. I believe in the butterfly effect. Everything would have been much different without you.

Fifth, I would like express my gratitude to my mother Serpil Coskun and my father Memet Coskun who always supported me in every step in my life. I would not be here without their infinite support.

My graduate studies was partially supported by fellowships from the Center for Pervasive Communications and Computing and the National Science Foundation under Grant No. 1307551.

CURRICULUM VITAE

Cemil Can Coskun

EDUCATION

Doctor of Philosophy in Electrical Engineering **2017**
University of California, Irvine *Irvine, CA*

Master of Science in Electrical and Electronics Engineering **2012**
Bilkent University *Ankara, Turkey*

Bachelor of Science in Electrical and Electronics Engineering **2010**
Bilkent University *Ankara, Turkey*

RESEARCH EXPERIENCE

Graduate Student Researcher **2012–2017**
University of California, Irvine *Irvine, California*

Engineering Intern **2013**
Broadcom Corporation *Sunnyvale, California*

Graduate Student Researcher **2010–2012**
Bilkent University *Ankara, Turkey*

JOURNAL PUBLICATIONS

Three-Stage Resource Allocation Algorithm for Energy-Efficient Heterogeneous Networks **2017**
IEEE Transactions on Vehicular Technology

Energy-Efficient Resource Allocation for Fractional Frequency Reuse in Heterogeneous Networks **2015**
IEEE Transactions on Wireless Communications

Energy-Efficient Base Station Deployment in Heterogeneous Networks **2014**
IEEE Wireless Communications Letters

CONFERENCE PUBLICATIONS

Energy-Spectral Efficiency Tradeoff for Heterogeneous Networks with QoS Constraints — **May 2017**
2017 IEEE International Conference on Communications

New Algorithms for Maximizing Cellular Wireless Network Energy Efficiency, — **Feb 2016**
IEEE Information Theory and Applications Workshop

An Energy-Efficient Resource Allocation Algorithm with QoS Constraints for Heterogeneous Networks — **Dec 2015**
2015 IEEE Global Communications Conference

A Greedy Algorithm for Energy-Efficient Base Station Deployment in Heterogeneous Networks — **June 2015**
2015 IEEE International Conference on Communications

ABSTRACT OF THE DISSERTATION

Energy and Spectral Efficiency in Wireless Heterogeneous Networks

By

Cemil Can Coskun

Doctor of Philosophy in Electrical and Computer Engineering

University of California, Irvine, 2017

Professor Ender Ayanoglu, Chair

The focus of this dissertation is investigating energy and spectral efficiency in wireless heterogeneous networks (HetNets). Our goal is to improve the energy efficiency and spectral efficiency of the HetNets while satisfying the minimum rate requirements of the users. The contributions of this dissertations are (i) to develop an energy-efficient base station deployment framework for HetNets, (ii) to increase energy efficiency of the HetNets while satisfying minimum rate requirements of users, and (iii) to investigate energy efficiency-spectral efficiency tradeoff in HetNets. First, we address the micro base station deployment problem in HetNets. Although micro base station deployment increases the total capacity of the network, increasing the number of micro base stations excessively may reduce the energy efficiency of the network. Therefore, we examine the energy efficiency aspect of the micro base station deployment problem. We propose a greedy deployment algorithm which is a constant-factor approximation of the optimal solution. Second, we investigate the energy efficiency of downlink transmission in multi-cell HetNets. Our objective is to satisfy the rate requirement of users while maximizing energy efficiency of the network. We divide the problem into three subproblems: cell-center region boundary selection for fractional frequency reuse (FFR), scheduling, and power allocation subproblems. We propose a three-stage algorithm, and apply it iteratively until convergence. We demonstrate that significant gains can be achieved in terms of energy efficiency and outage probability using the proposed al-

gorithm. Third, we investigate the energy efficiency-spectral efficiency tradeoff in multi-cell HetNets. Our objective is to maximize both energy efficiency and spectral efficiency of the network while satisfying the rate requirements of users. We define our objective function as the weighted summation of energy efficiency and spectral efficiency. We derive the Pareto optimal solution that strikes a balance between the spectral efficiency and energy efficiency.

Chapter 1

Introduction

Each year, new mobile devices such as smart phones, tablets, and phablets are introduced to users [1]. In 2016, around 8 billion mobile devices were accessing mobile networks worldwide and this number is expected to increase to 11.6 billion in 2021 [1]. Introduction of new and smarter mobile devices with increasing numbers also increases the mobile data traffic volume. These devices create around 8 exabytes of traffic per month and this number is expected to increase to 50 exabytes per month in 2021 with 47% cumulative annual growth rate [1]. Therefore, network operators have to meet more than 6 times traffic demand within 5 years. Several different solutions such as increasing spectral efficiency, expanding spectrum, and increasing node density are considered in the literature to meet this demand [2]. In this dissertation, small cell base station deployment, increasing energy efficiency, and increasing spectral efficiency cases have been investigated.

Increasing spectral efficiency utilizes the existing resources more efficiently and also provides higher data rates to users with same bandwidth allocation. Therefore, solutions that improve spectral efficiency help meet the increasing demand. However, the spectral efficiency metric does not provide any information about the energy efficiency of the network.

In fact, solutions that provides higher spectral efficiency usually works poorly in terms of energy efficiency. Improving the energy efficiency of the network has both economical and environmental benefits. Total worldwide electricity consumption of telecom operators are growing [3]. In 2007, the worldwide electricity consumption of communication networks increased from 203 TWh in 2007 to 334 TWh in 2012 and this trend is expected to continue [3]. By improving energy efficiency of the network, network operators can decrease their operational costs. In addition, increased energy consumption in wireless networks also causes the growth of greenhouse gases. Between 1970 to 2004, the emissions of greenhouse gases increased by 70% [4]. These gases create a blanket over the earth surface and warm the planet's surface. Improving the energy efficiency of the network decreases the amount of these gases in the atmosphere. Solutions that improve the spectral efficiency of the network have to consider energy efficiency of the network to decrease operational costs and to reduce negative environmental effects.

In this dissertation, heterogeneous networks are investigated to meet this increasing demand. In heterogeneous networks, small cell base stations are deployed into the coverage area of the macrocell base stations. Small cell base stations are preferred over the macrocell base stations due to the fact that they consume significantly lower power than macrocell base stations, they create less interference to the existing network, and they can provide significantly improved data rate to their coverage areas [5,6]. These base stations also eliminate the coverage holes in the network. In [5], it is shown that four times improvement in terms of throughput is obtained by picocell deployment. In [7], it is shown that both energy efficiency and spectral efficiency of the network can be improved with small cell base station deployment. Although small cell base station deployment has its own benefits, each additional base station comes with its capital and operational expenditures. Therefore, limiting the number of small cell base stations to be deployed while satisfying the increasing demand is a problem that needs to be investigated. In this dissertation, the small cell base station deployment problem is examined in Chapter 2. Second important problem that is experienced with small cell base

station deployment is the interference. Small cell base stations are deployed into the coverage area of the macrocell base stations. Therefore, coverage area of small cell base stations overlaps with the macrocell base stations. This structure is called an umbrella network [6]. Therefore, interference becomes a significant problem among these base stations. Several intercell interference cancellation and mitigation techniques have been investigated in the literature [8, 9]. Among different techniques, fractional frequency reuse (FFR) is important in next-generation networks, due to its efficiency and low complexity [9]. In this dissertation, FFR is addressed in Chapter 3 and Chapter 4 for energy-efficient resource allocation and energy- and spectral-efficient resource allocation, respectively.

In Chapter 2, an energy-efficient base station deployment framework is developed for heterogeneous wireless networks. This chapter investigates capacity improvement of the network with micro base station deployment. It shows that increasing the number of micro base stations excessively may reduce the energy efficiency of the network. This chapter examines the energy efficiency aspect of the micro base station deployment problem. This problem can be divided into two subproblems: choosing feasible candidate micro base station locations and selecting the optimum set of micro base stations among the candidate locations. The proposed algorithm first chooses the subset of the feasible locations as candidate locations, and then selects the micro base stations which maximize the energy efficiency of the network iteratively. It is shown that the proposed algorithm is a constant-factor approximation of the optimal solution. Simulation results demonstrate that the proposed algorithm improves the energy efficiency of the network up to 12% for low-loaded scenarios and 98% for the high-loaded scenarios.

Chapter 3 investigates the energy efficiency of downlink transmissions in heterogeneous networks (HetNets). Our objective is to satisfy the rate requirement of users while maximizing the energy efficiency of the network. The fractional frequency reuse (FFR) scheme is employed to increase the energy efficiency of downlink transmissions and to eliminate outages

for the cell-edge users. The problem is formulated as the joint cell-center boundary selection for FFR, scheduling, and power allocation. This formulation gives us a mixed discrete (selection of the cell-center boundary selection for FFR and scheduling) and continuous (power allocation) optimization problem which is hard to solve jointly. In order to solve this problem, a three-stage resource allocation algorithm is proposed. In the first stage, we propose a dynamic method to determine the cell-center region boundaries. In the second stage, the Lagrangian directed scheduler algorithm is employed to incorporate the rate requirements of users. The third stage solves the power allocation subproblem using the Levenberg-Marquardt method combined with dual decomposition. In order to make the base stations further reduce intercell interference, interference pricing mechanism is applied. This scheme penalizes the utility of a base station with the interference it creates. The performance of the proposed algorithm is simulated in a Long Term Evolution (LTE) network simulation tool. Numerical results reveal that significant gains in terms of energy efficiency can be achieved with the proposed algorithm. The outage probability is also significantly reduced.

In Chapter 4, energy efficiency and spectral efficiency tradeoff in multi-cell heterogeneous networks is investigated. Our objective is to maximize both energy efficiency and spectral efficiency of the network while satisfying the minimum rate requirements of the users. The objective function is defined as the weighted summation of energy efficiency and spectral efficiency functions. The fractional frequency reuse (FFR) scheme is employed to suppress intercell interference. We formulate the problem as cell-center boundary selection for FFR, frequency assignment to users, and power allocation. The optimal solution of this problem requires exhaustive search over all cell-center radii, frequency assignments, and power levels. A three-stage algorithm is proposed and applied consecutively until convergence. First, the cell-center radius is selected for the FFR method in each sector. Second, the frequency resources are assigned to users to satisfy their rate requirements and also maximize the objective function. Third, the power allocation subproblem is solved by using the Levenberg-Marquardt method. Minimum rate requirements of users are also included in the

solution by using dual decomposition techniques. Simulation results show a Pareto-optimal solution for energy efficiency and spectral efficiency. We present energy efficiency, spectral efficiency, outage probability, and average transmit power results for different minimum rate constraints. Among other results, in a particular setting, 13% energy efficiency increase can be obtained in a multi-cell heterogeneous wireless network by sacrificing 7% spectral efficiency.

In Chapter 5, all findings in this dissertation is summarized. In addition, future research directions are also discussed. Contribution of this dissertation is presented with the corresponding research directions.

Chapter 2

A Greedy Algorithm for Energy-Efficient Base Station Deployment in Heterogeneous Networks

2.1 Motivation

In the last two decades, the need for a fast and ubiquitous wireless network has increased to unexpected levels. The popularity of the smartphones and mobile applications, as well as the flat rate price policy of mobile operators show that this trend will continue. In order to meet this increasing demand, network operators seek coherent solutions such as expanding the spectrum, increasing node density per area, and deploying more, and smaller, cells [2]. Due to the dense deployment of macro base stations (BSs) today, adding more macro BSs to the cellular network significantly reduces the gain because of the elevated intercell interference.

Heterogeneous networks (HetNets) are one of the enabling technologies that can provide significantly improved data rates while creating less intercell interference to the existing architecture. HetNets have attracted attention in the literature, see, e.g., [8, 10, 11]. These works demonstrate that the deployment of HetNets is very promising to improve overall capacity and it decreases the outages in the next generation wireless networks.

However, the deployment of more BSs increases the energy consumption of the network, which is one of the nontrivial causes of the growth in the emission of greenhouse gases to very high levels. As a result, green cellular communication has attracted attention, see, e.g., [6, 12–14]. The main objective of the green cellular communication is to reduce energy consumption as much as possible while satisfying the demand of users. Reducing the energy consumption in wireless networks is also preferred due to economical reasons such as decreasing maintenance costs and longer battery life time for the mobile users.

In HetNets, each additional micro BS increases both the capital expenditures (CAPEX) and operational expenditures (OPEX) of the system. CAPEX mostly consists of the infrastructure costs, e.g., BS equipment, site installation, etc. [15]. On the other hand, OPEX includes other expenses such as electric bills, site lease, backhaul transmission lease, and operation and maintenance costs [16]. Therefore, if the number of BSs which meet the network requirements is lowered, both CAPEX and OPEX of the network automatically decrease. In addition, over 80% of the power is consumed by BSs in mobile cellular networks [17]. Micro BSs consume significantly lower power than macro BSs. Therefore, they are more desirable over macro BSs to decrease the OPEX of the network. In accordance with this observation, the proposed algorithm limits the number of additional micro BSs while satisfying the increasing traffic demand of the network.

Former works on HetNets have mostly concentrated on power control and resource allocation problems, see, e.g., [9,18–20]. However, the deployment of micro BSs and the energy efficiency aspects of the problem have not been investigated to their full potential. A similar study

in [21] investigates the area spectral efficiency (ASE) aspect of the micro BS deployment problem. The authors of [21] deploy micro BSs to an area which is covered by macro BSs to increase the ASE of the network. The cell boundaries are selected as candidate locations because the authors observe that the ASE improvement increases with the coverage of the BS. Then, a greedy algorithm is proposed to select micro BSs. The algorithm continues to run until the ASE requirement is reached. Reference [21] considers cell edges as good locations for the placement of new cells in order to increase ASE. However, cell edges may not always be good candidates if energy efficiency of the network is considered. In addition, the user distribution affects the energy efficiency of the network and the proposed algorithm in [21] works poorly for the clustered user distribution scenarios. The algorithm we will present in this chapter is designed to overcome this limitation. In [22], the authors aim to minimize the outage of the network by deploying additional low power BSs. The authors of [22] first deploy certain number of micro BSs to the network area, and then they iteratively shift the location of these BSs. However, system characteristics, path loss and shadowing, are strictly dependent on the location of the BSs. Although the proposed algorithm works well for the test cases, obtaining these parameters in every iteration may be impractical in real BS topologies. In [23], the authors investigate the energy efficiency of the micro BSs on hexagonal grids. They demonstrate that the power savings depend on the network load. Moderate gains are observed in fully loaded networks. In [23], micro BSs are located to the cell edges to minimize the intercell interference. However, depending on the user distribution in the network, larger gains can be obtained in terms of energy efficiency with different sets of micro BSs.

In this chapter, the algorithm we present is not affected by the user distributions and can be implemented in both clustered and dispersed networks. In addition, the proposed algorithm considers the feasibility of the candidate locations and minimizes the effect of environmental conditions. Moreover, this algorithm can be implemented in both hexagonal grid and real BS topologies. Furthermore, the proposed algorithm finds the set of micro BS locations

that maximizes the energy efficiency of the network while satisfying the increasing capacity demand of the network.

The remainder of the chapter is organized as follows. Section 2.2 introduces the system model. Section 2.3 presents the problem and discusses the possible approaches to solve it. Section 2.4 describes the proposed algorithm and compares the performance of the algorithm with the optimal solution. Numerical results and the performance improvements are presented in Section 2.5 and concluding remarks are made in Section 2.6.

2.2 System Model

In this section, the system model, power consumption of the BSs, and the energy efficiency problem formulation are presented.

Consider a wireless network in which all mobile users are served by sets of macro and micro BSs, denoted by $\mathcal{B}_M$ and $\mathcal{B}_m$, respectively. The subscript M is used to indicate macro BSs and m is for micro BSs throughout the rest of the chapter. All BSs in the network area are denoted by $\mathcal{B}$, i.e., $\mathcal{B} = \mathcal{B}_M \cup \mathcal{B}_m$. The mobile users are associated with the BS which provides the highest signal strength at the location of the user. If more than one BS provides equal power at the user location, the user selects one of the BSs randomly. We assume that the mobile users always have data to transmit, and thereby they require a bandwidth allocation. The signal-to-interference-plus-noise ratio (SINR) of a macrocell associated user k on subcarrier n can be written as

$$\gamma_k^{(n)} = \frac{P_M^{(n)} g_{k,b}}{\sum\limits_{b' \in \mathcal{B}_M, b' \neq b} P_M^{(n)} g_{k,b'} + \sum\limits_{b' \in \mathcal{B}_m} P_m^{(n)} g_{k,b'} + \sigma^2} \tag{2.1}$$

where $P_M^{(n)}$ and $P_m^{(n)}$ are the transmit power of a macrocell M and a microcell m on sub-

carrier n, respectively. We note that although in this chapter we focus on the downlink communication, the same ideas can be applied for the uplink as well. The channel gain from BS b to user k is denoted by $g_{k,b}$. The channel gain includes path loss attenuation, shadow fading, and multi-path fading components. The thermal noise effective over a subcarrier is denoted by σ^2. Similarly, the SINR for microcell user k on subcarrier n can be written as

$$\gamma_k^{(n)} = \frac{P_m^{(n)} g_{k,b}}{\sum\limits_{b' \in \mathcal{B}_M} P_M^{(n)} g_{k,b'} + \sum\limits_{b' \in \mathcal{B}_m, b' \neq b} P_m^{(n)} g_{k,b'} + \sigma^2}. \tag{2.2}$$

For simplicity, we use the same symbol $\gamma_k^{(n)}$ for SINR of both macro and microcell users. In the sequel, the capacity of user k can be written as

$$C\left(k, \mathcal{B}\right) = \sum_{n=1}^{N_k} W_k^{(n)} \log_2(1 + \gamma_k^{(n)}) \qquad \text{[bits/sec]} \tag{2.3}$$

where $W_k^{(n)}$ denotes the bandwidth of subcarrier n of user k and N_k is the number of subcarriers assigned to user k. In this chapter, equal bandwidth scheduling is employed [24]. In this scheduling, each BS shares its resources equally among its users. In LTE systems, the smallest granularity which can be assigned to a user is a resource block with 12 subcarriers. Therefore, if K users are associated with the BS b with N_{RB} RBs, $K_h =$ mod (N_{RB}, K) of the users get $12(\lfloor N_{RB}/K \rfloor + 1)$ subcarriers, whereas the rest of the users receive $12\lfloor N_{RB}/K \rfloor$ subcarriers. In this chapter, we assume that a BS allocates equal power on its subcarriers.

The energy efficiency of the network can be improved by either increasing the total capacity of the network while consuming the same power or decreasing the consumed power of the network and providing the same capacity. Traditional macro BSs provide better coverage and data rate, however they consume significantly higher power than the micro BSs. In addition, in densely deployed networks, this gain is substantially reduced due to intercell interference. On the other hand, the transmission power of micro BSs is significantly less than the macro BSs, thereby they cover less area. However, they consume less power and do

not interfere with the other transmissions as severe as macro BS transmissions. Therefore, they are more energy-efficient than the macro BSs especially in densely deployed networks. For this reason, in this dissertation, micro BSs are deployed to the network as an underlay for macro BSs to maximize the energy efficiency of the network and to satisfy the traffic demand.

The power consumption of a BS consists of two parts. The first part is the static power consumed by the BS with no transmission. The second part depends on the load and the transmission power of the BS. There are several power consumption models proposed in the literature, see, e.g., [25–27]. In this chapter, we use the power consumption model proposed in [25]. It is given by

$$\begin{aligned} P_M &= P_{0,M} + \Delta_M P_{tx} \\ P_m &= P_{0,m} + \Delta_m P_{tx} \end{aligned} \tag{2.4}$$

where P_M, P_m, and P_{tx} are the average consumed power per macro BSs, micro BSs, and transmission power, respectively. Δ_M and Δ_m scale the transmission power depending on the load. $P_{0,M}$ and $P_{0,m}$ denote the static part of the power consumption of the macro and micro BSs, respectively.

As stated earlier, we assume that users always have data to transmit with full buffer. In addition, no power control algorithm is used. Therefore, BSs are fully utilized and Δ_M and Δ_m are constant for all BSs. Then, the energy efficiency of the network can be written as

$$\eta_{EE}\left(\mathcal{B}\right) = \frac{\sum_{k \in \mathcal{K}} C(k, \mathcal{B})}{N_B \cdot P_M + N_b \cdot P_m} \qquad \text{[bits/Joule]} \tag{2.5}$$

where N_B and N_b are the number of macro and micro BSs in the network, respectively.

2.3 Problem Definition

In this section, we will first present the BS deployment problem. Then, we will discuss possible approaches to solve the problem.

A network operator would like to improve the capacity of the network with additional micro BSs to meet increasing traffic demand. In order to maximize the energy efficiency of the network and to limit CAPEX and OPEX, the network operator would like to deploy the micro BSs to optimum locations. In real-life scenarios, users are mobile and several user distributions can occur with different probabilities. During the peak hours, more users are active and total traffic of the network reaches to its maximum. However, most of the time BSs are underutilized. In [28], the authors present that 49.2% of the time, the total traffic of the network is below the 20% of the peak hour traffic. However, even if most of the time the traffic demand is low, additional micro BSs are to be deployed for the peak hour traffic. Existing BSs are sufficient during the off-peak hours and the additional BSs are needed during heavy traffic. Therefore, operators must consider only the user distributions with high load periods for the deployment. Therefore, we formulate the deployment problem as

$$\begin{aligned} \max \quad & \pi_r \eta_{EE}\left(\mathcal{B}\right) \\ \text{s.t.} \quad & \sum_{k \in \mathcal{K}_r} C\left(k, \mathcal{B}\right) \geq \lambda \cdot C_r \qquad \text{for all } r \in \mathcal{R} \end{aligned} \tag{2.6}$$

where C_r denotes the network capacity when only macro BSs are deployed for scenario r. The multiplier $\lambda \geq 1$ is the desired capacity increase over the C_r. Symbol π_r is the probability that scenario r occurs, and $\mathcal{R}$ and $\mathcal{K}_r$ represent the set of scenarios and users in scenario r, respectively.

Finding the optimal number of BSs and the position of the BSs are extremely complex

problems. Similar problems have been studied in the literature under the facility location research formulation [29]. Facility location problems focus on the optimal placement of facilities to minimize the costs while providing service constraints. The relation between the energy-efficient BS deployment and facility location problems is straightforward. One approach to simplify this problem is to select the set of candidate locations in the network area. These locations must be selected wisely to improve the performance of the algorithm. After selecting these locations, the second part of the problem is the determination of the optimal set of BSs among these candidates. Due to intercell interference, the individual and cumulative performance of the BSs are not directly correlated. Especially, if the BSs are located close to each other, the cumulative performance of the BSs can be worse than the individual performance of each BS. Therefore, this optimization problem is a combinatorial problem. It quickly becomes untractable when the number of scenarios and the candidate locations are large. Thus, we propose a greedy algorithm which is described in the next section.

2.4 Proposed Algorithm and Optimality Analysis

In this section, we first present the candidate selection and the greedy deployment algorithm, and then discuss its performance.

2.4.1 Candidate Selection

The authors in [21] suggest that the boundaries of the existing cells can be good candidate locations. However, authors in [21] do not consider the distribution of the users in the network and the algorithm they propose works poorly especially when the users are clustered close to macro BSs. In addition, these locations may not be available to deploy BSs depending

on the landform and structures. Second approach can be selecting all feasible locations as candidates. However, depending on the network size, these locations can be innumerably many and even heuristic approaches will be impractical to implement. Therefore, some of the feasible locations should be eliminated to improve the performance of the algorithm in a smart way. In order to overcome these problems, in this dissertation, we divide the network area into equal grids and select a candidate location in each grid. This approach performs well for both clustered and dispersed networks. However, it does not guarantee that a feasible location exists in every grid. In addition, if more than one feasible location exists in a grid, selection of the candidate location is another problem to solve. Therefore, the following approach is proposed in this dissertation. If all the neighboring grids of the center grid have at least one feasible location, the candidate location which is closest to the center of the grid is selected as a candidate. In cases where some of the neighboring grids do not have any feasible location, the closest feasible location to the centroid of the center grid and neighboring grids with no feasible location is selected as a candidate. An example scenario is shown in Fig. 2.1. In this figure, feasible locations, candidate locations, and the center of the centroid are denoted by empty triangles, filled triangles, and X, respectively. In the first case, all neighboring grids have at least one candidate. Therefore, a feasible location which is closest to the center of the grid is selected as the candidate. On the other hand, in the second case, three of the neighboring grids do not have any feasible location. Therefore, the feasible location which is closest to the centroid of these four grids is selected as the candidate location. This approach limits the effects of the user distribution to the performance of the proposed algorithm.

2.4.2 Deployment Algorithm

We propose a greedy algorithm that selects one micro BS to deploy in each iteration. The algorithm selects the candidate micro BS which maximizes the weighted sum of the energy

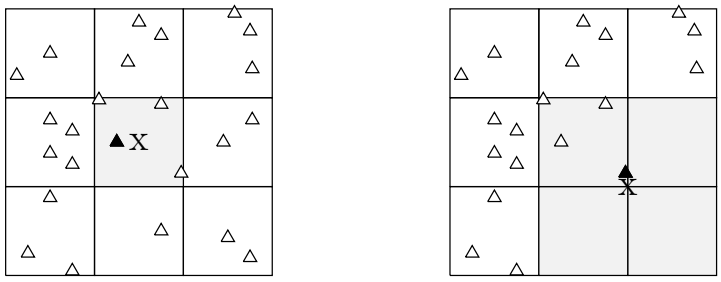

Figure 2.1: A candidate location selection example.

efficiency of all scenarios as next micro BS. This process continues until the required capacity of all scenarios are satisfied. In each iteration, the proposed algorithm assumes the previously selected micro BSs are deployed, and then calculates the energy efficiency over the updated set of BSs. This approach significantly reduces the complexity of the algorithm. The complexity of the optimal solution increases polynomially with $|\mathcal{R}|$ and $|\mathcal{B}_C|$ where $\mathcal{B}_C$ denotes the set of candidate micro BSs. The proposed algorithm solves the problem in linear time. In this dissertation, we assume that one type of micro BSs is deployed, however this work can be extended to cases where different types of BSs are to be deployed such as the deployment of picocells and femtocells. The proposed algorithm is given next, under the heading Algorithm 1.

Algorithm 1 Greedy Base Station Deployment Algorithm

1: Initialize $\mathcal{B}_m = \emptyset$ and $\eta_{EE}(\mathcal{B}) = \eta_{EE}(\mathcal{B}_M)$
2: **while** $\sum_{k \in \mathcal{K}_r} C\left(k, \mathcal{B}\right) < \lambda \cdot C_r$ for all $r \in \mathcal{R}$ **do**
3: $\quad \mathcal{B} = \mathcal{B}_M \cup \mathcal{B}_m$
4: $\quad b = \arg\max_{b \in \mathcal{B}_\mathcal{C}} \sum_{r \in \mathcal{R}} \pi_r \left(\eta_{EE}(\mathcal{B} \cup b) - \eta_{EE}(\mathcal{B})\right)$
5: $\quad \mathcal{B}_m \longleftarrow \mathcal{B}_m \cup \{b\}$
6: $\quad \mathcal{B}_\mathcal{C} \longleftarrow \mathcal{B}_\mathcal{C} \backslash \{b\}$
7: **end while**

2.4.3 Optimality Analysis

The proposed algorithm is a greedy heuristic algorithm. Therefore, it does not guarantee that the obtained solution is optimal. However, it is shown that in [30] if the greedy algorithm

satisfies *i)* $\eta_{EE}(\emptyset) = 0$, *ii)* η_{EE} is nondecreasing, and *iii)* η_{EE} is submodular, then it can be claimed that the algorithm performs better than $(e-1)/e$ times the performance of the optimal solution. The energy efficiency function violates the condition (*ii*). However, in [21], it is shown that ASE satisfies all these three properties. ASE is defined as summation of total capacity over an area times bandwidth. Therefore, over constant area and bandwidth, we can claim that capacity also satisfies these three properties. If we assume that the number of deployed micro BSs which satisfies the constraint is equal for the optimal solution and the proposed algorithm, then we can state that η_{EE} performs better than $(e-1)/e$ times the performance of the optimal solution.

2.5 Numerical Results

In this section, we first investigate the effects of the number of grids and number of active users on the performance of the algorithm, and then compare the performance of the proposed algorithm with the algorithm in [21]. A sample scenario for the deployment of macro BSs, a set of candidate micro BSs, and user distribution are provided in Fig. 2.2. Ten macro BSs are deployed in the 10x10km^2 simulation area. In order to avoid the edge effects, we collect the data over the 5x5km^2 area in the center as suggested in [21]. For simplicity, we assume that 15 different scenarios exist with equal probability. In order to observe the effect of the number of active users on the performance of the algorithm, we create three different types of scenarios: low-, moderate-, and high-loaded. Five of the scenarios are created as low-loaded with 30 active users. Another five of the scenarios are created as moderate-loaded with 100 active users, and the rest five of the scenarios are created as high-loaded with 200 active users. In all these scenarios, users are distributed uniformly over the observation area. All users are associated with the BSs in the observation area. The simulation models and parameters are provided in Table 4.2 [24]. We assume that 3-sector antennas are used for macro BSs

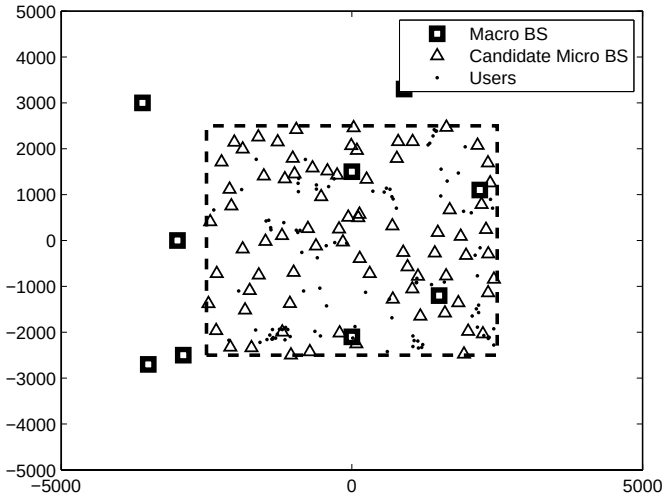

Figure 2.2: Macro BSs, candidate micro BSs, and user distribution for a sample scenario.

and omnidirectional antennas are used in the micro BSs. Multiple antenna transmission is not investigated in this chapter. The transmission and total operational powers for macro and micro BSs are summarized in Table 2.2 [25].

In Fig. 2.3, we investigate the effects of the number of the grids on the performance of the proposed algorithm. The edge length of the grids are decreased to the half in each case. We start with 4 grids and increase the number of grids until it reaches 65536. The performance of the algorithm significantly improves until the number of grids reaches 1024. However, the increase is slowed down after 1024. Increasing the number of grids from 1024 to 65536 improves the energy efficiency of the algorithm by 1%. However, due to the increase of the number of candidate locations, the complexity of the algorithm increases polynomially. After a certain number of grids, increasing the number of grids does not improve the performance of the algorithm notably and it requires a longer convergence time.

In Fig. 2.4, we compare the performance of three different types of user scenarios when the number of grids is selected as 1024. When the number of active users in the network increases, more micro BSs should be deployed to maximize the energy efficiency of the network. The

Table 2.1: Simulation Parameters

Parameter	**Setting**
Channel bandwidth	10 MHz
Total number of data RBs	50 RBs
User to Macro PL model	$128.1 + 37.6 \log_{10}(d)$
User to micro PL model	$140.7 + 36.7 \log_{10}(d)$
Effective thermal noise power	-174 dBm/Hz
User noise figures	9 dB
Macro antenna gain	14 dBi
Micro antenna gain	5 dBi
User antenna gain	0 dBi
Macro- and microcell shadowing	8 dB and 10 dB
Traffic model	Full buffer

Table 2.2: Power consumption models of different BS types

BS Type	P_M (W)	P_m (W)
Macro 20W	865	–
Micro 1W	–	38

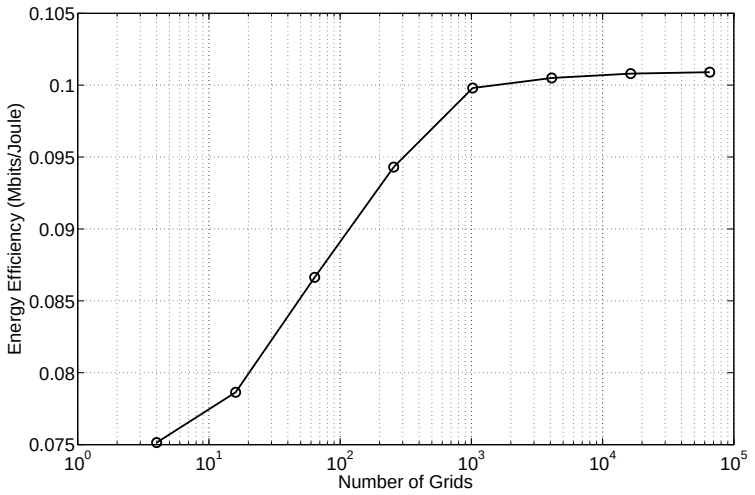

Figure 2.3: Grid size vs. average energy efficiency.

energy efficiencies of the network reach the maximum when 8, 20, and 28 micro BSs are deployed for low-, moderate-, and high-loaded scenarios, respectively. In future networks, it is expected that the number of active users in the network will be higher during the peak hours. Therefore, more additional micro BSs can be deployed to improve the energy efficiency

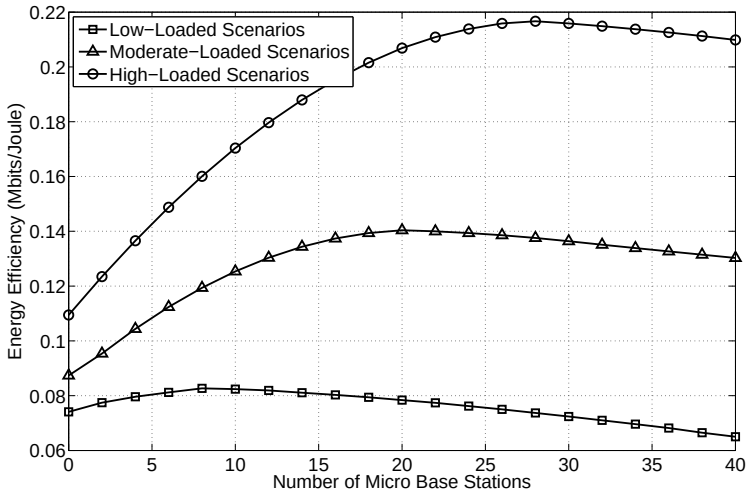

Figure 2.4: The number of active users vs. the energy efficiency.

of the network. In addition, the networks with more active users are more energy-efficient than the others. This improvement is the combination of multi-user diversity and increasing micro BS users.

Figs. 2.5(a)-(b) show the performance of the proposed algorithm and the algorithm in [21]. In this chapter, we particularly compare the energy efficiency gain and the total capacity improvement of the network. Both algorithms start with no micro BS and in each iteration one micro BS is deployed. In this simulation, moderate-loaded scenarios are considered. The number of grids is chosen as 1024 for the proposed algorithm. As the number of micro BSs is increased, the total throughput of the network increases monotonically. On the other hand, the energy efficiency is shaped such that it monotonically increases up to a certain point and then starts to decrease. In Fig. 2.5(a), 10 micro BSs are required for the proposed algorithm, when λ is equal to 1.5. On the other hand, the algorithm in [21] cannot reach the required capacity improvement, the maximum capacity improvement is slightly over 30%. The total capacity improvements of the proposed algorithm is 36% better than the algorithm in [21] when both algorithms reach their maximum. Similar energy efficiency improvement is observed.

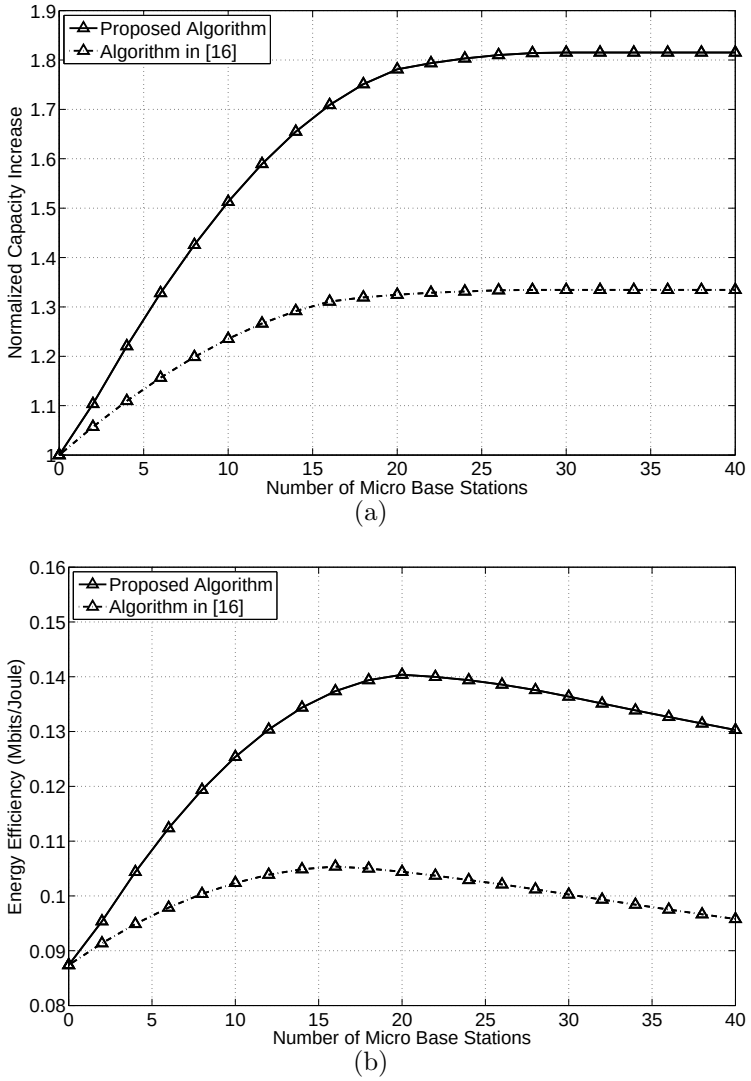

Figure 2.5: Network total capacity (a) and energy efficiency of the system (b) are depicted per iteration.

2.6 Conclusion

In this chapter, a greedy BS deployment algorithm is proposed to improve the energy efficiency of the network. Imprudent increase of the number of micro BSs may harm the energy efficiency of the network. The proposed algorithm first selects a set of feasible micro BS locations wisely, and then greedily deploys a subset of them until the required capacity of the network is satisfied. Due to the heuristic nature of the algorithm, the complexity of

the algorithm is significantly reduced. The simulations show that the proposed algorithm increases both the energy efficiency and the throughput of the network, while satisfying the capacity requirements.

This chapter is reproduced based on the material in [31, 32].

Chapter 3

Three-Stage Resource Allocation Algorithm for Energy-Efficient Heterogeneous Networks

3.1 Motivation

As discussed earlier, with the proliferation of the mobile devices such as smart phones, tablets, and laptops, ubiquitous, fast, and reliable wireless connections are needed. A recent study in [33] estimates that the number of mobile devices will reach 11.6 billion by 2020. According to the same source, this will be accompanied by an increase in mobile data traffic volume reaching a compounded annual growth rate of 53 percent between 2015 and 2020. Motivated by the financial and ecological concerns, network operators are pursuing energy-efficient solutions to keep their energy consumption at reasonable levels while satisfying this demand. These solutions have been studied in the literature under the general description "Green Communications," see, e.g., [6] and the references therein.

Resource allocation problem is an important research area in the field of game theory with wide applications in wireless communication networks, see, e.g., [34–39]. This problem arises when multiple agents or players with conflicting interests compete for the same resources. For example, resource allocation in heterogeneous networks (HetNets) reflects a case such that while each base station tries to maximize its utility by increasing its transmit power, this creates an excessive interference in the system for the neighboring cells. In this chapter, we employ interference pricing, which is introduced in [35–37]. Each base station is penalized according to the interference it creates. The penalty factor increases if the interference leads to outage of users in other sectors. The pricing algorithm defines the utility as the energy efficiency of a sector minus the created interference to other sectors. This makes Macrocell Base Stations (MBSs) decrease their transmission power, and the energy efficiency of the network is further improved. In addition, due to the drop of the interference level, the outage probability of users decreases.

Energy-efficient wireless networks have been widely investigated in the literature, see, e.g., [40–49] and the references therein. In [40], the authors formulate energy efficiency function with predetermined weights to user rates and propose three resource allocation algorithms: optimal, near optimal, and suboptimal. A suboptimal resource allocation algorithm is proposed in [41] in which each user is first assigned with one subcarrier and then the rest of the resources are assigned to minimize the power consumption. They show that energy efficiency function is quasiconcave for given subcarrier assignment. Then, multi-level water-filling algorithm is used for power allocation. The scheduling problem in a single-cell network is transformed into a fractional program in [42]. The water filling algorithm is used for power allocation. In [43], an energy-efficient water-filling algorithm is proposed. Energy-per-goodbit metric is defined for the optimization problem. However, all of these works investigate the problem in single-cell single-tier networks. The proposed algorithm in this chapter investigates resource allocation problem in multi-cell multi-tier networks. The following works investigate the energy-efficient wireless networks in multi-cell networks. An

iterative energy-efficient link adaptation framework is presented in [44]. This work considers the circuit power and transmit power jointly to determine the optimal solution that maximizes the energy efficiency in a non-cooperative manner. A similar link adaptation algorithm that considers interference to determine the transmit power levels is proposed in [45]. The work in [46] investigates energy-efficient resource allocation in an Orthogonal Frequency Division Multiple Access (OFDMA) network. It is shown that the maximum energy efficiency and spectral efficiency are achieved at the same point for the low-power regime. In [47], the authors show that energy efficiency maximization problem is equivalent to spectral efficiency maximization problem for small values of transmission power. However, rate requirements of users are not considered in [47]. Works in [44–47] employ universal frequency reuse (FR) and do not consider HetNet deployments. Contrary to these references, in what follows, we present an algorithm in this chapter that determines the MBS and picocell transmit power levels together in networks with Fractional Frequency Reuse (FFR).

Several interference cancellation and mitigation techniques have been investigated in the literature such as FFR, opportunistic scheduling, and almost blank subframes [8, 9]. In next-generation networks such as Long Term Evolution (LTE) and 5G, FFR has been identified as an efficient, and at the same time, a low-complexity method to mitigate intercell interference [9]. Although FFR has been mostly studied in the literature for single-layer networks, see, e.g., [50] and [51], its performance has not been investigated to its full potential in multi-tier networks. Recently, energy efficiency of heterogeneous cloud radio access networks is investigated in [52], and the soft-FFR method is employed to mitigate the interference between the high- and low-power nodes. It has been shown that heterogeneous cloud radio networks provide significant performance gain over both HetNets and cloud networks. In [53], the authors propose an energy-efficient resource scheduling algorithm for heterogeneous coordinated multi-point (CoMP) transmissions. The proposed algorithm in [53] converges quickly which is crucial in practical wireless systems. A novel multi-tier FFR scheme has been proposed in [54] and [55], which have investigated its throughput and out-

age probability in [54] and its spectral efficiency in [55] for constant cell-center boundaries. In this chapter, we will also employ the same FFR scheme, but with dynamic cell-center boundaries to maximize the energy efficiency.

The problems of energy efficiency maximization and satisfying rate constraints do not always coincide. On the contrary, these problems usually contradict with each other. In order to satisfy rate requirements of users, base stations may need to increase their transmission power to energy-inefficient levels. In the literature, these two problems are studied in [43, 44, 49]. However, none of these works considers intercell interference conditions that increase the complexity of the problem. In this chapter, we address this problem in a multicell environment in which the intercell interference is very critical.

The contributions of this chapter are as follows. We study energy efficiency maximization of HetNets with rate constraints using the FFR scheme and propose a dynamic algorithm to select cell-center radius, assign frequency resources, and solve the power allocation problem. First, a dynamic method is proposed to determine cell-center radius. Second, frequency resources are assigned to users considering the interference conditions and user rate requirements. As the majority of the network traffic is generated indoors [56], the first stage is typically solved at a large time scale. However, in this chapter, we combine the first and second stage and solve cell-center radius selection problem in small scale. Last, a Levenberg-Marquardt method-based approach is implemented to solve the power allocation problem. Dual decomposition techniques are used for minimum rate constraints of users. This reactive approach helps us further improve the energy efficiency and satisfy the rate requirements of users. Note that the third stage is updated more frequently at a smaller time scale. We have previously proposed a gradient ascent based power allocation method to solve the energy efficiency maximization problem without considering rate constraints of users, constant cell-center boundaries, and constant frequency assignments in [57]. In this chapter, we propose a Levenberg-Marquardt method-based approach to extend the framework to consider

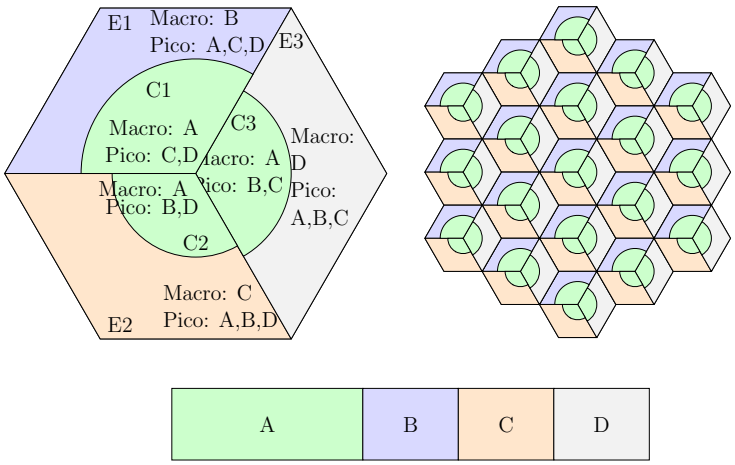

Figure 3.1: Dynamic cell-center region boundaries and spectrum assignments in a multi-tier FFR scheme. The network layout assumes a uniform 19 cell hexagonal grid in which the MBSs have three sector antennas and pico-BSs employ omnidirectional antennas.

Quality-of-Service (QoS) constraints and to increase the speed of convergence.

The remainder of this chapter is organized as follows. Section 3.2 introduces the system model and base station power consumption models. Section 3.3 formulates the energy-efficient resource allocation problem in HetNets. The proposed solution methods are presented in Section 3.4. Simulation results are presented to evaluate the performance gains in Section 3.5 and concluding remarks are presented in Section 3.6.

3.2 System Model

In this section, we first present the system model and the multi-tier FFR scheme. We then study a linearized base station power consumption model that will be used later to formulate the energy-efficient resource allocation problem in Section 3.3.

Consider a cellular layout of 19 hexagonal cells as depicted in Fig. 3.1. As is commonly done in the literature, we will use this layout together with the wrap-around technique, e.g., [57,58], to model a cellular network of infinite dimensions. Assume that macrocells employ 3-sector

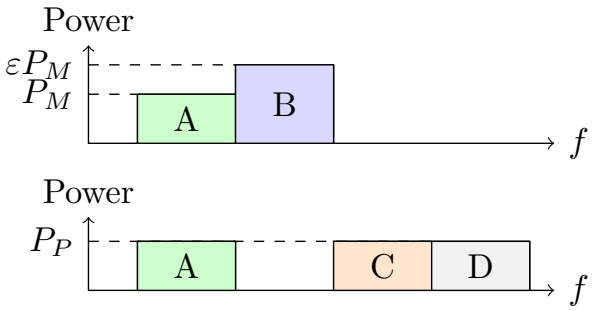

Figure 3.2: Illustration of the proposed spectrum and power utilization of an MBS and a cell-edge pico-BSs in Sector 1 with the multi-tier FFR scheme.

antennas and picocell base stations (pico-BSs) have omni-directional antennas. Spectrum allocation in the macrocell and picocell tiers is fundamental to determine the interference conditions and user rates at each tier. In densely deployed networks, intercell interference becomes a significant problem, limiting the system performance. The FFR scheme provides a solution by assigning the frequency resources in a coordinated manner such that high interference conditions are avoided. In this chapter, we employ the FFR scheme depicted in Fig. 3.1. We refer to the macrocell-associated users as MUEs and picocell-associated users as PUEs. The MUEs can be categorized into cell-center and cell-edge users depending on factors such as their received reference power, path loss, or traffic load within the sector [57]. In this process, the variable $r_{th,s}$ determines the cell-center region boundary of sector s. In Section 3.4.1, we elaborate on the selection process of $r_{th,s}$ in detail. In terms of spectrum allocation, the MBSs can allocate subcarriers in subband A to their cell-center users while the cell-edge MUEs are assigned to either one of the remaining three subbands. For example, in Sector 1, subband B is allocated to the cell-edge users. Pico-BSs in the cell-center region are assigned to orthogonal channels with respect to the subbands that the MBS operates at. This is to reduce the cross-tier interference as the cell-center pico-BSs are close to the MBS. For example, cell-center pico-BSs operate at subbands C and D. Note that, in a typical LTE deployment, the MBSs and pico-BSs have around 16 dB transmit power difference [59]. This would have detrimental effects for the cell-center PUEs in the downlink if they were not assigned to orthogonal channels with the MBS. For the cell-edge pico-BSs, subband A can

also be reused in order to increase the throughput. For example, cell-edge pico-BSs operate at subbands A, C, and D in Sector 1. Note that the multi-tier FFR scheme depicted in Fig. 3.1 favors the cell-center PUEs and cell-edge MUEs that would have been exposed to severe interference if, for example, universal FR had been employed. This also enables operation at a lower interference region such that the energy efficiency of the downlink transmissions can be significantly increased. This fact is demonstrated later in Section 3.5 through numerical simulations. We test our findings in an LTE scenario. In LTE, the smallest scheduling granularity is per resource block (RB) in which an RB consists of 12 subcarriers [59].

In this chapter, we employ constant power allocation across subbands. Let N_A, N_B, N_C, and N_D denote the total number of subcarriers in subbands A, B, C, and D, respectively. The total number of subcarriers is denoted by N, i.e., $N = N_A+N_B+N_C+N_D$. We introduce two variables, ε and β, to determine transmission power levels of base stations. The parameter ε denotes the ratio of the downlink transmissions of cell-edge MUEs to cell-center MUEs. This parameter is introduced to favor either cell-center or cell-edge users that do not satisfy their minimum rate requirements. This parameter is only defined for the MBSs. The variable β scales the transmission power of the base stations. This parameter introduces energy savings into the system. The corresponding spectrum and power utilization scheme is illustrated in Fig. 3.2. The downlink transmission per subcarrier of an MBS M for cell-center MUEs in Sector 1, P_M, is given by

$$P_M = \frac{\beta_s P_{\max,M}}{N_A + \varepsilon N_B}, \tag{3.1}$$

where $P_{\max,M}$ is the maximum transmit power of an MBS. Similarly, for the cell-edge MUEs, the MBS transmit power per subcarrier is εP_M. It is straightforward to obtain the expressions for Sectors 2 and 3 by replacing N_B with N_C and N_D, respectively. In the picocell tier, the downlink transmission across subcarriers is also considered to be constant. For example, the

transmit power per subcarrier of a pico-BS P, P_P, in Sector 1 can be expressed as

$$P_P^C = \frac{\beta_P P_{\max,P}}{N_C + N_D} \text{ and } P_P^E = \frac{\beta_P P_{\max,P}}{N_A + N_C + N_D}, \tag{3.2}$$

where P_P^C and P_P^E denote the transmit power of a cell-center and a cell-edge pico-BS per subcarrier, respectively. The maximum transmit power of a pico-BS is represented by $P_{\max,P}$. For pico-BSs in Sectors 2 and 3, a similar expression can be obtained by simply replacing the values of N_C and N_D with the respective subband values.

Let sector s consist of K_s active users, and $\mathcal{K}_{M,s}$ and $\mathcal{K}_{P,s}$ denote the sets of MUEs and sets of PUEs, respectively. Let k be the index of user and n be the index of the subcarrier. The vector $\boldsymbol{C}_{M,s}$ consists of binary variables denoting whether or not MUE is in the cell-center region, i.e., $\boldsymbol{C}_{M,s}^k = 1$ if MUE k is located in the cell center region and $\boldsymbol{C}_{M,s}^k = 0$ otherwise, where $\boldsymbol{C}_{M,s}^k$ is the kth entry of the vector $\boldsymbol{C}_{M,s}$. Likewise, the vector $\boldsymbol{C}_{P,s}$ consists of binary variables $\boldsymbol{C}_{P,s}^k \in \{0, 1\}$ denoting whether or not PUE is in the cell-center region. The matrix $\boldsymbol{F}_{M,s}$ is $|\mathcal{K}_{M,s}| \times N$ and its (n, k)th element denotes whether or not the subcarrier is assigned to MUE by a value of 1 or 0, respectively. The matrix $\boldsymbol{F}_{P,s}$ is $|\mathcal{K}_{P,s}| \times N$ and its (n, k)th element denotes whether or not the subcarrier is assigned to PUE by a value of 1 or 0, respectively. The matrices $\boldsymbol{R}_1$ and $\boldsymbol{R}_2$ are $N \times |\mathcal{K}_{M,s}|$, and the matrices $\boldsymbol{R}_3$ and $\boldsymbol{R}_4$ are $N \times |\mathcal{K}_{P,s}|$. The (n, k)th element of $\boldsymbol{R}_1$ and $\boldsymbol{R}_2$ is the throughput of MUE k on subcarrier n when the user k is located in the cell-center and cell-edge regions, respectively. Likewise, the (n, k)th element of $\boldsymbol{R}_3$ and $\boldsymbol{R}_4$ denotes the throughput of PUE k on subcarrier n when the user k is located in the cell-center and cell-edge regions, respectively. The aggregate throughput of a sector s can be expressed as

$$\begin{aligned} R_s = &\sum_{k \in \mathcal{K}_{M,s}} (\boldsymbol{C}_{M,s}^k \boldsymbol{F}_{M,s}^{(k,:)} \boldsymbol{R}_1^{(:,k)} + (1 - \boldsymbol{C}_{M,s}^k) \boldsymbol{F}_{M,s}^{(k,:)} \boldsymbol{R}_2^{(:,k)}) \\ &+ \sum_{k \in \mathcal{K}_{P,s}} (\boldsymbol{C}_{P,s}^k \boldsymbol{F}_{P,s}^{(k,:)} \boldsymbol{R}_3^{(:,k)} + (1 - \boldsymbol{C}_{P,s}^k) \boldsymbol{F}_{P,s}^{(k,:)} \boldsymbol{R}_4^{(:,k)}). \end{aligned} \tag{3.3}$$

Note that $\boldsymbol{X}^{(n,:)}$ corresponds to the nth row vector of the matrix $\boldsymbol{X}$. Likewise, $\boldsymbol{X}^{(:,k)}$ is the kth column vector of the matrix $\boldsymbol{X}$. Depending on the associated tier, region, and subband, the throughput terms in (4.4) can be expanded using the definitions in (4.2) and (3.2) as

$$\begin{aligned}
\boldsymbol{R}_1^{(n,k)} =& \Delta_n \log_2\left(1+\frac{P_M\, g_{k,M}^{(n)}}{I_1^{(k,n)}+N_0\Delta_n}\right), \quad \boldsymbol{R}_2^{(n,k)} = \Delta_n \log_2\left(1+\frac{\varepsilon_s P_M\, g_{k,M}^{(n)}}{I_2^{(k,n)}+N_0\Delta_n}\right), \\
\boldsymbol{R}_3^{(n,k)} =& \Delta_n \log_2\left(1+\frac{P_P^C\, g_{k,P}^{(n)}}{I_3^{(k,n)}+N_0\Delta_n}\right), \quad \boldsymbol{R}_4^{(n,k)} = \Delta_n \log_2\left(1+\frac{P_P^E\, g_{k,P}^{(n)}}{I_4^{(k,n)}+N_0\Delta_n}\right),
\end{aligned} \tag{3.4}$$

where $\boldsymbol{X}^{(n,k)}$ is the entry on the nth row and kth column of the matrix $\boldsymbol{X}$. The channel gain between user k and MBS M and between user k and pico-BS P on subcarrier n are denoted by $g_{k,M}^{(n)}$ and $g_{k,P}^{(n)}$, respectively. The interference incurred by user k on subcarrier n is denoted by $I_j^{(n,k)}$ in (4.5), where $j = 1, 2, 3, 4$. The value of $I_j^{(n,k)}$ can be calculated as follows

$$I_j^{(n,k)} = \begin{cases} \displaystyle\sum_{M' \neq M,\, M' \in \mathcal{B}_M^{(n)}} P_{M'}^{(n)} g_{k,M'}^{(n)} + \sum_{P \in \mathcal{B}_P^{(n)}} P_P^{(n)} g_{k,P}^{(n)} & \text{for } j = 1, 2 \\ \displaystyle\sum_{M' \in \mathcal{B}_M^{(n)}} p_{M'}^{(n)} g_{k,M'}^{(n)} + \sum_{P' \neq P,\, P' \in \mathcal{B}_P^{(n)}} P_{P'}^{(n)} g_{k,P'}^{(n)} & \text{for } j = 3, 4 \end{cases} \tag{3.5}$$

where $\mathcal{B}_M^{(n)}$ and $\mathcal{B}_P^{(n)}$ denote the sets of MBSs and pico-BSs that transmit on subcarrier n, respectively. The sets of interfering MBSs and pico-BSs differ based on the sector, associated tier, and whether the UE is in the cell-center or cell-edge region. The transmit power of an MBS M and a pico-BS P are represented by $p_M^{(n)}$ and $p_P^{(n)}$, respectively. Likewise, these power levels depend on the sector and transmission band. The thermal noise power per Hz and bandwidth of a subcarrier are represented by N_0 and Δ_n, respectively, $\Delta_n = 15$ kHz for LTE systems [59]. Notice that for the cell-edge PUEs that are assigned to Band A, the interference term in $\boldsymbol{R}_4^{(n,k)}$ includes the intra-sector interference contributions from the

MBS M to a cell-edge PUE k in the same sector, that is $P_M g_{k,m}^{(n)}$. Including these terms enables us to balance the cross-tier interference while maximizing the sector energy efficiency. Reference [60] presents an extensive survey on resource allocation methods with cooperating BSs. Our paper, in particular, can be categorized as a case where base stations share their channel state information (CSI), which are obtained through feedback channels, to coordinate their power and scheduling assignments among cooperating cells. In this chapter, we assume that there exists backhaul capacity to exchange CSI information among base stations.

Several base station power consumption models are proposed in the literature, see, e.g., [26, 61–64]. In [26], the authors provide a parameterized power model that especially considers the effects of transmission bandwidth and number of transmission chains. In [61, 62], the circuit power consumption is defined as a function of sum rate. In [63], the power consumption of base station is defined as a summation of the transmit power dependent power consumption and static power consumption. In [64], the authors propose a power model for various types of base stations and the individual contributions of the different equipment, such as the baseband unit, radio frequency transceiver, power amplifier, power supply unit, and cooling devices, are considered for total power consumption. This model also captures the power consumption during the sleep mode which is very crucial for next-generation networks [6]. In this chapter, base stations go into the sleep mode when they are not serving any user. Therefore, we employ the model in [64] in this paper. The power consumption at MBS M is given by

$$P_{\mathrm{MBS},M} = \begin{cases} N_M^{TRX}\left(P_{0,M} + \Delta_M \beta_s P_{\max,M}\right), & \text{if } 0 < \beta \leq 1, \\ N_M^{TRX} P_{\mathrm{sleep},M}, & \text{if } \beta = 0, \end{cases} \tag{3.6}$$

where $P_{\mathrm{MBS},M}$ and P_M^{TX} are the total power consumption at an MBS and RF transmit power, respectively. N_M^{TRX} is the number of transceiver chains and $P_{0,M}$ is the power consumption

at the minimum nonzero output power at an MBS. The slope of the load-dependent power consumption at an MBS is denoted by Δ_M. When an MBS does not transmit, it is considered to be in the sleep mode and its power consumption is captured in $P_{\text{sleep},M}$. In this model, the total power consumption depends on the transmit power or the load. Therefore, it is referred to as the load-dependent power consumption model [64]. Similarly, the power consumption of pico-BS P is given by

$$P_{\text{PBS},P} = \begin{cases} N_P^{TRX}\left(P_{0,P} + \Delta_P \beta_P P_P^{TX}\right), & \text{if } 0 < P_P^{TX} \leq P_P^{\max}, \\ N_P^{TRX} P_{\text{sleep},P}, & \text{if } P_P^{TX} = 0, \end{cases} \tag{3.7}$$

where $P_{\text{PBS},P}$, $P_{0,P}$, $P_{\text{sleep},P}$, and P_P^{TX} denote the total power consumption, power consumption at the minimum nonzero output power, power consumption in the sleep mode, and RF transmit power at pico-BS P, respectively. The number of transceiver chains at the pico-BSs is denoted by $N_{TRX,P}$. The slope of the load-dependent power consumption at pico-BS is denoted by Δ_P. In Table 3.1, we present the values of the linearized power consumption model parameters for MBSs and pico-BSs. Using (3.6) and (3.7), the power consumed in sector s can be expressed as

$$\psi_s(\beta_s, \boldsymbol{\beta}_{P,s}) = P_{\text{MBS}} + \sum_{P \in \mathcal{B}_{P,s}} P_{\text{PBS,P}}, \tag{3.8}$$

where $\boldsymbol{\beta}_{P,s}$ is the vector of all β parameters of all pico-BSs in sector s. The set of pico-BSs in sector s is denoted by $\mathcal{B}_{P,s}$.

Using the aggregate throughput and power consumption expressions in (3.3) and (3.8), the energy efficiency of sector s, in bits/Joule, is defined as

$$\eta_s(\varepsilon_s, \beta_s, \boldsymbol{\beta}_{P,s}) = \frac{R_s}{\psi_s(\beta_s, \boldsymbol{\beta}_{P,s})}. \tag{3.9}$$

Note that the MBS transmissions on Band A determine the cross-tier interference for the cell-

edge PUEs in the same sector as well as the intercell interference. However, as the downlink transmissions of the MBS and cell-center pico-BSs in the same sector are orthogonal, the MBS transmissions do not affect the throughput of cell-center PUEs in the same sector. In the next section, we formulate the energy efficiency maximization problem.

3.3 Joint Energy-Efficient Resource Allocation Problem

In this section, we develop the framework for a utility-based resource allocation algorithm in which the objective is to maximize the energy efficiency while satisfying the rate requirement of users. The energy efficiency maximization problem can be formulated as

$$\max_{\mathbf{x},\boldsymbol{\beta}_P,\mathbf{C},\mathbf{F}} \quad \sum_{s\in\mathcal{S}} \eta_s(\mathbf{x}_s,\boldsymbol{\beta}_{P,s})$$

$$\text{s.t.} \quad \boldsymbol{C}^k_{M,s}\boldsymbol{F}^{(k,:)}_{M,s}\boldsymbol{R}^{(:,k)}_1 + (1-\boldsymbol{C}^k_{M,s})\boldsymbol{F}^{(k,:)}_{M,s}\boldsymbol{R}^{(:,k)}_2 \geq R_{\min,k}, \tag{3.10a}$$

$$\text{for all } k\in\mathcal{K}_{M,s}, s\in\mathcal{S}$$

$$\boldsymbol{C}^k_{P,s}\boldsymbol{F}^{(k,:)}_{P,s}\boldsymbol{R}^{(:,k)}_3 + (1-\boldsymbol{C}^k_{P,s})\boldsymbol{F}^{(k,:)}_{P,s}\boldsymbol{R}^{(:,k)}_4 \geq R_{\min,k}, \tag{3.10b}$$

$$\text{for all } k\in\mathcal{K}_{P,s}, s\in\mathcal{S}$$

$$\sum_{\substack{k\in\mathcal{K}_{M,s}\\ \boldsymbol{C}^k_{M,s}=1}} \boldsymbol{F}^{(k,n)}_{M,s} = 1 \text{ and } \sum_{\substack{k\in\mathcal{K}_{M,s}\\ \boldsymbol{C}^k_{M,s}=0}} \boldsymbol{F}^{(k,n)}_{M,s} = 0 \quad \text{for all } n\in\mathcal{N}^C_{M,s}, s\in\mathcal{S} \tag{3.10c}$$

$$\sum_{\substack{k\in\mathcal{K}_{M,s}\\ \boldsymbol{C}^k_{M,s}=0}} \boldsymbol{F}^{(k,n)}_{M,s} = 1 \text{ and } \sum_{\substack{k\in\mathcal{K}_{M,s}\\ \boldsymbol{C}^k_{M,s}=1}} \boldsymbol{F}^{(k,n)}_{M,s} = 0 \quad \text{for all } n\in\mathcal{N}^E_{M,s}, s\in\mathcal{S} \tag{3.10d}$$

$$\sum_{k\in\mathcal{K}_{M,s}} \boldsymbol{F}^{(k,n)}_{M,s} = 0 \quad \text{for all } n\notin\mathcal{N}^C_{M,s}\cup\mathcal{N}^E_{M,s}, s\in\mathcal{S} \tag{3.10e}$$

$$\sum_{\substack{k\in\mathcal{K}^p_{P,s}\\ \boldsymbol{C}^k_{P,s}=1}} \boldsymbol{F}^{(k,n)}_{P,s} = 1 \text{ and } \sum_{\substack{k\in\mathcal{K}^p_{P,s}\\ \boldsymbol{C}^k_{P,s}=0}} \boldsymbol{F}^{(k,n)}_{P,s} = 0 \quad \text{for all } n\in\mathcal{N}^C_{P,s}, s\in\mathcal{S} \tag{3.10f}$$

$$\sum_{\substack{k\in\mathcal{K}^p_{P,s}\\ \boldsymbol{C}^k_{P,s}=0}} \boldsymbol{F}^{(k,n)}_{P,s} = 1 \text{ and } \sum_{\substack{k\in\mathcal{K}^p_{P,s}\\ \boldsymbol{C}^k_{P,s}=1}} \boldsymbol{F}^{(k,n)}_{P,s} = 0 \quad \text{for all } n \in \mathcal{N}^E_{P,s}, s \in \mathcal{S} \tag{3.10g}$$

$$\sum_{k\in\mathcal{K}^p_{P,s}} \boldsymbol{F}^{(k,n)}_{P,s} = 0 \quad \text{for all } n \notin \mathcal{N}^C_{P,s} \cup \mathcal{N}^E_{P,s}, s \in \mathcal{S} \tag{3.10h}$$

$$\boldsymbol{\varepsilon} \succeq \mathbf{0} \text{ and } \mathbf{0} \preceq \boldsymbol{\beta} \preceq \mathbf{1} \tag{3.10i}$$

$$0 \preceq \boldsymbol{\beta}_P \preceq \mathbf{1} \tag{3.10j}$$

where $R_{\min,k}$ is the minimum rate constraint of user k. The sets of subcarriers assigned to cell-center and cell-edge regions of MBS M in sector s are denoted by $\mathcal{N}^C_{M,s}$ and $\mathcal{N}^E_{M,s}$, respectively. Likewise, the sets of subcarriers assigned to cell-center and cell-edge regions of pico-BSs in sector s are denoted by $\mathcal{N}^C_{P,s}$ and $\mathcal{N}^E_{P,s}$, respectively. The set of sectors in the simulations area is $\mathcal{S}$. The set of PUEs that are associated with pico-BS P in sector s is denoted by $\mathcal{K}^p_{P,s}$. The vectors $\boldsymbol{\varepsilon}$ and $\boldsymbol{\beta}$ consist of ε_s and β_s for all sectors in the network. The vector $\boldsymbol{\beta}_P$ consists of $\boldsymbol{\beta}_{P,s}$ that denotes the power control variable for each pico-BSs in the sector s. The notation $\boldsymbol{\varepsilon} \succeq \mathbf{0}$ means that each element of $\boldsymbol{\varepsilon}$ is greater than or equal to 0. Throughout the rest of the chapter, the vector $\mathbf{x}_s$ will be used for the (ε_s, β_s) couple and the vector $\mathbf{x}$ will be used for the vector couple $(\boldsymbol{\varepsilon}, \boldsymbol{\beta})$. Constraints (3.10a) and (3.10b) ensure that minimum rate constraints of users are satisfied. Constraints (3.10c) and (3.10d) guarantee that cell-center MBS resources assigned to cell-center MUEs and cell-edge MBS resources are assigned to cell-edge MUEs, respectively. Constraint (3.10e) ensures that MBSs do not assign any resources that are not available to themselves. Constraints (3.10f) and (3.10g) guarantee that cell-center pico-BS resources assigned to cell-center PUEs and cell-edge pico-BS resources assigned to cell-edge PUEs, respectively. Constraint (3.10h) ensures that pico-BSs do not assign any resources that are not available to themselves. Constraints (3.10i) and (3.10j) state that parameters $\boldsymbol{\varepsilon}$, $\boldsymbol{\beta}$, and $\boldsymbol{\beta}_{P,s}$ are within the given limits.

This resource allocation problem needs to be jointly solved over the cell-center radius, frequency, and power domains to obtain the optimum solution. The problem is combinatorial over the first two domains and is non-convex over the power allocation domain [65, 66]. Therefore, obtaining the global solution to this problem requires an exhaustive search which is fairly impractical. For the power allocation problem, we have showed in [57] that for the same cell-center radius and frequency domain allocation, the energy efficiency function of a sector is quasiconcave over the power levels when the interference conditions are constant. To benefit from this property in the next section, we propose a three-stage algorithm in which the joint problem is divided into separate domains.

3.4 Proposed Solution

Our formulation in (3.10) enables us to develop an energy-efficient resource allocation algorithm. Similar resource allocation algorithms have been studied in the literature, see, e.g., [44,45], and Chapter 3 of [34]. In our proposed algorithm, we decouple the main problem into three subproblems. First, we start by selecting three candidate cell-center boundaries such that the cell-center and cell-edge MUEs are selected and the corresponding information is sent to the pico-BSs, identifying their regions and subbands. Second, we solve the frequency allocation problem for all candidate cell-center boundaries. Note that, the power control parameters that are obtained during the last time instant are used to calculate the Lagrangian function in this process. Then, among these candidate cell-center boundaries, the one that maximizes the Lagrangian function is selected. Last, we calculate the power control parameters for the MBS and the pico-BSs, consecutively. After each sector solves its power allocation subproblem, the interference prices and power levels are distributed among the network. By using this information, each sector first resets the cell-center radius, resolves the frequency allocation, and finally recalculates the power levels. The proposed algorithm

Algorithm 2 Proposed Energy-Efficient Resource Allocation Algorithm

1: **Initialize:** $r_{th,s}^{(0,c)} = r_{r,s}/2 \quad (\varepsilon_s^{(0)}, \beta_s^0, \boldsymbol{\beta}_{P,s}^{(0)}) = [1, 1, \mathbf{1}]$
2: $r_{th,s}^{(t,c)} = r_{th,s}^{(t-1,c)}$
3: **Stage 1:** Each sector determines $r_{th,s}^{(t,c-1)}$ and $r_{th,s}^{(t,c+1)}$ by using the cell-center radius selection algorithm in Section 3.4.1.
4: **for** $n := -1$ to 1 **do**
5: **Stage 2:** For cell-center radius, $r_{th,s}^{(t,c+n)}$, the frequency assignment algorithm is solved by using the algorithm in Section 3.4.2.
6: $\mathcal{L}_s^{(n)}$ which is described in Section 3.4.3 is calculated for the given frequency assignment.
7: Note that dual variables and power control parameters in previous time instant are used during the Lagrangian function calculation.
8: **end for**
9: The cell-center radius and the frequency assignments that maximize the Lagrangian function are selected.
10: **Stage 3:** For this cell-center radius and frequency assignment, the power control parameters are determined by the proposed power control algorithm in Section 3.4.3.
11: Go to Step 2 and repeat.

is presented under the heading Algorithm 2. In the sequel, we discuss each stage of the proposed algorithm in detail.

3.4.1 The Cell-Center Region Boundaries

The first stage of the proposed algorithm determines the cell-center region boundary of each sector. It is shown in [55] that over 10% throughput improvement can be achieved by proper selection of the constant cell-center region boundaries. Further improvements can be obtained by selecting the boundaries dynamically in each sector. For single-layer networks, the cell-center boundary categorizes its users into the cell-center and cell-edge MUEs. MUEs can typically be distinguished into cell-center and cell-edge users based on the reference signal received power (RSRP) or reference signal received quality (RSRQ) measurements fed back from UEs to MBSs. The RSRP signal indicates the path loss between the serving base station and users, whereas the RSRQ measurement gives the ratio of the reference signal to

the interference. Since it is shown in [67] that the performance of both schemes are similar, in this chapter, we also distinguish users into cell-center and cell-edge users based on the RSRP measurements. If the RSRP of a user is higher than a threshold, it is considered to be in the cell-center region, and vice versa.

For two-tier networks, the cell-center boundary also determines the available RBs for each pico-BS. For example, consider the multi-tier FFR scheme depicted in Figure 3.1. If a pico-BS is located in the cell-center region, the number of available RBs for this pico-BS reduces. This frequency allocation alleviates the cross-tier interference between the cell-center MUEs and cell-edge PUEs. On the other hand, if a pico-BS is located in the cell-edge region, all subbands, except the subband which is used by cell-edge MUEs, are available to this pico-BS. Therefore, when a pico-BS is located in the cell-center region, the available RBs and correspondingly the total throughput of the pico-BS significantly decreases.

In two-tier networks, due to the high power difference of the reference signal between the MBSs and pico-BSs, PUEs are typically located close to the pico-BS [68]. For this reason, PUEs typically have low path loss values, or equivalently, high channel gains to their serving pico-BSs. When the number of subbands available to the pico-BS is decreased, it can be expected that the total throughput of PUEs will be reduced. However, due to the reduction in the cross-tier interference, the signal-to-interference-plus-noise ratio (SINR) of the cell-center MUEs increases subsequently. In [57], we proposed two different cell-center selection algorithms. The first algorithm (CSSA2) is proposed to maximize the throughput and the energy efficiency of the network at the cost of fairness. On the other hand, the second one (CSSA3) maximizes fairness among users at the cost of throughput. In CSSA2, the MUE that is closest to the MBS is selected to be in the cell-center region, while the rest of the MUEs are in the cell-edge region. This algorithm achieves higher energy efficiency and throughput while it leads to the starvation of some users, due to the lack of resources for cell-edge users. There is even the possibility of some users not getting any resources when the network is

crowded. On the other hand, CSSA3 achieves significantly higher fairness by sacrificing the energy efficiency of the network. We will evaluate the performance of CSSA2 and CSSA3 in Section 3.5. To benefit the advantage of both algorithms, we propose a new cell-center radius selection method (CSSA1) that dynamically updates the radius. In heterogeneous networks, shifting the cell-center radius is only effective if the new radius changes the region of an MUE or a pico-BS. Otherwise, the change will be useless. Therefore, CSSA1 compares the Lagrangian function of the previous cell-center radius with two cell-center radii: one more MUE or pico-BS is included in the cell-center region and one MUE or pico-BS is excluded from the cell-center region. The MUE or pico-BS that is going to be included in the cell-center region is the closest MUE or pico-BS to the cell-center radius and located in the cell-edge region for the previous cell-center radius. Likewise, the MUE or pico-BS that is going to be excluded from the cell-center region is the closest MUE or pico-BS to cell-center radius and located in the cell-center region. Note that RSRP measurements are used to determine the users or pico-BSs that are going to change their region. In addition, only the region of one MUE or pico-BS changes at each iteration. After that, CSSA1 selects the cell-center radius that maximizes the Lagrangian function among these three radii. In order to calculate the Lagrangian function, the frequency assignment problem needs to be solved. Therefore, the frequency assignment problem that is going to be explained in Section 3.4.2 has to be solved for all these three radii. When the rate requirements of the users are small, CSSA1 shrinks the cell-center radius and improves the energy efficiency of the network. On the other hand, when the rate requirements of the users increase, a more fair cell-center radius selection helps satisfy the rate requirements of users.

3.4.2 Frequency Assignment Problem

In the second stage of the problem, we determine the frequency assignments. There are many scheduling methods discussed in the literature, see, e.g., [59, 69]. Each scheduler has

an efficiency and fairness tradeoff. In general, both of these utilities cannot be increased at the same time. In the LTE radio protocol stack, scheduling is handled by the medium access control (MAC) layer [59]. The scheduler in each base station is responsible from the distribution of frequency resources and this is left to the network operator for implementation. Green scheduling schemes have been surveyed in [69] and references therein. These schemes can significantly improve energy efficiency of the system and decrease the transmission powers. In this chapter, we propose a novel scheduling algorithm to satisfy the rate requirements of users and to maximize the energy efficiency of the sector. For fairness purposes, we first assign one RB to each user. Then, the rest of the resources are assigned to users that provide the highest improvement to the Lagrangian function which is described in Section 3.4.3. When the rate requirements of the users are not satisfied, the dual prices significantly decrease the value of the Lagrangian function. Therefore, the proposed algorithm favors those users that could not satisfy the rate requirement with the current assignment. On the other hand, when the rate requirements of all users are satisfied, the proposed algorithm assigns RBs to the user that provides the highest increase to the Lagrangian function. This user is usually the one who has the best average channel gain among all users. We describe the scheduler algorithm next.

Lagrangian Directed Scheduler (LDS): In the LDS, RBs are distributed among users to maximize the Lagrangian function. Note that, we run this algorithm twice in the MBSs, one for the cell-center MUEs and one for the cell-edge users, due to the fact that these users do not compete for the same RB sets. In LTE standards, the smallest granularity is RB. Therefore, we assign all subcarriers in one RB to one user during the scheduling process. In the proposed scheduling algorithm, the scheduler first assigns one RB to each user. The RB that has the best average channel gain among the available RBs is assigned to the user. After that, if there are still unassigned RBs, the proposed algorithm calculates the increase in the Lagrangian function for an RB and this RB is assigned to the user that provides the highest improvement to the Lagrangian function. This process continues until all RBs are

assigned to the users.

In the sequel, we will compare the proposed LDS with the Equal Bandwidth (EBW) scheduler and Max-Min Fair (MMF) scheduler whose descriptions are given below.

EBW Scheduler: The EBW scheduler distributes RBs equally among users in the following manner. Assume that there are K users and N_{RB} RBs. These RBs are assigned to users such that $\lfloor N_{RB}/K \rfloor + 1$ RBs to $K_h =$ mod (N_{RB}, K) users and $\lfloor N_{RB}/K \rfloor$ RBs to $K_i = K - K_h$ users.

MMF Scheduler: In the MMF scheduler, RBs are distributed among users to maximize the minimum throughput. We adopt the scheduler that has been described in [70]. The primary difference between these two algorithms is the scheduler granularity. The one described in [70] allocates subcarriers to users, however the smallest granularity in the LTE standard is RB. Therefore, we need to adopt the algorithm in [70] to work at the RB level. In the MMF scheduler, each user is assigned the RB with the best average channel gain. We then remove this user from the user set and the corresponding RB from the RB set. This process continues until one of the sets is empty. If the user set is empty first, then the users are sorted according to their actual rates with current assignment. Then the RB that has the best channel is assigned to the first user and users are sorted again according to updated rates. This process continues until all RBs are assigned.

3.4.3 Power Control Problem

The third stage of the proposed solution determines the power assignments such that the optimal power levels are assigned to each subband in order to maximize the energy efficiency and satisfy the rate requirements in the sector. Given the frequency assignments from the previous stage, it remains to solve this power control problem. As we discussed earlier,

this problem is non-convex over the power allocation subdomain and the solution requires exhaustive search over all power control parameters. However, we showed that energy efficiency function $\eta_s(\mathbf{x}_s, \boldsymbol{\beta}_{P,s})$ is quasiconcave over the power control parameters ε_s and β_s in [57]. Therefore, when we divide the power allocation problem into $|S|$ subproblems such that each sector maximizes its own energy efficiency while satisfying the rate requirements of its users where the number $|S|$ corresponds to the number of sectors in the network, each problem is quasiconcave and has a unique maximum over the power control parameters ε_s and β_s. In the maximization problem, the received interference is assumed to be constant. In addition, the region of the users in the sector and frequency assignment of the users have to be determined before calculating the power levels. After these steps, by using convex optimization techniques, the optimal β_s, ε_s, and $\boldsymbol{\beta}_{P,s}$ that maximize the energy efficiency of the sector s and satisfy the rate constraints of users can be obtained.

The pico-BSs are expected to become significantly dense to meet the increasing rate demands [2]. Therefore, updating the power control parameters of MBSs and all pico-BSs in the sector concurrently requires significant data exchange between base stations. This may create congestion in the backhaul network. In addition, this process requires significant computation time and may not be obtained in real time especially in denser networks. Therefore, we split the power control problem into two subproblems. In the first part of the algorithm, MBS determines optimum β_s and ε_s. During this process, the power control parameters of pico-BSs, $\boldsymbol{\beta}_{P,s}$, are assumed to be constant. In the second part of the process, pico-BSs concurrently calculate their power control parameters for the determined β_s and ε_s in the first part. Note that each pico-BS assumes that the transmission power level of the other pico-BSs in the sector are not changing during this process.

MBS Power Control Problem

In the first part, MBSs determine the optimum power control parameters in each sector. Due to the fact that each MBS tries to satisfy the rate requirement of its users, the transmission power of the MBSs may increase imprudently. This not only reduces the energy efficiency of the network, but also augments the intercell interference and elevates the outage probabilities of the users in the other sectors. Therefore, we study the pricing mechanism to account for the interference caused to the users associated with other base stations. The pricing mechanism reduces the intercell interference by giving incentives to MBSs for decreasing their transmit powers.

The pricing function penalizes the utility of an MBS based on the interference it creates. If the interference leads to outage of the users in other sector, the penalty factor increases. Let $\theta_s(\mathbf{x}_s)$ denote the pricing function of sector s. The energy efficiency maximization problem with the pricing function per sector can be formulated as

$$\begin{aligned} \max_{\mathbf{x}_s} \quad & \eta_s(\mathbf{x}_s, \boldsymbol{\beta}_{P,s}) - \theta_s(\mathbf{x}_s) \\ \text{s.t.} \quad & \boldsymbol{C}^k_{M,s}\boldsymbol{F}^{(k,:)}_{M,s}\boldsymbol{R}^{(:,k)}_1 + (1-\boldsymbol{C}^k_{M,s})\boldsymbol{F}^{(k,:)}_{M,s}\boldsymbol{R}^{(:,k)}_2 \geq R_{\min,k}, \text{for all } k \in \mathcal{K}_{M,s} \\ & \boldsymbol{C}^k_{P,s}\boldsymbol{F}^{(k,:)}_{P,s}\boldsymbol{R}^{(:,k)}_3 + (1-\boldsymbol{C}^k_{P,s})\boldsymbol{F}^{(k,:)}_{P,s}\boldsymbol{R}^{(:,k)}_4 \geq R_{\min,k}, \text{for all } k \in \mathcal{K}_{P,s} \\ & \varepsilon_s \geq 0 \text{ and } 0 \leq \beta_s \leq 1 \end{aligned} \tag{3.11}$$

Several pricing functions have been proposed in the literature. For example, in [38] and [39], the authors propose to use $\theta_s(\mathbf{x}_s) = c_s\beta_s P_M^{\max}$, where c_s is a constant. The cost function proposed in [38] and [39] penalizes the utility of an MBS with the total amount of power it transmits. In this chapter, we pursue an alternative approach and penalize the interference that an MBS creates. This type of pricing function was first proposed in [35–37]. In this

approach, the pricing function is defined as

$$\theta_s(\mathbf{x}) = \sum_{n \in \mathcal{N}_M} p_M^{(n)} \sum_{l \neq k, l \in \mathcal{K}^{(n)}} \frac{\partial \eta_{s'}}{\partial p_M^{(n)}}, \tag{3.12}$$

where the transmit power of MBS M on subcarrier n is denoted by $p_M^{(n)}$. The set of subcarriers that MBS M allocates for the cell-center and cell-edge regions is denoted by $\mathcal{N}_M$. Let $\mathcal{K}^{(n)}$ denote the set of users that are assigned to subcarrier n. Then, the set of users that MBS m interferes on subcarrier n are represented by $l \in \mathcal{K}^{(n)}$. Let a user l be in sector s', then the energy efficiency of the sector s' is denoted by $\eta_{s'}$. The term $\partial \eta_{s'} / \partial p_M^{(n)}$ denotes the derivative of energy efficiency of sector s' with respect to the transmit power of MBS M of sector s. Thus, the penalty function (3.12) characterizes the marginal change in the utility of a neighboring sector s' per unit power change in MBS M of sector s. In addition, this approach prevents the base stations from increasing their transmission power to very high levels when the minimum rate requirement of one or more of their users cannot be satisfied without causing outage of the other users. In LTE standards, the X2 interface provides a fast and reliable backhaul link between base stations [59]. In this chapter, we use this interface for three reasons: First, pico-BSs send the CSI for their users to MBS where these are processed. Second, the CSI of users is distributed among MBSs. Third, for the pricing method, the same interface distributes the interference prices between MBSs. The Lagrangian of the problem in (3.11) can be written as

$$\begin{aligned}
\mathcal{L}(\mathbf{x}_s, \boldsymbol{\beta}_{P,s}, \boldsymbol{\lambda}, \nu_s, \tau_s, \rho_s) =& \eta_s(\mathbf{x}_s, \boldsymbol{\beta}_{P,s}) - \theta_s(\mathbf{x}_s) - \sum_{k \in \mathcal{K}_{M,s}} \lambda_{k,s} \big(R_{\min,k} - (\boldsymbol{C}_{M,s}^k \boldsymbol{F}_{M,s}^{(k,:)} \boldsymbol{R}_1^{(:,k)} \\
&+ (1 - \boldsymbol{C}_{M,s}^k) \boldsymbol{F}_{M,s}^{(k,:)} \boldsymbol{R}_2^{(:,k)}) \big) - \sum_{k \in \mathcal{K}_{P,s}} \lambda_{k,s} \big(R_{\min,k} \\
&- (\boldsymbol{C}_{P,s}^k \boldsymbol{F}_{P,s}^{(k,:)} \boldsymbol{R}_3^{(:,k)} + (1 - \boldsymbol{C}_{P,s}^k) \boldsymbol{F}_{P,s}^{(k,:)} \boldsymbol{R}_4^{(:,k)}) \big) \\
&+ \nu_s \beta_s + \tau_s (1 - \beta_s) + \rho_s \varepsilon_s.
\end{aligned} \tag{3.13}$$

For simplicity, we will use $\mathcal{L}_s$ for $\mathcal{L}(\mathbf{x}_s, \boldsymbol{\beta}_{P,s}, \boldsymbol{\lambda}, \nu_s, \tau_s, \rho_s)$ throughout the rest of the chapter.

Since the downlink transmissions of an MBS M in sector s, $p_M^{(n)}$, are characterized by ε_s and β_s, we need to adopt (3.12). In addition, we need to include the effect of interference to the rate constraints of users in other sectors. Therefore, the pricing function can be written as

$$\begin{aligned}\theta_s(\mathbf{x}_s) =& \mathbf{x}_s^T \sum_{\substack{s' \in \mathcal{S} \\ s' \neq s}} \Bigg(\nabla_{\mathbf{x}_s} \eta_{s'}(\mathbf{x}_{s'}, \boldsymbol{\beta}_{P,s'}) + \sum_{k \in \mathcal{K}_{M,s'}} \lambda_{k,s'} \Big(\boldsymbol{C}_{M,s'}^k \boldsymbol{F}_{M,s'}^{(k,:)} \boldsymbol{R}_1^{(:,k)} \\ & + (1 - \boldsymbol{C}_{M,s'}^k) \boldsymbol{F}_{M,s'}^{(k,:)} \boldsymbol{R}_2^{(:,k)} \Big) + \sum_{k \in \mathcal{K}_{P,s'}} \lambda_{k,s'} \Big(\boldsymbol{C}_{P,s'}^k \boldsymbol{F}_{P,s'}^{(k,:)} \boldsymbol{R}_3^{(:,k)} \\ & + (1 - \boldsymbol{C}_{P,s'}^k) \boldsymbol{F}_{P,s'}^{(k,:)} \boldsymbol{R}_4^{(:,k)} \Big) \Bigg). \end{aligned} \tag{3.14}$$

Hence, the pricing function in (3.14) reflects the marginal costs of the variables ε and β. The detailed expressions of the terms in (3.14) are given in the Appendix A.

For the solution, we will employ the Levenberg-Marquardt method. The Levenberg-Marquardt method is a modification to the Newton method. The Newton method premultiplies the gradient ascent direction by the inverse of the Hessian matrix. The motivation of the Newton method is to find a suitable direction based on the quadratic approximation of a function, whereas the gradient ascent method seeks to find a linear approximation of a function. Consider the Lagrangian function in (3.13). Its quadratic approximation evaluated at $\mathbf{y}_s^{(l)} = (\varepsilon_s^{(l)} \;\; \beta_s^{(l)})^T$ can be expressed as

$$g(\mathbf{y}) = \mathcal{L}_s + \nabla \mathcal{L}_s^T (\mathbf{y} - \mathbf{y}_s^{(l)}) + \frac{1}{2} (\mathbf{y} - \mathbf{y}_s^{(l)})^T \nabla^2 \mathcal{L}_s (\mathbf{y} - \mathbf{x}_s^{(l)}), \tag{3.15}$$

where $\nabla^2 \mathcal{L}_s$ is the Hessian matrix of $\mathcal{L}$ evaluated at $\mathbf{y}_s^{(l)}$. Note that we are going to use $\mathbf{y}_s^{(l)}$ for $(\varepsilon_s^{(l)} \;\; \beta_s^{(l)})$ pair for the Newton iteration l and the parameter $\mathbf{x}_s^{(t)}$ will be used for the same pair at time instant t. The parameter updates that maximize $g(\mathbf{y})$ are given by

$$\mathbf{y}_s^{(l+1)} = \mathbf{y}_s^{(l)} - \mu_l (\nabla^2 \mathcal{L}_s^{(l)})^{-1} \nabla \mathcal{L}_s^{(l)}, \tag{3.16}$$

where the Newton search direction is $\mathbf{d}_l^N = -(\nabla^2 \mathcal{L}_s^{(l)})^{-1} \nabla \mathcal{L}_s^{(l)}$. In general, convergence of the Newton method is not guaranteed [71]. This is due to the fact that the Hessian can be singular or the search direction, $\mathbf{d}_l^N$, may not even give an ascent direction. Therefore, even when the inverse of the Hessian matrix exists, it does not necessarily imply that $\mathcal{L}_s^{(l+1)}$ is greater than $\mathcal{L}_s^{(l)}$. However, when the starting point $\mathbf{y}_s^{(0)}$ is close enough to the optimal $\mathbf{y}^*$ such that $\nabla \mathcal{L}_s^{(l)*} = 0$ and $\nabla^2 \mathcal{L}_s^{(l)*}$ is full rank, then the Newton method converges to the optimal $\mathbf{y}^*$ [71, 72]. In order to address the convergence problem of the Newton method, several methods have been proposed in the literature, see Chapter 8 of [71] and Chapter 5.2.4 of [72]. In this chapter, we employ the Levenberg-Marquardt method due to its guarantee of convergence. With the Levenberg-Marquardt method, the parameter updates are given by

$$\mathbf{y}_s^{(l+1)} = \mathbf{y}_s^{(l)} - \mu_l (\nabla^2 \mathcal{L}_s^{(l)} - \xi \mathbf{I})^{-1} \nabla \mathcal{L}_s^{(l)}, \tag{3.17}$$

where $\mathbf{d}_l^{LM} = -(\nabla^2 \mathcal{L}_s^{(l)} - \xi \mathbf{I})^{-1} \nabla \mathcal{L}_s^{(l)}$ is the search direction evaluated at $\mathbf{y}_s^{(l)}$ and $\mathbf{I}$ is the identity matrix. The constant ξ ensures all the eigenvalues of $\mathbf{D} = (\nabla^2 \mathcal{L}_s^{(l)} - \xi \mathbf{I})$ are negative such that $\mathbf{D}$ is negative definite. It is called as the damping or the Levenberg-Marquardt parameter [71]. If the largest eigenvalue of $\nabla^2 \mathcal{L}_s^{(l)}$ is negative, then ξ will be equal to zero and the Levenberg-Marquardt method reduces to the Newton method, that is $\mathbf{d}_{(l)}^{LM} = \mathbf{d}_{(l)}^N$. Under this condition, quadratic convergence is achieved. If the largest eigenvalue of the Hessian is non-negative, then we take $\xi = \omega_{\max} + \sigma$, where $\omega_{\max}$ is the largest eigenvalue of $\nabla^2 \mathcal{L}_s^{(l)}$ and $\sigma > 0$ is a sufficiently large number. This operation forces the Hessian to be negative definite. In our simulations, this offset is taken as $\sigma = 1$. The proposed approach using the interference pricing method is depicted under the heading Algorithm 3, where $l_{\max}$ is the maximum number of iterations and ϵ is a sufficiently small positive number to determine when to exit the algorithm. The parameter $\alpha_{k,s}$ in Step 10 is the positive scalar step size. In addition, the controlled increase mechanism in Step 15 is used to update the power levels. When the power level of the MBSs changes largely between two consecutive time instants,

Algorithm 3 Proposed Power Control Algorithm with Pricing

1: % Each sector solves (3.11) by using the Levenberg-Marquardt Method
2: **for** $l := 1$ to $l_{\max}$ **do**
3: **if** $\omega_{\max} = \max(\text{eig}(\nabla^2_{\mathbf{y}} \mathcal{L}_s^{(l)})) < 0$ **then**
4: $\xi = 0$.
5: **else**
6: $\xi = \omega_{\max} + \sigma$.
7: **end if**
8: $\mathbf{d}_l^{LM} = -(\nabla^2 \mathcal{L}_s^{(l)} - \xi \mathbf{I})^{-1} \nabla \mathcal{L}_s^{(l)}$.
9: Update the power control parameters, $\mathbf{y}_s^{(l+1)}$, using

$$\mathbf{y}_s^{(l+1)} = \mathbf{y}_s^{(l)} + \mu_l \mathbf{d}_l^{LM},$$

10: Update the Lagrange multiplier, $\lambda_{k,s}^{(l+1)}$ for all $k \in \mathcal{K}_{M,s}^C$ and $\mathcal{K}_{M,s}^E$, using

$$\lambda_{k,s}^{(l+1)} = \left[\lambda_{k,s}^{(l)} + \alpha_{k,s} \big(R_{\min,k} - (\boldsymbol{C}_{M,s}^k \boldsymbol{F}_{M,s}^{(k,:)} \boldsymbol{R}_1^{(:,k)} + (1 - \boldsymbol{C}_{M,s}^k) \boldsymbol{F}_{M,s}^{(k,:)} \boldsymbol{R}_2^{(:,k)}) \big) \right]^+.$$

11: **if** $\left| \nabla \mathcal{L}_s^T \mathbf{d}_l^{LM} \right| \leq \epsilon$ **then**
12: **Break**
13: **end if**
14: **end for**
15: $\mathbf{x}_s^{(t+1)} = (1 - \zeta) \mathbf{x}_s^{(t)} + \zeta \mathbf{y}_s^{(l)}$
16: *Price Update:* Each user calculates interference prices and feeds these values back to its base station.
17: Interference prices are distributed among base stations.

the interference pricing mechanism does not accurately model the effect of the interference over the utilities of the other sectors [36]. The controlled increase mechanism in Step 15 prevents large changes of the power levels. In this step, the selection of small ζ slows down the convergence of the algorithm. On the other hand, large ζ may cause large changes in the power levels. Therefore, an adaptive algorithm is used to select ζ in this chapter. The parameter ζ is equal to $t/(2t+1)$ where t is the time instant [34]. When t goes to infinity ζ will converge to $1/2$.

Note that the Levenberg-Marquardt method guarantees convergence regardless of the starting point [71, p. 312]. Using the Levenberg-Marquardt method, the parameters are updated in Step 9 of Algorithm 3. The expression $\sqrt{(\nabla \mathcal{L}_s^{(l)})^T \mathbf{d}_l^{LM}}$ is called as the Newton incre-

ment [73]. It is used as a stopping criterion in iterative line search algorithms [73]. Note that this stopping criterion is also the condition to check whether a search direction $\mathbf{d}_l^{LM}$ is an ascent direction or not, that is, to check if $\nabla \mathcal{L}_s^{(l)T} \mathbf{d}_l^{LM} > 0$ is true. The loop terminates when the convergence condition is satisfied or the maximum number of iterations is reached.

In general, the main computational effort in Algorithm 3 is at Step 3 and Step 8 where the eigenvalues of matrix $\nabla^2 \mathcal{L}_s^{(l)}$ and the inverse of matrix $\nabla^2 \mathcal{L}_s^{(l)} - \xi \mathbf{I}$ are calculated [71]. Using classical approaches such as the Gauss-Jordan elimination method, the computational complexity of calculating eigenvalues and taking the inverse of an $n \times n$ matrix is $\mathcal{O}(n^3)$. For large-scale problems, this operation becomes prohibitively complex. Consider the centralized resource allocation approach where we solve for 57 (ε, β) pairs, one pair for each sector. Taking the inverse of this big matrix would require $\mathcal{O}(114^3)$ floating point operations (flops). Fortunately, with the proposed distributed algorithm, we only need to calculate the eigenvalues of $\nabla^2 \mathcal{L}_s^{(l)}$ and take the inverse of $\nabla^2 \mathcal{L}_s^{(l)} - \xi \mathbf{I}$, which are both 2×2 matrices, and these calculations are straightforward. The computational complexity of finding the maximum eigenvalue and updating power control parameters is $\mathcal{O}(n)$. Those steps require significantly less amount of time. The computational complexity of updating the Lagrange multipliers is independent from the number of power control parameters and it depends on the number of users in the sector. Under these conditions, the computational complexity of both the gradient and Levenberg-Marquardt methods are on the same order per iteration step. In addition, due to the distributed nature of the algorithm, increasing the number of sectors in the simulation area does not change the required time due to parallel processing. However, the total required time increases linearly due to the fact that more sectors run the proposed algorithm. Along with similar computational complexity, the Levenberg-Marquardt based-method has significantly faster convergence rate compared to the gradient-based method. The convergence properties of the algorithm are inherited from the detailed analysis in [57]. Also, note that the expressions of the gradient and Hessian of the energy efficiency function, η_s, are presented in detail in the Appendix of [57].

Picocell Power Control Problem

In the second part of the power problem, each pico-BS determines its own power control parameter separately. When the power control parameters for MBS are selected, the problem will be similar to the MBS power control problem. However, instead of two power control parameters, we only need to determine one power control parameter for each pico-BS. During this process, we assume that all power control parameters of other pico-BSs in sector s are constant. Then, the energy efficiency maximization problem with pricing function for pico-BS P can be formulated as

$$\begin{aligned} \max_{\beta_{P,s}} \quad & \eta_s(\mathbf{x}_s, \boldsymbol{\beta}_{P,s}) - \theta_s(\beta_{P,s}) \\ \text{s.t.} \quad & \boldsymbol{C}^k_{M,s}\boldsymbol{F}^{(k,:)}_{M,s}\boldsymbol{R}^{(:,k)}_1 + (1-\boldsymbol{C}^k_{M,s})\boldsymbol{F}^{(k,:)}_{M,s}\boldsymbol{R}^{(:,k)}_2 \geq R_{\min,k}, \text{for all } k \in \mathcal{K}_{M,s} \\ & \boldsymbol{C}^k_{P,s}\boldsymbol{F}^{(k,:)}_{P,s}\boldsymbol{R}^{(:,k)}_3 + (1-\boldsymbol{C}^k_{P,s})\boldsymbol{F}^{(k,:)}_{P,s}\boldsymbol{R}^{(:,k)}_4 \geq R_{\min,k}, \text{for all } k \in \mathcal{K}_{P,s} \\ & 0 \leq \beta_{P,s} \leq 1. \end{aligned} \tag{3.18}$$

The pricing function, $\theta_s(\beta_{P,s})$, will be similar to the one in (3.14) except the derivatives are calculated with respect to $\beta_{P,s}$. Therefore, we do not repeat it here for simplicity.

The Lagrangian of the problem in (3.18) can be written as

$$\begin{aligned} \mathcal{L}_s =& \eta_s(\mathbf{x}_s, \boldsymbol{\beta}_{P,s}) - \theta_s(\beta_{P,s}) - \sum_{k\in\mathcal{K}_{M,s}} \lambda_{k,s}\big(R_{\min,k} - (\boldsymbol{C}^k_{M,s}\boldsymbol{F}^{(k,:)}_{M,s}\boldsymbol{R}^{(:,k)}_1 \\ & + (1-\boldsymbol{C}^k_{M,s})\boldsymbol{F}^{(k,:)}_{M,s}\boldsymbol{R}^{(:,k)}_2)\big) - \sum_{k\in\mathcal{K}_{P,s}} \lambda_{k,s}\big(R_{\min,k} - (\boldsymbol{C}^k_{P,s}\boldsymbol{F}^{(k,:)}_{P,s}\boldsymbol{R}^{(:,k)}_3 \\ & + (1-\boldsymbol{C}^k_{P,s})\boldsymbol{F}^{(k,:)}_{P,s}\boldsymbol{R}^{(:,k)}_4)\big) + \nu_{P,s}\beta_{P,s} + \tau_s(1-\beta_{P,s}). \end{aligned} \tag{3.19}$$

The optimum $\beta_{P,s}$ can be calculated by using the Levenberg-Marquardt method-based algorithm similar to the algorithm that is described in Section 3.4.3. In Section 3.4.3, the algorithm determines two power control parameters concurrently. However, we only de-

termine one power control parameter in each pico-BS. Therefore, the complexity of this algorithm is lower than the one in Section 3.4.3. In addition, this process is done concurrently at all pico-BSs in sector s and increasing the number of pico-BSs in sector does not affect the required time for this calculation.

In this chapter, we are maximizing the energy efficiency of the network while satisfying the rate constraints of users. This particular approach is beneficial for applications such as Voice-over-IP, video call, streaming, and real-time gaming applications that require minimum rate to perform properly. As we will show next in Section 3.5, when we enforce higher rates, the energy efficiency of the network may decrease.

3.5 Simulation Results

In this section, first, we show the convergence behavior of the Levenberg-Marquardt method at the first time instant. Second, we evaluate the performance of the proposed algorithm in terms of energy efficiency, outage probability, and power consumption for different rate constraints. Third, we compare the performance of the dynamic cell-center radius with constant cell-center region boundary selection algorithms. Fourth, we assess the effect of the scheduler on the energy efficiency and the outage probabilities. Fifth, we compare the performance of the proposed algorithm with no power control and non-cooperative power control algorithms in terms of energy efficiency and outage probabilities. Sixth, we study the efficiency of the proposed algorithm by comparing it with an exhaustive search algorithm over all possible cell-center radii and power levels.

For the FFR method, the spectrum allocation scheme is such that 14 RBs are assigned to subband A. The remaining 36 RBs are divided into three equal segments and assigned to subbands B, C, and D. The simulation layout is illustrated in Fig. 3.1. The simulation

area consists of 19 hexagonal cells with wrap-around edges. Single antenna transmission is considered, i.e., $N_{TRX,M} = 1$ and $N_{TRX,P} = 1$ for all sectors. Two pico-BSs are randomly generated in each sector. Although we present the results for the two pico-BS case, the proposed algorithm can easily be implemented for a network that has more pico-BSs per sector. Twenty users are generated in each sector. First, two users are generated within the radius of 40 meters for each pico-BS. Then, the rest of the users are uniformly distributed in the sector area. The highest RSRP method is used for the cell-association [68]. The simulation parameters, distance constraints in generating new nodes, and the base station power consumption values are given in Table 3.1 [24]. Furthermore, the initial values are chosen as $(\boldsymbol{\varepsilon}^{(0)}, \boldsymbol{\beta}^{(0)}, \boldsymbol{\beta}_P^{(0)}) = (\mathbf{1}, \mathbf{1}, \mathbf{1})$ where $\mathbf{1}$ is defined as a vector all of whose members are equal to 1.

In the first part of the simulations, we assume that all MUEs in the network have the same guaranteed-bit-rate (GBR) requirements, i.e., $R_{min,k} = R_{min}$, for all $k \in \mathcal{K}_{M,s} \cup \mathcal{K}_{P,s}$ and $s \in \mathcal{S}$. Six different rate constraints are considered, R_{min} is equal to 16, 32, 64, 128, 256, and 512 kbits/sec (kbps). In the second part of the simulations, we compare the performance of the proposed dynamic cell-center radius selection algorithm with the ones that are described in [57]. In the third part of the simulations, we study the importance of the scheduler. The LDS, the EBW scheduler, and the MMF scheduler described in Section 3.4.2 are considered for no rate constraint and various rate constraint cases.

Fig. 3.3 depicts the average energy efficiency function of the network for each iteration at first time instant when R_{min} is equal to 0, 16, 32, 64, and 128 kbps. The average energy efficiency of the sector increases significantly at the first iteration, then Levenberg-Marquardt based-method updates the power control parameters every iteration until the convergence. Convergence behavior is independent from the rate requirements of users and in our simulations, it took around 20 to 25 iterations for convergence to be achieved.

Fig. 3.4(a) shows the energy efficiency of the network for the proposed algorithm when R_{min}

Table 3.1: Simulation Parameters

Parameter	**Setting**
Channel bandwidth	10 MHz
Total number of RBs	50 RBs
Freq. selective channel model (CM)	Extended Typical Urban CM
UE to MBS PL model	$128.1 + 37.6 \log_{10}(d)$
UE to pico-BS PL model	$140.7 + 36.7 \log_{10}(d)$
Effective thermal noise power, N_0	-174 dBm/Hz
UE noise figures	9 dB
MBS and pico-BS antenna gain	14 dBi and 5 dBi
UE antenna gain	0 dBi
Antenna horizontal pattern, $A(\theta)$	$-\min(12(\theta/\theta_{3\text{dB}})^2, A_m)$
A_m and $\theta_{3\text{dB}}$	20 dB and 70°
Penetration loss	20 dB
Macrocell and picocell shadowing	8 dB and 10 dB
Inter-site distance	500 m
Minimum MBS to user distance	50 m
Minimum pico-BS to user distance	10 m
Minimum pico-BS to MBS distance	75 m
Minimum pico-BS to pico-BS distance	40 m
Traffic model	Full buffer
Power Consumption Parameters	MBS: (130W, 75W, 46dBm, 4.7)
(P_0, P_{sleep}, $P_{\max}$, Δ)	Pico-BS: (56W, 39W, 30dBm, 2.6)

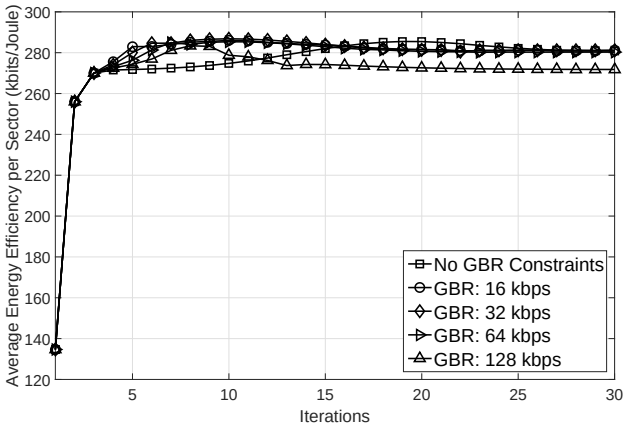

Figure 3.3: The average energy efficiency of the network at the first time instant for lower GBR requirements of users.

is equal to 0, 16, 32, 64, and 128 kbps. Note that in this range of R_{min} values, the algorithm uniformly improves the energy efficiency of the system. Not surprisingly, the improvement decreases as R_{min} increases. For the case without rate constraints, the energy efficiency of the network is 2.2%, 6.9%, 12.6%, and 20.2% higher than the cases with R_{min} is equal to 16, 32, 64, and 128 kbps, respectively. For the lower rate constraints, the reduction in energy efficiency is marginal due to the fact that the rate constraints of most of the users are

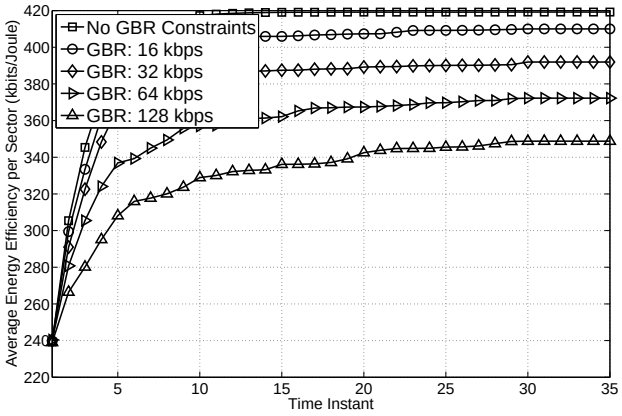

(a)

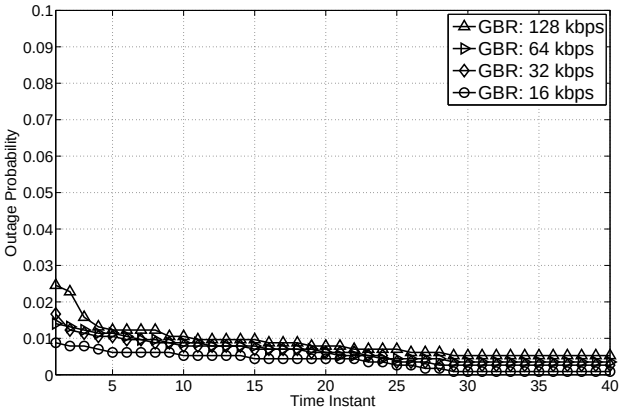

(b)

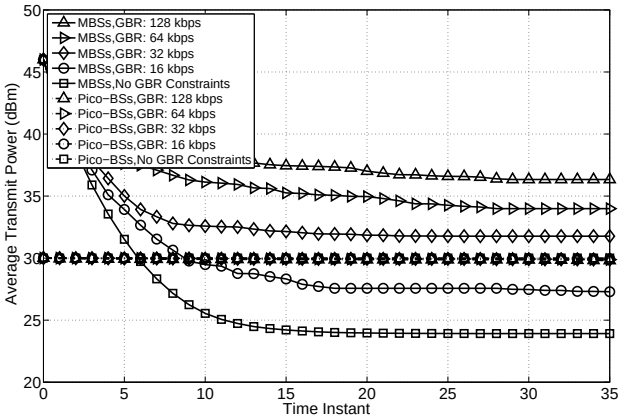

(c)

Figure 3.4: The average energy efficiency per sector (a), the outage probabilities (b), and average transmission power (c) for lower GBR requirements of users.

already satisfied at the energy-efficient optimum power level. Therefore, only small changes are required to satisfy the rate constraints of the rest of the users. In Fig. 3.4(b), the

outage probabilities of the network using the proposed algorithm are shown for the same rate constraints. A user is assumed to be in outage if the actual rate of the user is less than its rate requirement. The outage probabilities are very low for these rate constraints, even for the early time instances that the transmission power levels of the base stations have not converged. The highest outage probability is 0.5% when the rate requirement is 128 kbps. The efficiency of the proposed algorithm in terms of outage will become clear in the sequel when higher rate constraints are forced. Fig. 3.4(c) illustrates the power savings of the proposed algorithm. The average transmission power of the MBSs decreases every time instant until the convergence. Due to the fact that the rate constraints of the users are low, the proposed algorithm provides significant power savings. The average transmission power decreases more than 20 dB when users do not have any rate requirements. When the rate constraints are enforced, it leads to higher average transmission power and that is the main reason of the smaller gain in energy efficiency by using the algorithm. On the other hand, pico-BSs always transmit at the full power for the given rate constraints. Due to the fact that the interference from the pico-BSs to MBS does not cause outages of the users and pico-BSs reach their most energy-efficient case when they are transmitting at the full power, the pico-BSs transmit at the full power.

In Fig. 3.5(a), the energy efficiency of the network is illustrated for higher rate constraints, 256 and 512 kbps. Different from the previous cases, the average energy efficiency of the network now decreases in each time instant. The energy efficiency of the network drops 4.9% and 27.3% from the first time instant to the last time instant when R_{min} is equal to 256 and 512 kbps, respectively. The reason behind that is threefold. First, MBSs increase their transmission power to energy-inefficient levels in order to satisfy the higher minimum rate requirements of users. Second, the increased transmission power elevates the interference to the users that are in other sectors and using the same subchannels. Due to the elevated interference, base stations increase power levels to be able to support the minimum rate requirements which gives rise to more interference and a chain reaction starts. Third, pico-

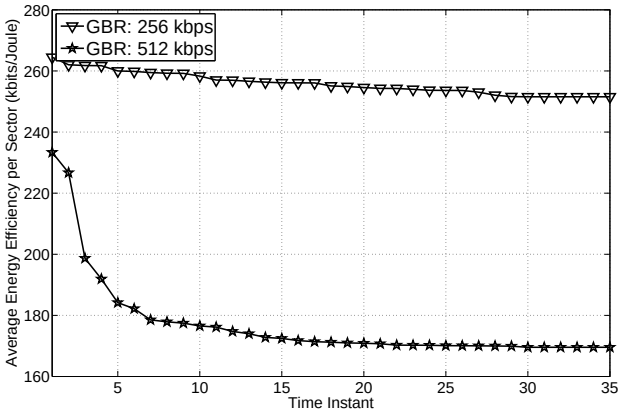

(a)

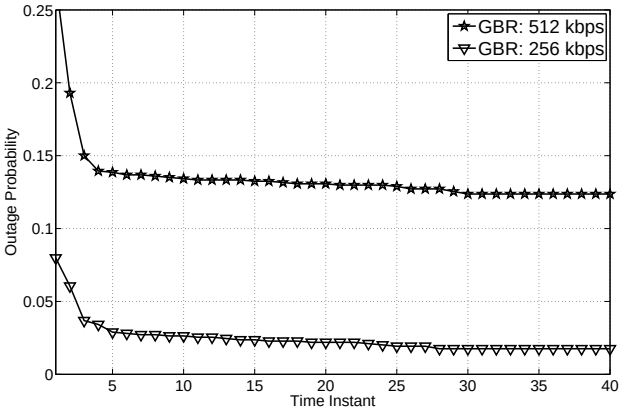

(b)

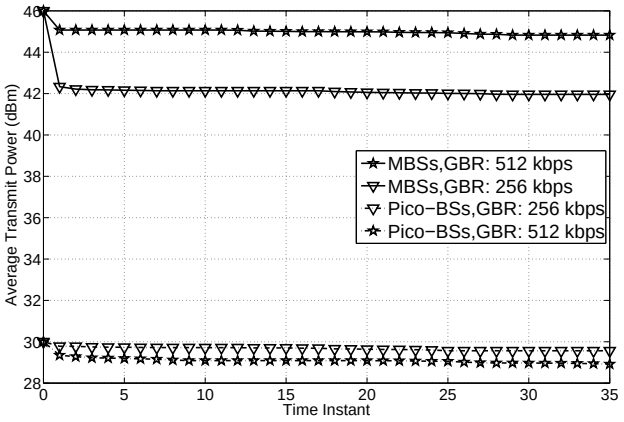

(c)

Figure 3.5: The average energy efficiency per sector (a), the outage probabilities (b), and average transmission power (c) for higher GBR requirements of users.

BSs decrease their transmission power in order to decrease the interference to MBSs. The result is the reduction in energy efficiency manifested in Fig. 3.5(a). In Fig. 3.5(b), the

outage probabilities of MUEs are shown for the higher rate constraints. As expected, the outage probability of users increases for the higher rate requirements as compared to lower rates shown in Fig. 3.4(b). At the first iteration, the outage probabilities are 7.9% and 27.0% for GBR requirements 256 and 512 kbps, respectively. After 40 time instants, the outage probabilities become 1.8% and 12.4% for the GBR requirements in the same order as before. When the rate requirement of users increases, energy-efficient power levels cause significant outages and that needs to be adjusted to decrease outage probabilities to tolerable levels. If we continue to increase the rate requirements of users, that requires further sacrifice from the energy efficiency of the network. This points out to the tradeoff between the network energy efficiency and outage probability, which becomes more severe at higher GBR requirements. Nevertheless, it is worthwhile to state that while an outage probability of 27.0% is unacceptable, 12.4% can be acceptable, pointing out to the fact that although the algorithm does not improve energy efficiency for these high rates, it is useful for a substantial reduction in outage probability. In Fig. 3.5(c), the average transmission power of base stations is shown. When higher rate constraints are enforced; the average transmission power of MBSs reaches the lowest level at the first time instant, and then it increases each time instant until the convergence. In order to satisfy the rate requirements of the users, MBSs need to transmit at higher levels compared to lower rate cases. Therefore, compared to Fig. 3.4(c), the power savings of the network is significantly lower. For example, when the GBR requirement is equal to 256 kbps, the power saving of the MBSs is less than 5 dB. The power savings are even lower when the rate constraints are 512 kbps. The decline in the power savings is the main cause of the decrease in energy efficiency. Yet, it is worthwhile to note that there is a gain in transmitted power, although it does not translate into improved energy efficiency. The transmission power of the pico-BSs decreases when the higher rate requirement constraints are enforced. When the rate requirements of the users increase, some of the MUEs will be in outage. In order to satisfy the rate requirement of these MUEs, pico-BSs decrease their transmission powers and consequently the interference they create

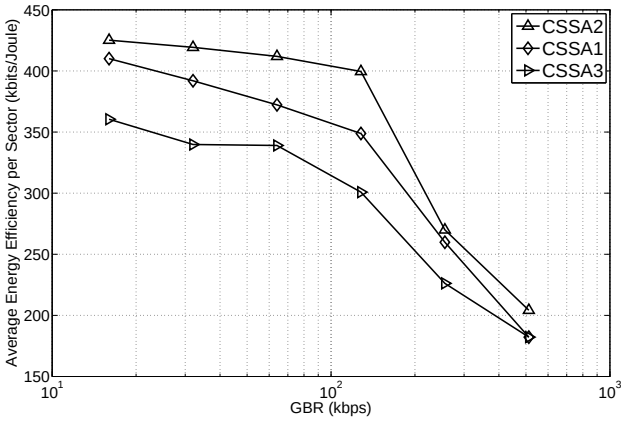

(a)

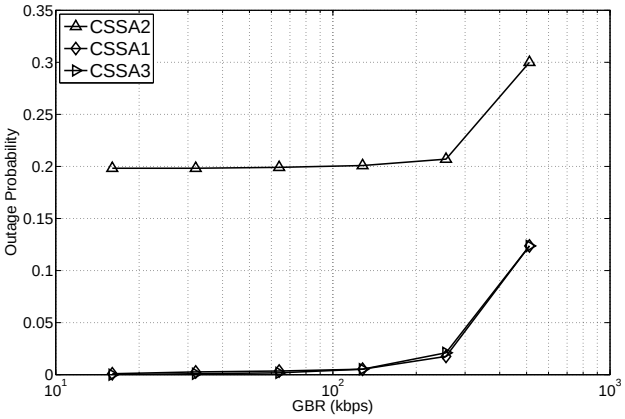

(b)

Figure 3.6: The average energy efficiency per sector (a) and the outage probabilities (b) for different cell-center radius selection algorithms.

Table 3.2: The Outage Profile of the Different User Types

	Nr. of users (Outage probability)		
Minimum GBR (kbps)	Cell-center MUE	Cell-edge MUE	PUE
-	348 (0%)	616 (0%)	176 (0%)
16	358 (0%)	606 (0.2%)	176 (0%)
32	366 (0%)	598 (0.5%)	176 (0%)
64	396 (0.2%)	568 (0.5%)	176 (0%)
128	447 (0.4%)	517 (0.8%)	176 (0%)
256	482 (1.7%)	482 (2.5%)	176 (0.5%)
512	517 (10%)	447 (15.2%)	176 (12%)

to these users. For example, when the GBR requirement is equal to 512 kbps, the pico-BSs decrease their transmission power more than 1 dB.

In Table 4.3, we further investigate the relationship between the outage probability and cell-center region boundaries. The users in the network are divided into three categories, cell-center MUEs, cell-edge MUEs, and PUEs. Based on the minimum rate requirements, the cell-center regions are dynamically adjusted. As we increase the GBR requirements, we observe that the number of cell-center MUEs increases. As discussed in Section 3.4.1, the proposed cell-center radius selection algorithm behaves similar to CSSA3 to share resources more fairly among users. Although the FFR scheme decreases the interference that cell-edge MUEs suffer from, due to the fact that they are located away from the MBS, they encounter higher outage probabilities. When the minimum rate requirement of users is less than 256 kbps, all PUEs in the network satisfy their rate requirement. However, when the rate requirement is 512 kbps, 12% of PUEs cannot satisfy their rate requirement. As shown in Fig. 3.5(c), the transmission power of the pico-BSs decreases when the rate requirement is 512 kbps in order to decrease the interference on cell-center MUEs. Therefore, 12% of the PUEs is in outage when GBR is 512 kbps.

In Fig. 3.6(a-b), we investigate the effect of the cell-center radius selection algorithms in terms of energy efficiency and outage probabilities. The proposed cell-center radius selection algorithm (CSSA1) is compared with the ones that are proposed in [57]. Our simulation results show that CSSA1 performs significantly better than CSSA3 in terms of energy efficiency when the rate constraints are below 128 kbps. For example, when the GBR requirement is equal to 16 kbps, CSSA1 performs 16% better than CSSA3 in terms of energy efficiency. CSSA1 converges to CSSA3 to meet the rate constraints of more users when the rate constraints become aggressive. For example, when the rate constraints are 512 kbps, the selected cell-center radii are the same for these two algorithms for most of the sectors in the network. On the other hand, CSSA1 performs worse than CSSA2 in terms of energy efficiency when users have nonzero rate requirements. CSSA1 selects a cell-center radius such that each user is assigned at least one RB when users have nonzero rate requirements. However, CSSA2 does not consider the rate requirements of the users and for example 19.8% of the users are

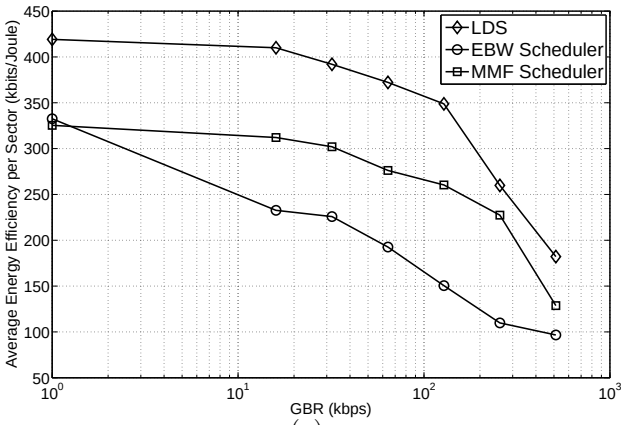

(a)

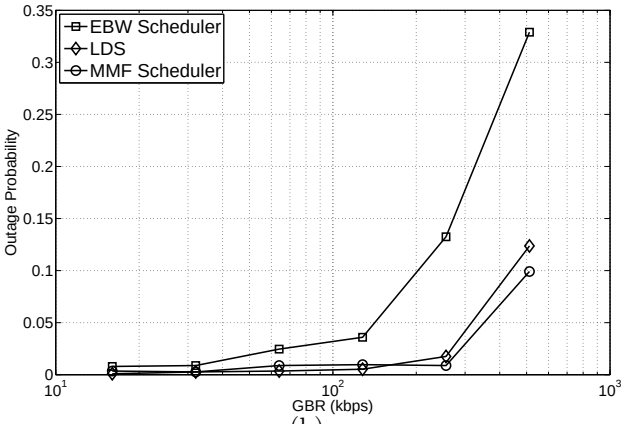

(b)

Figure 3.7: The average energy efficiency per sector (a) and outage probability of the network (b) for the LDS, EBW, and MMF schedulers.

not assigned any resources for the given network. While this approach increases the energy efficiency of the network, it causes unacceptable outage probabilities. For example, the energy efficiency of CSSA1 is 3.7% less than CSSA2 when the GBR requirement is 256 kbps. However, the outage probability of CSSA1 is 1.8%, while CSSA2 is 21%. Thus, the outage probability of CSSA2 is not acceptable. The proposed cell-center region selection algorithm benefits from the advantages of both algorithms. It selects more aggressive cell-center radii when the rate constraints are small. On the other hand, it selects more fair cell-center radii when the rate constraints are higher.

Fig. 3.7(a) shows the average energy efficiency per sector for the LDS, the EBW, and the

MMF schedulers. The LDS performs significantly better than the other two schedulers for all GBR requirements. For example, when no GBR requirement is enforced, LDS performs 26% and 28.8% better than the EBW and MMF scheduler, respectively. When no GBR requirement is enforced, the dual prices will always be zero. Therefore, after assigning one RB to each user, the LDS will assign the rest of the RBs to the user that has the best channel. This approach significantly increases the energy efficiency of the network. On the other hand, the EBW scheduler performs better than the MMF scheduler when no GBR requirement is enforced. The EBW scheduler disregards the rate requirement of users and the channel quality between the user and the base station during the resource allocation process. Each user obtains equal amount of RBs. Therefore, users with better channel qualities get significantly better rates than the other users. On the other hand, the MMF scheduler assigns most of the resources to the users with worse channel conditions to maximize the minimum throughput. Therefore, when there are no GBR requirements, the throughput and corresponding energy efficiency of the EBW scheduler are better than the ones for the MMF scheduler. When we enforce rate requirements, LDS still performs significantly better than the EBW and MMF scheduler. For example when the GBR requirement is 128 kbps, LDS performs 34% and 132% better than the MMF and the EBW schedulers, respectively. When the minimum rate requirements of users increase, LDS starts to assign resources to users with worse channels in MBSs due to the dual prices. On the other hand, the minimum rate requirement of the PUEs can be easily satisfied with fewer RBs. Therefore, the dual prices will still be zero and most of the RBs are going to be assigned to the user with the best channel. This approach increases the overall energy efficiency of the network. In addition, when users have minimum rate requirements, higher power transmission levels are necessary for the EBW scheduler to satisfy the rate requirements of users that are in outage. Therefore, the energy efficiency of the sector decreases. In addition, the intercell interference becomes the more significant problem because of these high transmission levels. Due to the fact that the MMF scheduler assigns more resources to the user with worse channel

conditions, less power might suffice to satisfy the rate requirement of these users. Therefore, when users have nonzero minimum rate requirements, the MMF scheduler performs better than the EBW scheduler in terms of energy efficiency. In Fig. 3.7(b), we compare the outage probabilities of the network. Due to the fact that MBSs need to transmit in higher transmission power levels to satisfy the rate requirements, the intercell interference becomes a significant problem for the EBW scheduler. Due to the higher intercell interference and fewer resource block allocation to users with worse channel conditions, the outage probability of the EBW scheduler becomes significantly higher than the one for the LDS and MMF scheduler. For example, the outage probability of the EBW scheduler is 13.2%, whereas the one for the LDS is 1.7% and the MMF scheduler is 0.9% when the GBR requirement is 256 kbps. When the rate requirement of the user increases the outages of the LDS becomes higher than the MMF scheduler. The LDS assigns the RB to the user that provides highest increment to the Lagrangian function. Therefore, more users will be in outage than the MMF scheduler to have higher energy efficiency. These results indicate the significance of the scheduler selection.

Fig. 3.8(a-b) illustrates the average energy efficiency per sector and outage probabilities of the network for no power control, non-cooperative power control, and the proposed algorithm with LDS. When the rate constraints are below 128 kbps, the proposed algorithm provides gain over the non-cooperative power control algorithm in terms of energy efficiency. In addition, both of them perform significantly better than the no-power control algorithm, as expected. The outage probabilities of all three algorithms are at acceptable levels. It is less than 10% when the GBR requirement is equal to 128 kbps. When the rate constraints are low, the transmission power of the MBSs is relatively low and MBSs can satisfy the rate requirements of almost all of their users without cooperation. The cooperation only helps to improve the average energy efficiency of the network. However, when we have more strict rate requirements, cooperation is required to satisfy rate requirements of the users. For example, when the GBR requirement is equal to 256 kbps, the outage probability of the

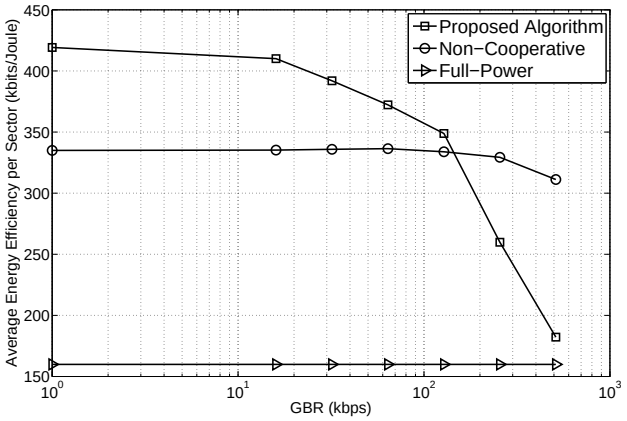

(a)

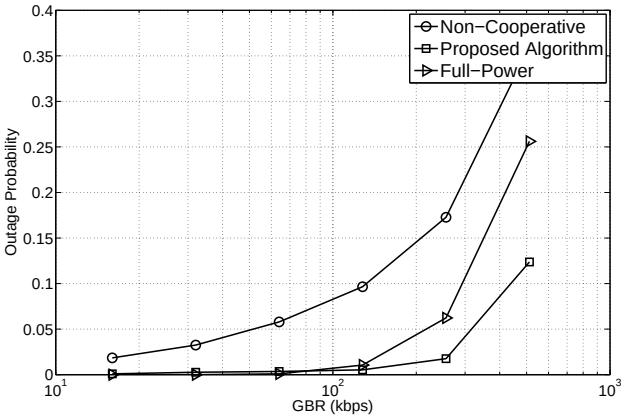

(b)

Figure 3.8: The average energy efficiency per sector (a) and outage probability of the network (b) for no power control, non-cooperative power control, and the proposed algorithm with the LDS scheduler.

non-cooperative algorithm is 17.3% and it is beyond the tolerable levels. On the other hand, outage probabilities of the network are 6.2% for the full power transmission for the same case. Due to the fact that the non-cooperative power control algorithm does not consider intercell interference conditions during the resource allocation process, it leads to a large number of users being at outage. The proposed power control algorithm decreases the network outage probability to 1.7% when the GBR requirement is equal to 256 kbps. Although the outage probabilities of the full-power case and the proposed algorithm are close, the energy efficiency of the proposed algorithm is 62.5% better than the full power transmission when the GBR requirements are equal to 256 kbps.

Table 3.3: Simulation Results

Methods	Average Sector Energy Efficiency (kbits/Joule) (Outage Probabilities)			Required Time (minutes)
	0 kbps	128kbps	512kbps	
The Proposed Algorithm	130.81(0%)	128.48(0%)	121.16(14%)	1.45
The Exhaustive Search Algorithm	131.11(0%)	128.71(0%)	121.19(14%)	9855

Table 3.3 shows the average energy efficiency per sector for the proposed algorithm and the exhaustive search algorithm. For the purposes of this table, the proposed algorithm and the exhaustive search algorithm are implemented over three sectors that are using the same frequency bands (i.e., shown with the same color in Fig. 3.1) while the rest of the sectors transmit in full power. The exhaustive search algorithm searches over all possible β and ε pairs and cell-center radii over these three sectors. Due to the fact that searching over the frequency domain increases exponentially with the number of RBs, we use the EBW scheduler for both the proposed algorithm and the exhaustive search algorithm and use the same frequency allocation over all searches. Table 3.3 shows that the performance of the proposed algorithm and the exhaustive search algorithm are very similar to each other. In addition, when we increase the minimum rate requirements, the difference between the proposed algorithm and the exhaustive search algorithm decreases. The difference between the proposed algorithm and the exhaustive search algorithm is approximately 0.23% in terms of energy efficiency when there are no minimum rate constraints. The difference becomes 0.18% and 0.02% when the minimum rate requirements are 128 kbps and 512 kbps, respectively. In addition, the outage probabilities of the network are the same for the proposed algorithm and the exhaustive search algorithm and they are 0% and 14% when the rate requirements are 128 kbps and 512 kbps, respectively. In our simulation tool, while the proposed algorithm obtains the results in 1.45 minutes, the exhaustive search algorithm requires 9855 minutes to obtain the results. As we discussed in Section 3.4, when we increase the number of sectors that implement the proposed algorithm, the required time increases linearly. On the other hand, the required time increases exponentially for the exhaustive search algorithm and it

requires decades to obtain results for the 19 cell hexagonal grid layout depicted in Fig. 3.1.

3.6 Conclusion

In this chapter, we studied the energy efficiency of HetNets. We have proposed an energy-efficient resource allocation algorithm in which the cell-center radius selection, scheduling, and power allocation problems are decoupled. The proposed algorithm maximizes the sector energy efficiency while satisfying the rate requirement of users. The interference pricing mechanism is introduced to prevent selfish behavior of base stations. The proposed algorithms employ the Levenberg-Marquardt method to solve the power allocation problem. Furthermore, the effect of cell-center radius selection is investigated. Based on our simulation results, we demonstrate that significant energy savings can be achieved, while the outage probability is also reduced.

There is a range of GBR requirements our approach improves energy efficiency, outage probabilities, and reduces average transmit power, substantially in some cases. For the tested traffic mixes of the same GBR requirements, this range is $0, 16, 32, 64, 128$ kbps within the transmission parameters studied. Within the experimental parameters, for GBR requirements of 256 and 512 kbps, the energy efficiency becomes worse but the outage probability improves. The improvement is such that the outage probability can move from an unacceptable level to acceptable one. The transmit power improves but not uniformly, unlike the parameters in the previous case. We note that in these simulation setups, the GBR requirements for all users are considered the same. In a real-life situation, there will be a mix of GBR requirements, and the effects of these higher GBR requirements will be less. The newly introduced cell-center selection algorithm (CSSA1) performs better than the two we proposed earlier, namely CSSA2 and CSSA3. The LDS performs better in terms of both energy efficiency and outage probability. Interference pricing mechanism reduces outages

significantly. The proposed approach achieves the same energy efficiency as the exhaustive search whereas the exhaustive search takes an unacceptable amount of time.

This chapter is reproduced based on the material in [74, 75].

Chapter 4

Energy-Spectral Efficient Resource Allocation Algorithm for Heterogeneous Networks

4.1 Motivation

As discussed earlier in thesis, in recent years, the rapid increase of mobile devices such as smart phones, tablets, and wearable computers and mobile applications brought the need for higher throughput and the problem of coverage simultaneously. The capacity of the wireless networks needs to increase to meet this demand. In [2], expanding spectrum and increasing spectral efficiency are proposed among several solutions for this problem. Although increasing spectral efficiency eliminates these problems, the spectral efficiency metric does not provide any intuition about the efficiency of energy consumption. In fact, solutions that improve spectral efficiency may be inefficient in terms of energy efficiency. The increased energy consumption in wireless networks contributes to the growth of greenhouse gases. The

information and communication technologies cause about $2-4\%$ of all carbon footprint generation [6]. This topic has been investigated in the literature under the theme of "Green Communications," see, e.g., [6] and the references therein. In this chapter, we investigate the tradeoff between energy efficiency and spectral efficiency in multi-cell heterogeneous wireless networks.

To meet the increasing throughput demand and eliminate coverage holes, heterogeneous networks (HetNets) are investigated in the literature [5]. In [7], it is shown that both energy efficiency and spectral efficiency can be improved with dense small cell deployment. Due to the fact that low-powered base stations are deployed into the coverage area of a macrocell base station (MBS), the coverage regions of MBS and small cells overlap. Therefore, interference becomes a significant problem in HetNets. To overcome this problem, intercell interference cancellation and mitigation techniques are investigated in the literature [8,9]. In this chapter, we employ the fractional frequency reuse (FFR) scheme for multi-tier networks, studied in [55,57]. FFR is preferred over other intercell interference solutions due to its low complexity. In this scheme, a virtual cell-center radius is selected to divide the sector area into two regions and then subbands are assigned to the base stations depending on their regions. In [55], same cell-center radius is used in each sector independent of the user distribution. Our prior work in [57] has employed the same FFR scheme, but the cell-center radii were selected depending on the user distribution. In this chapter, we employ the same FFR scheme, however we update cell-center boundaries dynamically depending on the requirements of users. A similar approach is also used in our prior work in [75]. This approach helps us satisfy the rate requirements of users and improve our objective. Although the FFR scheme mitigates some portion of the interference in the network, intercell interference is still a significant problem. To further suppress the interference, the pricing mechanism has been studied to maximize the system utility in the literature, see, i.e., [35–38]. In [38], the transmission power times a predefined constant is used for the penalty function. This method prevents base stations from transmitting at high power levels. On the other hand, in [35–37], an interference-based

penalty function is suggested. This approach lets the base stations transmit at high levels if the utility decrease due to interference is less than the improvement of the system utility with transmission power increase. In this chapter, we employ a similar method where each base station is penalized with respect to the amount of interference it creates. This approach prevents the base station from increasing its transmission power to levels that hurt the utility of the other sectors which in turn causes a decrease of the total utility of the network.

As stated earlier, optimizing energy efficiency and spectral efficiency usually contradict with each other [15]. Therefore, this tradeoff has attracted attention in the literature recently. In [15], the authors show that the energy efficiency function is strictly quasi-concave over spectral efficiency. In addition, it is shown that the power consumption minimization problem and the maximization of the energy efficiency problem do not have to coincide. Therefore, these problems should be investigated separately. In [76], the energy efficiency and spectral efficiency tradeoff is investigated for OFDMA networks with optimal joint resource allocation of transmission power and bandwidth. The authors show that when the cell size decreases, the energy efficiency of the network increases. Papers [15, 76] study the energy efficiency and spectral efficiency tradeoff for single-tier networks. When low-powered base stations are deployed with MBSs, intra-cell interference becomes a significant problem. The proposed algorithm in this chapter and [77] investigate energy efficiency and spectral efficiency tradeoff for heterogeneous networks. In [77], the energy efficiency and spectral efficiency tradeoff has been investigated in interference-limited networks. The authors show that the problem is non-convex and NP-hard to solve. Therefore, they propose an iterative power allocation algorithm which guarantees convergence to a local optimum. They define the problem as maximizing energy efficiency of the network under minimum rate constraints. The proposed algorithm in this chapter investigates maximizing the energy efficiency and spectral efficiency simultaneously.

The aforementioned papers investigate energy efficiency and spectral efficiency functions

separately. Another approach to investigate this problem is to combine these metrics under one metric. For this purpose, multi-objective optimization techniques have been widely investigated in the literature [78]. These techniques are successfully used to investigate the energy efficiency and spectral efficiency tradeoff. The first approach to combine energy efficiency and spectral efficiency is the Cobb-Douglas production method [79, 80]. In the Cobb-Douglas method, different powers of the energy efficiency and spectral efficiency metrics are multiplied. In [79], it is shown that the metric that is obtained by using the Cobb-Douglas production method is quasi-concave over the power function. By using the same metric, authors in [80] investigate the relation between energy efficiency, spectral efficiency, and the base station density. In [81], authors study the resource allocation problem in downlink OFDMA multi-cell networks with a similar metric. Papers [80, 81] investigate the problem for homogeneous networks. On the other hand, the algorithm we proposed in this chapter investigates the energy efficiency and spectral efficiency tradeoff in heterogeneous networks. Another method to combine energy efficiency and spectral efficiency metrics is to sum these metrics with appropriate weights [82–84]. This method is called the weighted summation model. The logarithm of the metric in the Cobb-Douglas method corresponds to the weighted summation method of the logarithms of the spectral efficiency and energy efficiency metrics. Authors in [82] investigate the energy efficiency with proportional fairness for downlink distributed antenna systems. The tradeoff between transmission power and bandwidth requirement in single-tier single-cell networks is investigated in [83]. This paper shows that the tradeoff between energy efficiency and spectral efficiency can be exploited by balancing the occupied bandwidth and power consumption. Authors in [84] propose a novel bargaining cooperative game for dense small cell networks. They show that both the energy efficiency and the spectral efficiency of the network can be improved with cooperation among base stations. In [84], the problem in the single-cell network is investigated. In this chapter, we investigate the energy efficiency and spectral efficiency tradeoff in multi-cell multi-tier networks. We also implemented weighted summation model to combine energy efficiency

and spectral efficiency metrics. In our prior work [85], we investigated the same problem. However, in [85], all resources are assigned to users during the frequency assignment process and abandoning a resource block is not considered. In this work, we extend our work in [85] and abandon the resource blocks depending on the network conditions.

In this chapter, we study the joint maximization of energy efficiency and spectral efficiency in multi-cell heterogeneous wireless networks. The minimum rate constraints of users are addressed. The weighted summation method has been implemented to combine energy efficiency and spectral efficiency metrics. The given optimization problem is a mixture of combinatorial and non-convex optimization problems. The optimal solution requires checking all possible cell-center radii, all possible frequency allocations, and all possible power levels for all sectors in the network. Therefore, obtaining the optimum solution is extremely hard. In this chapter, we propose a multi-stage algorithm whereby at each stage the solution is updated while assuming the other network conditions are constant. We show the convergence of the proposed algorithm. In the first stage, each sector selects the cell center radius that maximizes its objective function. In the second stage, the frequency resources are assigned to the users while considering the rate requirement of the users and the interference conditions of the network. In the last stage, a Levenberg-Marquardt method-based power allocation algorithm is implemented that considers the rate requirements of the users. We investigate optimal and suboptimal power updates. In the optimal approach, the Levenberg-Marquardt method-based algorithm updates all power control parameters in the sector concurrently. In the suboptimal approach, the macrocell and the low-powered base stations update their power control parameters separately. The proposed algorithm iteratively solves these three stages until convergence.

The contributions of this chapter are as follows. First, we show that a Pareto optimal solution exists such that the sacrifices in terms of spectral efficiency can be transformed into gain in terms of energy efficiency or vice versa. Second, we investigate the relation between the

energy efficiency and spectral efficiency tradeoff and minimum rate constraints of the users. We show that maximizing energy efficiency of the network performs better than the spectral efficiency maximization in terms of outages. Third, we show that fewer resource blocks are allocated when we increase the minimum rate constraints of users or increase the weight of the spectral efficiency in the objective metric.

The remainder of this chapter is organized as follows. Section 4.2 introduces the system model, base station power consumption, and energy efficiency and spectral efficiency definitions. Section 4.3 formulates the resource allocation problem in HetNets. The proposed algorithm is presented in Section 4.4. Simulation results are discussed in Section 4.5. Section 4.6 concludes the chapter.

4.2 System Model

In this section, we first present our system model and describe the power consumption model of the base station. Second, we define the energy efficiency and spectral efficiency metrics.

Consider a wireless network with a 19-cell hexagonal layout as depicted in Figure 4.1. The edges are wrapped around to create the effect of an infinite network. In this chapter, we employ the multi-tier FFR scheme described in [55, 57]. In each cell, one MBS is deployed along with picocell base stations (Pico-BSs). MBSs employ 3-sector antennas, whereas omnidirectional antennas are used in Pico-BSs. The overall network area is divided into 57 sectors. Each sector is divided into two regions: cell center and cell edge. In the cell-center region, macrocell associated users (MUEs) are allocated on Subband A in all sectors. On the other hand, cell-edge MUEs are allocated on Subbands B, C, or D depending on their sector. In order to limit intra-sector interference, cell-center picocell associated users (PUEs) are allocated on the remaining two subbands that the MBS does not transmit on. Cell-edge

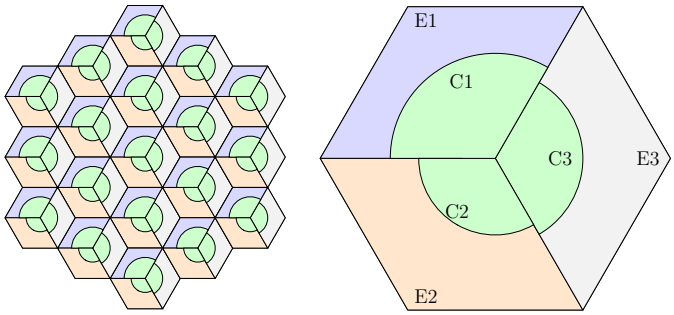

Figure 4.1: Dynamic cell-center region boundaries in a multi-tier FFR scheme. The network layout assumes a uniform 19 cell hexagonal grid in which the MBSs have three sector antennas and Pico-BSs employ omnidirectional antennas.

Table 4.1: Spectrum assignment in a multi-tier FFR scheme

Base Station Type	Sector 1		Sector 2		Sector 3	
	Cell-Center(C1)	Cell-Edge(E1)	Cell-Center(C2)	Cell-Edge(E2)	Cell-Center(C3)	Cell-Edge(E3)
MBS	A	B	A	C	A	D
Pico-BS	C and D	A, C, and D	B and D	A, B, and D	B and C	A, B, and C

PUEs also use Subband A in addition to two subbands that cell-center PUEs are using. The transmission powers of the Pico-BSs are significantly lower than the MBSs, therefore the intra-sector interference from cell-edge Pico-BSs to cell-center MUEs will be limited. The spectrum allocation is shown in Table 4.1.

In this chapter, we study constant power allocation across the subbands. The total bandwidth of the network is divided into 4 disjoint subbands. The number of subcarriers in subbands A, B, C, and D are denoted by N_A, N_B, N_C, and N_D, respectively. The total number of subcarriers is denoted by N, i.e., $N = N_A + N_B + N_C + N_D$. In order to characterize the power assignment of base stations, we introduce two power control parameters β and ε. The parameter β is used to scale the transmission power of base stations. This parameter is defined for both MBSs and Pico-BSs. On the other hand, the parameter ε is only defined for MBSs and determines the ratio of the transmission power of MBSs on the cell-edge and the cell-center subcarriers. We can write the signal-to-interference-plus-noise

ratio (SINR) of MUE k on subcarrier n as follows

$$\gamma_k^{(n)} = \frac{P_M^{(n)} g_{k,M}^{(n)}}{\sum\limits_{\substack{M' \in \mathcal{B}_M \\ M' \neq M}} P_{M'}^{(n)} g_{k,M'}^{(n)} + \sum\limits_{P \in \mathcal{B}_P} P_P^{(n)} g_{k,P}^{(n)} + N_0 \Delta_n} \tag{4.1}$$

where $P_M^{(n)}$ and $P_P^{(n)}$ are the downlink transmit powers of macrocell M and picocell P on subcarrier n, respectively. The channel gain between user k and MBS M on subcarrier n is represented as $g_{k,M}^{(n)}$. The same gain between user k and Pico-BS P is $g_{k,P}^{(n)}$. The sets of MBSs and Pico-BSs in the simulation area are denoted by $\mathcal{B}_M$ and $\mathcal{B}_P$, respectively. The bandwidth of a subcarrier n is represented by Δ_n. The thermal noise power per Hz is N_0. The SINR of PUEs can be generated by using the same approach. The downlink transmission power of MBS M for cell-center MUEs that are in sector s can be written as

$$P_M = \frac{\beta_M P_{\max,M}}{N_A^s + \varepsilon_s N_B^s}, \tag{4.2}$$

where $P_{max,M}$ is the maximum transmission power of the MBS M. The numbers of assigned subcarriers on subband A and B in sector s are denoted by N_A^s and N_B^s, respectively. The downlink transmission power for cell-edge users is $\varepsilon_M P_M$. The downlink transmission power of the MBSs in other sectors can be obtained by replacing N_A^s and N_B^s with the corresponding number of subcarriers. The downlink transmission power of cell-center and cell-edge Pico-BSs in Sector 1 are denoted by P_P^C and P_P^E, and are given by

$$P_P^C = \frac{\beta_P P_{\max,P}}{N_C^s + N_D^s}, \quad P_P^E = \frac{\beta_P P_{\max,P}}{N_A^s + N_C^s + N_D^s}. \tag{4.3}$$

The numbers of assigned subcarriers on subband C and D in sector s are denoted by N_C^s and N_D^s, respectively. For the Pico-BSs in other sectors, the transmission power can be calculated similarly, by replacing N_A^s, N_C^s, and N_D^s with the corresponding number of subcarriers.

Consider sector s to consist of $K_{M,s}$ MUEs and $K_{P,s}$ PUEs. The sets of MUEs and PUEs are

denoted by $\mathcal{K}_{M,s}$ and $\mathcal{K}_{P,s}$, respectively. We use index k for user k and index n for subcarrier n. We define vector $\boldsymbol{C}_{M,s}$ to show whether MUE is in the cell center or not. The size of this vector is $K_{M,s}$. If an MUE k is located in the cell center, $\boldsymbol{C}^k_{M,s} = 1$, otherwise $\boldsymbol{C}^k_{M,s} = 0$. Likewise, the vector $\boldsymbol{C}_{P,s}$ denotes whether PUE is in cell center or not. The size of $\boldsymbol{C}_{P,s}$ is $K_{P,s}$. If PUE k is located in the cell center, $\boldsymbol{C}^k_{P,s} = 1$, otherwise $\boldsymbol{C}^k_{P,s} = 0$. The matrices $\boldsymbol{F}_{M,s}$ and $\boldsymbol{F}_{P,s}$ denote whether the subcarrier n is assigned to user k or not. The size of the matrices $\boldsymbol{F}_{M,s}$ and $\boldsymbol{F}_{P,s}$ are $K_{M,s} \times N$ and $K_{P,s} \times N$, respectively. If the subcarrier n is assigned to MUE k, the (n,k)th element of $\boldsymbol{F}_{M,s}$ will be 1, otherwise it will be 0. The same approach is used for frequency allocation of $\boldsymbol{F}_{P,s}$. The matrices $\boldsymbol{R}_1$ and $\boldsymbol{R}_2$ denote the throughput of MUEs. The size of these matrices are $N \times K_{M,s}$. The (n,k)th element of matrix $\boldsymbol{R}_1$ is the throughput of MUE k on subcarrier n when MUE k is in the cell-center region. The same element of $\boldsymbol{R}_2$ corresponds to the same value when the user is located in the cell-edge region. The matrices $\boldsymbol{R}_3$ and $\boldsymbol{R}_4$ consist of the throughput of PUEs. The size of these matrices are $N \times K_{P,s}$. The (n,k)th element of $\boldsymbol{R}_3$ and $\boldsymbol{R}_4$ is the throughput of PUE k on subcarrier n when the user is in cell center and cell edge, respectively. Then, we can calculate the aggregate throughput of the sector s as

$$\begin{aligned} R_s = &\sum_{k \in \mathcal{K}_{M,s}} (\boldsymbol{C}^k_{M,s} \boldsymbol{F}^{(k,:)}_{M,s} \boldsymbol{R}^{(:,k)}_1 + (1 - \boldsymbol{C}^k_{M,s}) \boldsymbol{F}^{(k,:)}_{M,s} \boldsymbol{R}^{(:,k)}_2) \\ &+ \sum_{k \in \mathcal{K}_{P,s}} (\boldsymbol{C}^k_{P,s} \boldsymbol{F}^{(k,:)}_{P,s} \boldsymbol{R}^{(:,k)}_3 + (1 - \boldsymbol{C}^k_{P,s}) \boldsymbol{F}^{(k,:)}_{P,s} \boldsymbol{R}^{(:,k)}_4). \end{aligned} \tag{4.4}$$

Note that $\boldsymbol{X}^{(n,:)}$ and $\boldsymbol{X}^{(:,k)}$ are the nth row vector of the matrix $\boldsymbol{X}$ and the kth column vector of the matrix $\boldsymbol{X}$, respectively. The throughput terms in (4.4) can be expanded by using the definitions in (4.1) as

$$\boldsymbol{R}^{(n,k)}_i = \Delta_n \log_2 \left(1 + \gamma^{(n)}_k\right), \quad \text{for all } i \in 1,2,3,4, \tag{4.5}$$

where $\boldsymbol{X}^{(n,k)}$ is the entry on the nth row and kth column of the matrix $\boldsymbol{X}$.

4.2.1 Base Station Power Consumption Models

Modeling the energy consumption of the base stations has attracted some attention in the literature, see, e.g., [26,63,64]. Several components contribute to the energy consumption of the base stations such as power amplifier, power supply, cooling device, etc. A good model must include the contribution of all components. In order to quantify the energy savings properly, a load-dependent model is required. In this chapter, we use the power consumption model that is described in [64]. In this model, the power consumption of the base station is broken down into two parts: load-dependent and static power consumption. The load-dependent part changes depending on the transmission power of the base station. On the other hand, static power is independent of the transmission power and it will be consumed if the base station is on. If the base station has no user to serve, then it goes into the sleep mode. During the sleep mode, energy consumption of the base station is lower than the static power consumption of the base station. This model is given by

$$P_{Total} = \begin{cases} N_{TRX}\left(P_0 + \Delta \cdot P_{TX}\right) & 0 < P_{TX} \leq P_{\max} \\ N_{TRX} P_{sleep} & P_{out} = 0 \end{cases} \tag{4.6}$$

where P_{Total}, P_{TX}, and P_{sleep} are the overall power consumption of the base station, load-dependent transmission power, and the power consumption during the sleep mode. The maximum transmission power of the base station is denoted by $P_{\max}$. The number of the transceiver chains is represented by N_{TRX}. The slope of the load-dependent power consumption is Δ. By using this model, the power consumption of the MBSs and Pico-BSs can be written as

$$P_M = N_{TRX,M}\left(P_{0,M} + \Delta_M P_{TX,M}\right) \text{ and } P_P = N_{TRX,P}\left(P_{0,P} + \Delta_P P_{TX,P}\right) \tag{4.7}$$

where P_M and P_P denote the overall power consumption of MBS M and Pico-BS P, respectively. The parameters $P_{0,M}$ and $P_{0,P}$ are the static power consumption at MBS M and Pico-BS P, respectively. The transmission power of the MBS M and Pico-BS P are denoted by $P_{TX,M}$ and $P_{TX,P}$, respectively. The numbers of transceiver chains for MBS M and Pico-BS P are represented by $N_{TRX,M}$ and $N_{TRX,P}$, respectively. The slopes of the power consumption for MBS M and Pico-BS P are denoted by Δ_M and Δ_P, respectively. If no user is associated with a base station, the corresponding base stations go into sleep mode. The power consumptions of the MBS M and Pico-BS P during the sleep mode are denoted by $P_{sleep,M}$ and $P_{sleep,P}$, respectively.

4.2.2 Energy Efficiency and Spectral Efficiency Definition

Let η_s denote the energy efficiency of sector s which can be expressed as

$$\eta_s(\boldsymbol{\varepsilon}, \boldsymbol{\beta}) = \frac{R_s}{\psi_s(\varepsilon_s, \boldsymbol{\beta}_s)}, \tag{4.8}$$

where the vectors $\boldsymbol{\varepsilon}$ and $\boldsymbol{\beta}$ denote the optimization variables of transmission power for all sectors in the network. The scalar parameter ε_s is the ε value of the sector s. The vector $\boldsymbol{\beta}_s$ consists of all β values of the base stations in sector s. The total power consumption in sector s is denoted by $\psi_s(\varepsilon_s, \boldsymbol{\beta}_s)$ which can be calculated as

$$\psi_s(\varepsilon_s, \boldsymbol{\beta}_s) = P_M + \sum_{P \in \mathcal{N}_{\text{Pico},s}} P_P, \tag{4.9}$$

where $\mathcal{N}_{\text{Pico},s}$ is the set of Pico-BSs in sector s. Thus, the energy efficiency $\eta_s(\boldsymbol{\varepsilon}, \boldsymbol{\beta})$ has the unit bits/Joule.

In the same fashion, we can calculate the spectral efficiency of the sector s as follows

$$\nu_s(\boldsymbol{\varepsilon}, \boldsymbol{\beta}) = \frac{R_s}{W_s}, \tag{4.10}$$

where W_s is the total bandwidth allocated by MBS and Pico-BSs in sector s. The unit of $\nu_s(\boldsymbol{\varepsilon}, \boldsymbol{\beta})$ is bits/s/Hz.

4.3 Problem Formulation

In this section, we develop a framework to investigate energy efficiency and spectral efficiency tradeoff in multi-cell heterogeneous networks. Our objective is to maximize both energy efficiency and spectral efficiency of the network while satisfying the minimum rate requirements of users. As stated earlier, the problems of maximizing energy efficiency and spectral efficiency of the network usually contradict with each other. Therefore, we introduce a multi-objective optimization-based formulation to maximize energy efficiency and spectral efficiency simultaneously. Multi-objective problems are usually solved by combining objectives under a single objective. In that manner, we use the weighted summation method to combine the energy efficiency and spectral efficiency metrics. However, the units of these metrics are not the same. The unit of energy efficiency is bits/Joule and the unit of spectral efficiency is bits/s/Hz. To ensure the units of these metrics are the same in weighted summation form, we multiply the spectral efficiency function with W_{tot}/P_s. The parameter W_{tot} is the total bandwidth of the network and P_s is the total amount of power consumption of sector s when all BSs in this sector transmit at full power. A similar approach is also used in [83]. In addition, we introduce the unitless parameter α, $0 \leq \alpha \leq 1$, to tune the objective metric. This parameter helps us tune the network towards energy efficiency or spectral efficiency depending on the network conditions. During the peak hours, increasing spectral efficiency is more important than the energy efficiency to satisfy the demand of

more users. On the other hand, during the off-peak hours, maximizing energy efficiency becomes more important to decrease the energy consumption of the network. The objective metric moves towards spectral efficiency when parameter α increases. On one extreme, when α is 1, the problem becomes spectral efficiency maximization; on the other extreme, when α is 0, the problem is energy efficiency maximization. Thus, α allows a service provider to make a judicious decision between the two efficiency measures depending on their own criteria. In addition, for constant α, when we increase W_{tot}, the weight of the spectral efficiency function increases in the objective function. When there is sufficient bandwidth, the objective function emphasis is on saving more bandwidth and maximizing the efficiency of the occupied bandwidth. On the other hand, if we have sufficient power, the importance of the energy efficiency in the objective function increases. A multi-objective optimization problem employing the variables we specified above can be defined as follows

$$\max_{\boldsymbol{\beta},\boldsymbol{\varepsilon},\mathbf{C},\mathbf{F}} \quad \sum_{s\in\mathcal{S}}(1-\alpha)\eta_s(\boldsymbol{\varepsilon},\boldsymbol{\beta}) + \alpha\frac{W_{tot}}{P_s}\nu_s(\boldsymbol{\varepsilon},\boldsymbol{\beta})$$

$$\text{s.t.} \quad \boldsymbol{C}^k_{M,s}\boldsymbol{F}^{(k,:)}_{M,s}\boldsymbol{R}^{(:,k)}_1 + (1-\boldsymbol{C}^k_{M,s})\boldsymbol{F}^{(k,:)}_{M,s}\boldsymbol{R}^{(:,k)}_2 \geq R_{\min,k}, \text{for all } k\in\mathcal{K}_{M,s}, s\in\mathcal{S} \tag{4.11a}$$

$$\boldsymbol{C}^k_{M,s}\boldsymbol{F}^{(k,:)}_{M,s}\boldsymbol{R}^{(:,k)}_3 + (1-\boldsymbol{C}^k_{M,s})\boldsymbol{F}^{(k,:)}_{M,s}\boldsymbol{R}^{(:,k)}_4 \geq R_{\min,k}, \text{for all } k\in\mathcal{K}_{P,s}, s\in\mathcal{S} \tag{4.11b}$$

$$\sum_{\substack{k\in\mathcal{K}_{M,s}\\ \boldsymbol{C}^k_{M,s}=1}} \boldsymbol{F}^{(k,n)}_{M,s} \leq 1 \text{ and } \sum_{\substack{k\in\mathcal{K}_{M,s}\\ \boldsymbol{C}^k_{M,s}=0}} \boldsymbol{F}^{(k,n)}_{M,s} = 0 \quad \text{for all } n\in\mathcal{N}^C_{M,s}, s\in\mathcal{S} \tag{4.11c}$$

$$\sum_{\substack{k\in\mathcal{K}_{M,s}\\ \boldsymbol{C}^k_{M,s}=0}} \boldsymbol{F}^{(k,n)}_{M,s} \leq 1 \text{ and } \sum_{\substack{k\in\mathcal{K}_{M,s}\\ \boldsymbol{C}^k_{M,s}=1}} \boldsymbol{F}^{(k,n)}_{M,s} = 0 \quad \text{for all } n\in\mathcal{N}^E_{M,s}, s\in\mathcal{S} \tag{4.11d}$$

$$\sum_{k\in\mathcal{K}_{M,s}} \boldsymbol{F}^{(k,n)}_{M,s} = 0 \quad \text{for all } n\notin\mathcal{N}^C_{M,s}\cup\mathcal{N}^E_{M,s}, s\in\mathcal{S} \tag{4.11e}$$

$$\sum_{\substack{k\in\mathcal{K}^p_{P,s}\\ \boldsymbol{C}^k_{P,s}=1}} \boldsymbol{F}^{(k,n)}_{P,s} \leq 1 \text{ and } \sum_{\substack{k\in\mathcal{K}^p_{P,s}\\ \boldsymbol{C}^k_{P,s}=0}} \boldsymbol{F}^{(k,n)}_{P,s} = 0 \quad \text{for all } n \in \mathcal{N}^C_{P,s}, p \in \mathcal{N}_{Pico,s}, s \in \mathcal{S} \tag{4.11f}$$

$$\sum_{\substack{k\in\mathcal{K}^p_{P,s}\\ \boldsymbol{C}^k_{P,s}=0}} \boldsymbol{F}^{(k,n)}_{P,s} \leq 1 \text{ and } \sum_{\substack{k\in\mathcal{K}^p_{P,s}\\ \boldsymbol{C}^k_{P,s}=1}} \boldsymbol{F}^{(k,n)}_{P,s} = 0 \quad \text{for all } n \in \mathcal{N}^E_{P,s}, p \in \mathcal{N}_{Pico,s}, s \in \mathcal{S} \tag{4.11g}$$

$$\sum_{k\in\mathcal{K}^p_{P,s}} \boldsymbol{F}^{(k,n)}_{P,s} = 0 \quad \text{for all } n \notin \mathcal{N}^C_{P,s} \cup \mathcal{N}^E_{P,s}, p \in \mathcal{N}_{Pico,s}, s \in \mathcal{S} \tag{4.11h}$$

$$\boldsymbol{\varepsilon} \succeq \mathbf{0} \text{ and } \mathbf{0} \preceq \boldsymbol{\beta} \preceq \mathbf{1}, \tag{4.11i}$$

where $\mathcal{S}$ is the set of all sectors in the simulation area. The minimum rate requirement of user k is denoted by $R_{\min,k}$. The parameters $\mathcal{N}^C_{M,s}$ and $\mathcal{N}^E_{M,s}$ are the set of subcarriers that are assigned to cell-center and cell-edge MUEs, respectively. Likewise, the parameters $\mathcal{N}^C_{P,s}$ and $\mathcal{N}^E_{P,s}$ are the set of subcarriers that are assigned to cell-center and cell-edge PUEs, respectively. The notation $\mathbf{x} \succeq \mathbf{0}$ forces that each element of vector $\mathbf{x}$ is greater than or equal to 0. Constraints (4.11a) and (4.11b) ensure that rate constraints of the MUEs and PUEs are satisfied, respectively. Constraints (4.11c) to (4.11h) guarantee that available resources to a base station for a region are assigned to users that are associated with the base station and in the corresponding region and unavailable resources are not assigned to these users. Constraint (4.11i) guarantees that parameters $\boldsymbol{\varepsilon}$ and $\boldsymbol{\beta}$ are within the given limits.

The objective function in (4.11) is non-convex, therefore the optimal solution requires exhaustive search over all possible cell-center radii, frequency assignments, and power levels for all sectors. To tackle this problem, we divide our problem into $|S|$ subproblems so that each sector maximizes its own objective function simultaneously. This resource allocation problem still needs to be solved over the cell-center radius, frequency, and power domains jointly. This problem is combinatorial over the first two domains and non-convex over the

power allocation domain [65, 66]. Therefore, obtaining the optimum solution still requires exhaustive search over all domains. Therefore, instead of solving these problems jointly, we propose a three-stage algorithm that solves each problem consecutively. In the next section, we will describe these stages and discuss the complexity and convergence analysis of the proposed algorithm.

4.4 Proposed Solution

Our formulation in (4.11) enables us to develop an energy- and spectral-efficient resource allocation algorithm. We first divide the problem in (4.11) into $|S|$ subproblems such that each sector maximizes own objective function. Then, the proposed algorithm decouples the problem into three stages and solves them iteratively until convergence. In the first stage, we select the cell-center radius to divide MUEs into two groups as cell-center MUEs and cell-edge MUEs and also determine the available resources to the Pico-BSs depending on their regions. Second, MBS and Pico-BSs assign frequency resources to their users. This stage has two steps. In the first step, MBS and Pico-BSs assign the resource blocks to their users to maximize the objective metric and satisfy the rate requirements of their users. In the second step, the MBS and all Pico-BSs in the sector make a judicious decision to maximize the overall objective among the following: abandon one of the assigned resource block from all base stations, allocate one more resource block among the available ones, or protect the current allocation. By this approach, the available resources to each sector are updated in each iteration until the optimum allocation is found. Last, we determine the power control parameters ε and βs in each sector concurrently. The minimum rate requirements of the users are included in the power control subproblem by using dual decomposition techniques. After these three stages, the MBS sends the updated information to the other base stations in the network. Then, these stages are repeated in every sector until convergence. The proposed

Algorithm 4 Proposed Energy- and Spectral-Efficient Resource Allocation Algorithm

1: **Initialize:** $r_{th,s}^{(0,c)} = r_{r,s}/2 \quad (\varepsilon_s^{(0)}, \boldsymbol{\beta}_s^0) = [1, \mathbf{1}]$
2: $r_{th,s}^{(t,0)} = r_{th,s}^{(t-1,0)}$
3: First, three-candidate cell-center region boundaries are selected by using the cell-center radius algorithm in Section 4.4.1: $r_{th,s}^{(t,-1)}$, $r_{th,s}^{(t,0)}$, and $r_{th,s}^{(t,1)}$.
4: $r_{th,s}^{(t,0)} = r_{th,s}^{(t-1,0)}$. The cell-center radius $r_{th,s}^{(t,-1)}$ is obtained by shrinking $r_{th,s}^{(t,0)}$, and $r_{th,s}^{(t,1)}$ is obtained by expanding $r_{th,s}^{(t,c)}$.
5: **for** $c := -1$ to 1 **do**
6: For cell-center radius, $r_{th,s}^{(t,c)}$, run the frequency assignment algorithm in Section 4.4.2 for each base station in the sector.
7: Calculate the Lagrangian functions, $\mathcal{L}_s^{(c)}$, which is described in the Section 4.4.3.
8: Note that while calculating the Lagrangian function, power control parameters that are obtained at the end of the previous time instant are used.
9: **end for**
10: Among all three Lagrangian function, the maximum one is selected for the cell-center radius and the frequency assignments.
11: Then, run the power control algorithm that is described in Section 4.4.3 to determine the power control parameters.
12: Go to Step 2 and repeat until the convergence.

algorithm is presented under the heading Algorithm 4. The flowchart of this algorithm is depicted in Figure 4.2. In the sequel, we discuss each step of the proposed algorithm in detail.

4.4.1 The Cell-Center Region Boundaries

In the first stage of the proposed algorithm, we need to set the cell-center region boundaries in each sector to select the region of the MUEs and also determine the available resources to Pico-BSs. In [57], we showed that more than two times gain can be obtained in terms of energy efficiency and throughput by proper selection of cell-center radii. In [57], we proposed two cell-center radius selection algorithms. The first algorithm selects a cell-center radius to maximize the throughput of the sector. The second algorithm aims to distribute resources evenly among MUEs. However, neither of these algorithms considers the minimum rate requirements of users. For example, when the minimum rate requirements of users are low,

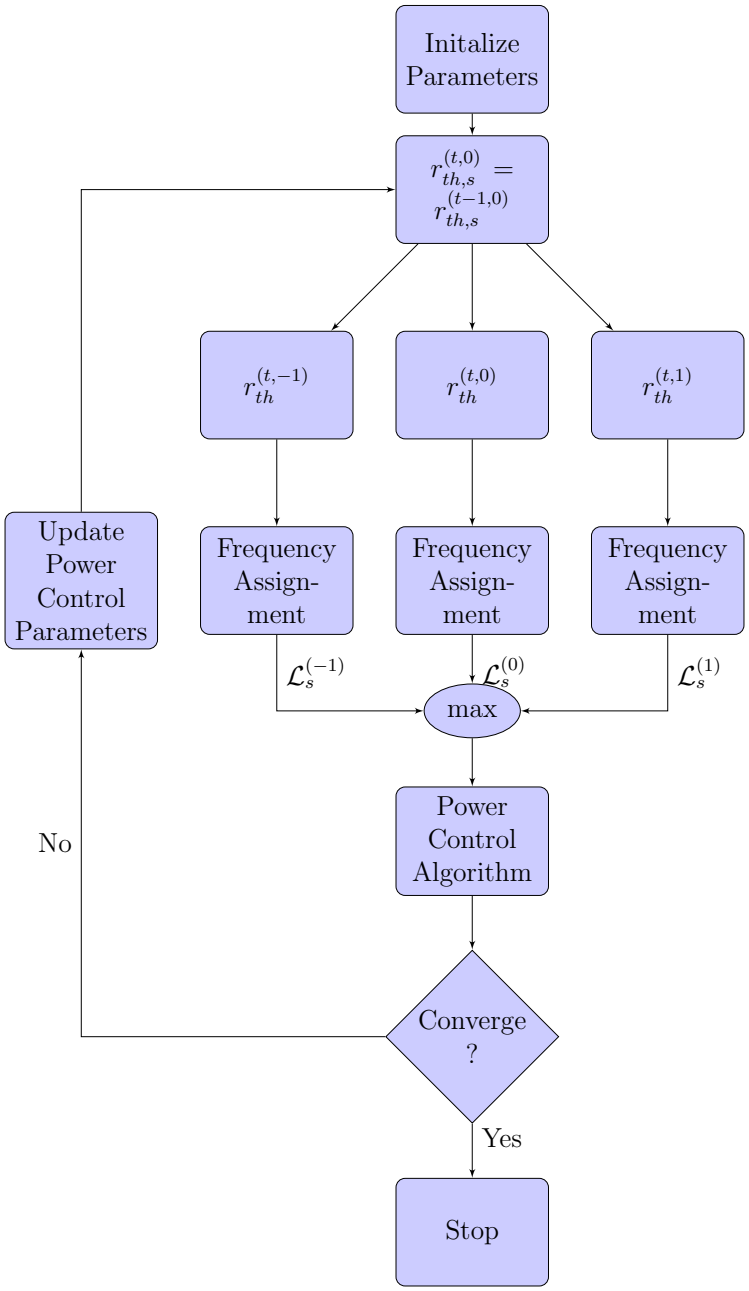

Figure 4.2: Flowchart of proposed algorithm in Algorithm 4.

the first algorithm is preferable over the second one to maximize the objective metric. On the other hand, if users have higher rate requirements, the second algorithm should be selected over the first one to satisfy the rate requirements of more users. Therefore, in order to benefit from the advantages of both algorithms, we propose a dynamic cell-center selection algorithm in this chapter. First, we will provide a useful observation.

Observation 1. *The resource distribution of the FFR scheme changes only when one of the cell-center MUEs or cell-center Pico-BSs passes to the cell-edge region or vice versa.*

When we expand or shrink the cell-center radius without changing the region of an MUE or a Pico-BS, the region of all users and Pico-BSs will be the same. Therefore, the solution of the frequency assignment and power assignment problems will be the same.

Therefore, $K_{M,s} + N_{\text{Pico},s} + 1$ different cell-center radii can be selected for sector s. When the number of users in the sector or the number of pico-BSs in the sector increases, exhaustive search over all radii requires a significant amount of time. In addition, the frequency assignment problem that will be discussed in the next subsection needs to be solved for every radius option. Therefore, we need to eliminate some of these radii choices judiciously. In this chapter, we propose an iterative algorithm for cell-center radius selection. The proposed algorithm compares the Lagrangian function of the current cell-center radius with two cell-center radii: one more MUE or Pico-BS is included in the cell-center region from the cell-edge region and one more MUE or Pico-BS is excluded to the cell-edge region from the cell-center region. Among these three cell-center radii, the one that maximizes the Lagrangian function is selected as the cell-center radius. This approach decreases the number of cell-center radii that will be checked in every iteration from $K_{M,s} + N_{\text{Pico},s} + 1$ to three. Therefore, a significant amount of time will be saved by this approach. We used a similar algorithm in our prior work [75].

4.4.2 Frequency Assignment Problem

In the second stage of the algorithm, frequency resources are assigned to users. In the literature, several scheduling algorithms are discussed, see, e.g., [59]. Each scheduler has its own priorities such as minimizing latency, maximizing fairness, etc. In [65], it is shown that the optimal resource allocation among $K_{M,s}$ users and $N^C_{M,s}$ resource blocks requires $K_{M,s}^{N^C_{M,s}}$

searches. This approach is impractical in real time applications. Therefore, we propose a two-step opportunistic scheduling algorithm in this chapter. Before discussing the proposed scheduling algorithm, we will provide some useful theorems.

Theorem 4.1. *The power consumption of a base station is minimized when the maximum of* $R_{\min,k}/R_{curr,k}$*,* R_{ratio}*, is minimized where* $R_{curr,k}$ *is the current rate of user* k *when no power control is implemented.*

Proof: Let us compare two different cases of scheduling that consume equal amount of power. Assume the minimum rate requirements of all users is satisfied with the current power assignment and R^1_{ratio} is bigger than R^2_{ratio}, i.e., $1 > R^1_{ratio} > R^2_{ratio}$. The power control algorithm that minimizes the power consumption will increase both ratios to 1. While the total power consumption of the first case is $R^1_{ratio} \cdot P$, that of the second case will be $R^2_{ratio} \cdot P$. Therefore, less power will be consumed in the second case than the first case.

Theorem 4.2. *The spectral efficiency of the resource block is maximized when a resource block is assigned to a user that has the best average channel gain over the subcarriers of the resource block.*

Proof: The proof of this theorem is straightforward. When a user has the best average channel gain over the subcarriers of the resource block, it has the highest capacity. Due to the fact that the total bandwidth of the resource block will be the same for all users, the user who has the highest channel gain will also provide the highest spectral efficiency for that resource block.

The proposed scheduling algorithm has two steps. In the first step, the available resource blocks are assigned to users. The proposed algorithm assigns the resource blocks to users iteratively. In each iteration, one resource block is assigned to a user. Our priority is satisfying the minimum rate requirements of more users. For this purpose, if there are users that could not satisfy their rate requirement with the current assignment, assigning a

resource block to one of these users is the most judicious choice. In order to maximize our objective, we assign the resource block to the user that provides the largest improvement in terms of the Lagrangian among the users that could not satisfy their rate requirement. If all users satisfy their rate requirement with the current assignment, available resource blocks are assigned to the user that provides the largest Lagrangian improvement among all users. By this approach, first, the rate requirement of more users are satisfied. Second, the power consumption of the network is minimized. Third, the spectral efficiency of the network is maximized. During this step, power allocations in the previous time instant are used to calculate the rates of the users with the current assignment. In the second step of the algorithm, all base stations in a sector determine whether to protect the current assignment, abandon one resource block, or assign one more resource block among the available but unassigned ones. When a resource block is not allocated by any user in a sector, the intercell interference to users in the other sector is lowered which increases the utility function of the other sectors. In addition, fewer resource blocks are assigned by base stations in the sector, therefore power assignment of other resource blocks increases. This may also increase the spectral efficiency of the sector. In the next section, we present the two steps of the opportunistic scheduling algorithm and then discuss the complexity of the algorithm.

Opportunistic Scheduler Algorithm: The opportunistic scheduler algorithm shares resource blocks among users to maximize the objective metric. Due to the fact that the cell-center and cell-edge MUEs are allocated different subbands, this algorithm runs for both sets separately. First, the proposed algorithm assigns a resource block to a user that provides maximum improvement to the Lagrangian function that is described in Section 4.4.3. If the rate requirement of the corresponding user is satisfied with the current assignment, this user is removed from the assignment set. The proposed algorithm continues to allocate resource blocks to users in the assignment set. If the minimum rate requirements of all users are satisfied with the current assignment (i.e., the assignment set is empty), the proposed algorithm assigns the rest of the available resource blocks to users that provide the largest

Lagrangian improvement. The resource allocation algorithm for cell-center MUEs is given under the heading Algorithm 5. The same approach can be used for the cell-edge MUEs and Pico-BSs.

Due to the interference conditions in the network, not assigning a resource block to any user in the sector may improve the overall utility of the network. In addition, when a resource block is not assigned by all base stations in a sector, the denominator of the spectral efficiency function becomes smaller. This may also improve the spectral efficiency of the sector. In order to benefit from these properties, we decide among the following three cases in each iteration: abandoning one of the resource blocks from all base stations, allocating one more resource block among the available ones, or protecting the current situation. For each resource block, we calculate the utility function without assigning this resource block. In addition, for each unassigned but available resource block, we calculate the utility function when this resource block is assigned. Among all these cases the one that has the largest Lagrangian function is selected as the current frequency resource allocation.

Complexity Analysis

In the first step of the scheduling algorithm, each base station calculates the rate of each available resource blocks for each user in the sector. Therefore, the complexity of the first step is $\mathcal{O}(NK)$ for each base station when there are N resource blocks to assign to K users. In the second step, the complexity of the algorithm is different for MBSs and Pico-BSs. In MBSs, the rate of each resource block is required to be recalculated for one more resource block assignment and one more resource block abandonment. When we look at the formula in (4.2), abandoning or assigning a cell-center resource block and cell-edge resource block has affected the downlink transmission power of the MBS differently. Therefore, we have to calculate different rates for all these cases. In the first step, the resource blocks are already assigned to users, therefore we have to calculate the rate of each resource block for

Algorithm 5 Proposed Frequency Allocation Algorithm

Initialize: $\boldsymbol{F}_{M,s} = \mathbf{0}$
$\mathcal{N}_{M,s}^{C,t} = \mathcal{N}_{M,s}^{C,t-1}$. $\mathcal{N}_{M,s}^{C,t-1}$ is the frequency resources that are assigned at time instant $t-1$
$\mathcal{K}_{M,s}^{C,U} = \mathcal{K}_{M,s}^{C}$
while $\mathcal{N}_{M,s}^{C,t}$ and $\mathcal{K}_{M,s}^{C,U}$ are not empty **do**
    $k = \arg \max_{k \in \mathcal{K}_{M,s}^{C,U}} \mathcal{L}_s^{(C,k,n)}$
    $\boldsymbol{F}_{M,s}^{(k,n)} = 1$
    if $\boldsymbol{F}_{M,s}^{(k,:)} \boldsymbol{R}_1^{(:,k)} \geq R_{\min,k}$ **then**
        $\mathcal{K}_{M,s}^{C} \longleftarrow \mathcal{K}_{M,s}^{C} \backslash \{k\}$
    end if
    $\mathcal{N}_{M,s}^{C,t-1} \longleftarrow \mathcal{N}_{M,s}^{C,t} \backslash \{n\}$
end while
while $\mathcal{N}_{M,s}^{C,t}$ is not empty **do**
    $k = \arg \max_{k \in \mathcal{K}_{M,s}^{C}} \mathcal{L}_s^{(C,k,n)}$
    $\boldsymbol{F}_{M,s}^{(k,n)} = 1$
    $\mathcal{N}_{M,s}^{C,t-1} \longleftarrow \mathcal{N}_{M,s}^{C,t} \backslash \{n\}$
end while

these four cases. The complexity of this process becomes $\mathcal{O}(4N)$. On the other hand, the effect of abandoning or assigning a resource block from different subbands on the downlink transmission power will be the same. Therefore, the complexity of this process at Pico-BSs is $\mathcal{O}(2N)$.

4.4.3 Power Control Problem

In the third stage of the algorithm, we determine the power levels on each subband that maximize our objective metric and also satisfy the rate requirements of the users. Given the cell-center radius vector and the frequency assignment matrix, we need to determine the power control parameters $\boldsymbol{\beta}_s$ and ε_s. We use convex optimization techniques to obtain optimum $\boldsymbol{\beta}$ and ε parameters.

Lemma 1. *The energy efficiency and spectral efficiency per sector expression* $(1-\alpha)\eta_s(\boldsymbol{\varepsilon}, \boldsymbol{\beta}) + \alpha \frac{W_{tot}}{P_s} \nu_s(\boldsymbol{\varepsilon}, \boldsymbol{\beta})$ *in (4.11) is quasiconcave in* ε_s *and* $\boldsymbol{\beta}_s$.

Proof: The proof is given in the Appendix B.

During obtaining optimum power control parameters, we assume that the power control parameters of the other sectors are constant. Therefore, the interference conditions from the other sectors are assumed to be constant. However, if the base stations increase their transmission powers to high levels without considering the other sector, this harms the transmissions in other sectors and causes outages and decrease in the overall utility. To prevent this, we introduce the interference pricing mechanism. Several pricing algorithms are discussed in the literature. In [38] and [39], each base station is penalized with the transmission power level of the base station. The penalty term is a constant term times the transmission power level of the base station. Although this approach forces the base stations to decrease their transmission power, the penalty term will be independent of the interference that the base stations create. Therefore, the improvement in overall network utility may not reach its actual potential. For this reason, we use an interference-based pricing mechanism in this chapter. The pricing mechanism penalizes each sector by the amount of the interference it creates. This approach was first proposed in [35–37]. We use $\theta_s(\varepsilon_s, \boldsymbol{\beta}_s)$ to denote the interference pricing function for sector s. The interference pricing function proportionally increases with the interference that the base station creates. In addition, if the interference causes the outages of users in other sectors, the penalty term becomes more severe.

Section 4.4.2 guarantees that constraints (4.11c) to (4.11h) are satisfied for each base station. In addition, when the minimum rate requirement of the users increases, some users may not be allocated any resources to decrease the overall outage probabilities of the network. When this is the case, the minimum rate requirement of these users cannot be satisfied with the power control algorithm. Therefore, we exclude these users from the power control problem and define sets of MUEs and PUEs that are assigned to at least one resource block as $\mathcal{K}^U_{M,s}$ and $\mathcal{K}^U_{P,s}$, respectively. When we write the Lagrangian of the problem (4.11) for the remaining

constraints and users, we obtain

$$\begin{aligned}\mathcal{L}_s(\mathbf{x}_s) =&(1-\alpha)\eta_s(\boldsymbol{\varepsilon},\boldsymbol{\beta})+\alpha\frac{W_{tot}}{P_s}\nu_s(\boldsymbol{\varepsilon},\boldsymbol{\beta})-\theta_s(\varepsilon_s,\boldsymbol{\beta_s})-\sum_{k\in\mathcal{K}^U_{M,s}}\lambda_{k,s}\big(R_{\min,k}\\ &-(\boldsymbol{C}^k_{M,s}\boldsymbol{F}^{(k,:)}_{M,s}\boldsymbol{R}^{(:,k)}_1+(1-\boldsymbol{C}^k_{M,s})\boldsymbol{F}^{(k,:)}_{M,s}\boldsymbol{R}^{(:,k)}_2)\big)\\ &+\sum_{k\in\mathcal{K}^U_{P,s}}\lambda_{k,s}\big(R_{\min,k}-(\boldsymbol{C}^k_{M,s}\boldsymbol{F}^{(k,:)}_{M,s}\boldsymbol{R}^{(:,k)}_3+(1-\boldsymbol{C}^k_{M,s})\boldsymbol{F}^{(k,:)}_{M,s}\boldsymbol{R}^{(:,k)}_4)\big)\\ &+\tau^L_M\beta_M+\tau^U_M(1-\beta_M)+\sum_{P\in\mathcal{N}_{\text{Pico},s}}\tau^L_P\beta_P+\sum_{P\in\mathcal{N}_{\text{Pico},s}}\tau^U_P(1-\beta_P)+\rho_s\varepsilon_M.\end{aligned}\tag{4.12}$$

For simplicity, we will use $\mathcal{L}_s(\mathbf{x}_s)$ for $\mathcal{L}(\varepsilon_s,\boldsymbol{\beta}_s,\boldsymbol{\lambda},\boldsymbol{\tau^L}_s,\boldsymbol{\tau^U}_s,\rho_s)$ throughout the rest of the chapter.

In this chapter, the transmission power of the MBS M depends on β_M and ε_M and the transmission power of the Pico-BS P depends on β_P. The interference pricing function accounts for the interference that all base stations in the sector s are subject to. We define a vector, $\mathbf{z}_s=[\beta_M\ \ \varepsilon_M\ \ \beta^1_P\dots\beta^{N_{P,s}}_P]$ where $N_{P,s}$ is the number of Pico-BSs in sector s. Then, we can write the interference pricing function as follows

$$\theta_s(\varepsilon_s,\boldsymbol{\beta}_s)=\mathbf{z}^T_s\sum_{\substack{s'\in\mathcal{S}\\ s'\neq s}}\nabla_{\mathbf{z}_s}\mathcal{L}_{s'}(\mathbf{x}_{s'}).\tag{4.13}$$

The pricing function reflects the marginal costs of the variables β_M, ε_M, and β_Ps for all Pico-BSs.

In each sector, there are $2+N_{Picos}$ power control parameters. In order to obtain the optimum power control parameters, we will employ the Levenberg-Marquardt method. The Levenberg-Marquardt method is a variant of the Newton method. The Newton method provides quadratic convergence. The quadratic approximation of the Lagrangian function in

(4.12) can be expressed as

$$g(\mathbf{z}) = \mathcal{L}_s(\mathbf{x}_s) + \nabla\mathcal{L}_s(\mathbf{x}_s)^T(\mathbf{z} - \mathbf{z}_s^{(t,l)}) + \frac{1}{2}(\mathbf{z} - \mathbf{z}_s^{(t,l)})^T\nabla^2\mathcal{L}_s(\mathbf{x}_s)(\mathbf{z} - \mathbf{z}_s^{(t,l)}), \tag{4.14}$$

where l and t denote the Newton iteration and time instant, respectively. The Hessian matrix of the $\mathcal{L}_s(\mathbf{x}_s)$ at $\mathbf{z}_s^{(t,l)}$ is denoted by $\nabla^2\mathcal{L}_s(\mathbf{x}_s)$. However, the Newton method does not guarantee convergence [71]. The reason behind this is that the Hessian matrix can be singular or the direction may not be correct. In order to overcome this problem, several methods have been investigated in the literature [71, 72]. In this chapter, we employ the Levenberg-Marquardt method due to its guarantee of convergence. Then, the power control parameters that maximize $g(\mathbf{z})$ can be obtained by

$$\mathbf{z}_s^{(t,l+1)} = \mathbf{z}_s^{(t,l)} - \mu_l(\nabla^2\mathcal{L}_s^{(l)}(\mathbf{x}_s) - \xi\mathbf{I})^{-1}\nabla\mathcal{L}_s^{(l)}(\mathbf{x}_s), \tag{4.15}$$

where $\mathbf{I}$ is the identity matrix. The term $\xi\mathbf{I}$ should be selected in such a way that all the eigenvalues of $\mathbf{D} = (\nabla^2\mathcal{L}_s^{(l)}(\mathbf{x}_s) - \xi\mathbf{I})$ are negative. This approach guarantees that $\mathbf{D}$ is negative definite. The parameter ξ should be selected larger than the highest positive eigenvalue of the $\nabla^2\mathcal{L}_s^{(l)}(\mathbf{x}_s)$. If all eigenvalues of $\nabla^2\mathcal{L}_s^{(l)}(\mathbf{x}_s)$ are already negative, then ξ should be selected as 0 and the Levenberg-Marquardt works as the Netwon method. The proposed algorithm is depicted under the heading Algorithm 6. The parameter $l_{\max}$ is the maximum number of iterations, and ϵ is a control parameter to determine when to exit the algorithm when the change between two iterations is sufficiently small. We use a controlled increase mechanism for the power control updates. If the difference between the power control parameters during two consecutive time instants is large, this may cause the interference pricing mechanism not to accurately estimate the interference prices [36]. Therefore, we employ the controlled increase mechanism in this chapter. The controlled increase mechanism in Step 17 prevents the base stations from changing their transmission powers by a large amount. Therefore, the estimation of the interference levels at the other

Algorithm 6 Proposed Power Control Algorithm with Pricing

Initialize: $\mathbf{z}_s^{(t,0)} = (\varepsilon_M^{(t-1,l_{max}+1)} \;\; \boldsymbol{\beta}_s^{(t-1,l_{max}+1)^T})$ and set $l = 0$
% Each sector solves (4.12) by using the Levenberg-Marquardt Method
for $l := 1$ to $l_{\max}$ **do**
  if $\omega_{\max} = \max(\text{eig}(\nabla^2_{\mathbf{z}} \mathcal{L}_s^{(l)}(\mathbf{x}_s))) < 0$ **then**
    $\xi = 0$.
  else
    $\xi = \omega_{\max} + \sigma$.
  end if
  $\mathbf{d}_l^{LM} = -(\nabla^2 \mathcal{L}_s^{(l)}(\mathbf{x}_s) - \xi \mathbf{I})^{-1} \nabla \mathcal{L}_s^{(l)}(\mathbf{x}_s)$.
  Update the power control parameters, $\mathbf{z}_s^{(l+1)}$, using

$$\mathbf{z}_s^{(t,l+1)} = \mathbf{z}_s^{(t,l)} + \mu_l \mathbf{d}_l^{LM},$$

  Update the Lagrange multiplier, $\lambda_{k,s}^{(l+1)}$ for all $k \in \mathcal{K}_{M,s}^U$, using

$$\lambda_{k,s}^{(l+1)} = \left[\lambda_{k,s}^{(l)} + \phi_{k,s} \big(R_{\min,k} - (\boldsymbol{C}_{M,s}^k \boldsymbol{F}_{M,s}^{(k,:)} \boldsymbol{R}_1^{(:,k)} + (1 - \boldsymbol{C}_{M,s}^k) \boldsymbol{F}_{M,s}^{(k,:)} \boldsymbol{R}_2^{(:,k)}) \big) \right]^+.$$

  Update the Lagrange multiplier, $\lambda_{k,s}^{(l+1)}$ for all $k \in \mathcal{K}_{P,s}^U$, using

$$\lambda_{k,s}^{(l+1)} = \left[\lambda_{k,s}^{(l)} + \phi_{k,s} \big(R_{\min,k} - (\boldsymbol{C}_{M,s}^k \boldsymbol{F}_{M,s}^{(k,:)} \boldsymbol{R}_3^{(:,k)} + (1 - \boldsymbol{C}_{M,s}^k) \boldsymbol{F}_{M,s}^{(k,:)} \boldsymbol{R}_4^{(:,k)}) \big) \right]^+.$$

  if $\left| \nabla \mathcal{L}_s^T \mathbf{d}_l^{LM} \right| \leq \epsilon$ **then**
    Break
  end if
end for
$\mathbf{z}_s^{(t,l_{max}+1)} = (1 - \zeta) \mathbf{z}_s^{(t-1,l_{max}+1)} + \zeta \mathbf{z}_s^{(t,l_{max})}$
Price Update: Each user calculates interference prices and feds these values back to its base station.
Interference prices are distributed among base stations.
Go to Step 2 and repeat.

sectors is accurate. However, the parameter ζ in Algorithm 6 should be selected optimally. Small ζ slows down the algorithm and convergence takes too much time. On the other hand, large ζ fails the purpose of the controlled increase mechanism. Therefore we use an adaptive ζ in this chapter. The parameter ζ depends on the current time instant. It is selected as $t/(2t+1)$ [34].

Complexity Analysis

The main computational effort of the proposed algorithm is taking the inverse of the matrix $\mathbf{D} = (\nabla^2 \mathcal{L}_s^{(l)} - \xi \mathbf{I})$. Therefore, the complexity of the proposed power control increases with the number of power control parameters. When the number of Pico-BSs in the sector increases, the complexity of the algorithm increases with N_{Picos}^3. For example, when there are 2 Pico-BSs in each sector, the matrix becomes 4×4 and taking the inverse of this matrix is straightforward. However, the Pico-BSs are expected to be significantly dense in the future [2]. Taking the inverse of the matrix may not be feasible in real time. Therefore, to overcome this problem, we also propose a suboptimal algorithm. The proposed suboptimal algorithm significantly reduces the complexity of the algorithm and the complexity of the algorithm will be independent of the number of Pico-BSs in the sector.

Suboptimal Power Control Algorithm

In the optimal algorithm, all base stations in the sector update their power control parameters together. Therefore, the optimal algorithm reaches the power control parameters that maximize the Lagrangian function. However, this requires calculation of the inverse of matrix $\mathbf{D}$ at every iteration. This becomes computationally costly when the number of Pico-BSs in the sector increases. Therefore, we propose a suboptimal algorithm that calculates the power control parameters of the MBS and Pico-BSs separately. Each base station assumes that the power control parameters of the other base stations in the same sector are constant during updates. The Hessian matrix $\mathbf{D}$ will become 2×2 for MBSs. In addition, Pico-BSs calculate their own power control parameter. Each Pico-BS has only one power control parameter. In simulation results, we will compare the performance of the suboptimal algorithm with the optimal power control algorithm.

4.5 Numerical Results

In this section, we evaluate the performance of the proposed algorithm. First, we investigate the effect of the parameter α over energy efficiency and spectral efficiency. We show that the proposed algorithm achieves the Pareto optimal solution for all α values. Second, we investigate the effect of the parameter α on outage probabilities. We show that smaller α (i.e., maximizing the energy efficiency of the network) performs better than maximizing spectral efficiency in terms of outage probabilities for this particular setting. Third, we investigate the performance of the proposed frequency assignment algorithm. We evaluate the usage rate of the subbands with different α values and rate constraints. We show that fewer resource blocks are assigned to the users when α and rate constraints increase. Fourth, we investigate the power consumption of the base stations with different α values and minimum rate requirements. We show that MBSs and Pico-BSs show different behaviors with increasing rate constraints. While average transmission powers of the MBSs increase with the rate requirements of the users, the average transmission power of the Pico-BSs decreases. Last, we study the performance of the optimum and suboptimal algorithms. We show that the performance of the proposed suboptimal algorithm is close to the optimal algorithm.

First, we will describe our simulation environment. In the FFR method, we distribute the 50 resource blocks with the following approach. First, 14 resource blocks are assigned to subband A, and then the remaining 36 are evenly distributed among the subbandds B, C, and D. In our simulation area, 19 MBSs are deployed and each cell is divided into 3 sectors. Therefore, our simulation area has been divided into 57 sectors. We use the wraparound technique to avoid edge effects. In each sector, two Pico-BSs are randomly deployed. Both MBS and Pico-BSs employ single antennas, i.e., $N_{TRX,M} = 1$ and $N_{TRX,P} = 1$. In each sector, we generate 20 users. First, we generate two users within 40 meters radius of the Pico-BSs. Then, the rest of the users are randomly generated under the settings in Table 4.2. The highest RSRP method is used for the cell associations. Even though we generate two

Table 4.2: Simulation Parameters

Parameter	**Setting**
Channel bandwidth	10 MHz
Total number of RBs	50 RBs
Freq. selective channel model (CM)	Extended Typical Urban CM
UE to MBS PL model	$128.1 + 37.6 \log_{10}(d)$
UE to Pico eNB PL model	$140.7 + 36.7 \log_{10}(d)$
Effective thermal noise power, N_0	-174 dBm/Hz
UE noise figures	9 dB
MBS and Pico eNB antenna gain	14 dBi and 5 dBi
UE antenna gain	0 dBi
Antenna horizontal pattern, $A(\theta)$	$-\min(12(\theta/\theta_{3\text{dB}})^2, A_m)$
A_m and $\theta_{3\text{dB}}$	20 dB and 70°
Penetration loss	20 dB
Macrocell and picocell shadowing	8 dB and 10 dB
Inter-site distance	500 m
Minimum MBS to user distance	50 m
Minimum Pico-BS to user distance	10 m
Minimum Pico-BS to MBS distance	75 m
Minimum Pico-BS to Pico-BS distance	40 m
Traffic model	Full buffer
Power Consumption Parameters	MBS: (130W, 75W, 46dBm, 4.7)
(P_0, P_{sleep}, $P_{\max}$, Δ)	Pico-eNB: (56W, 39W, 30dBm, 2.6)

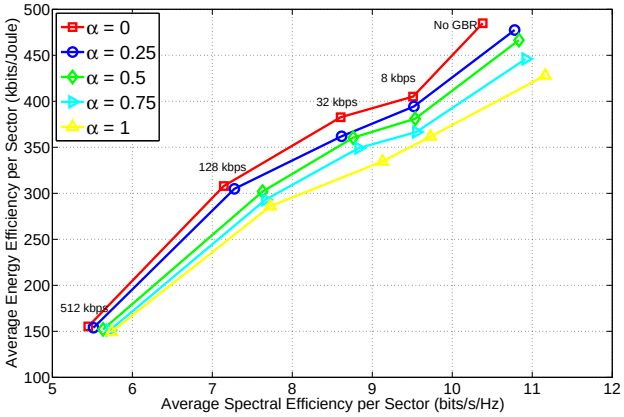

Figure 4.3: The average energy efficiency versus average spectral efficiency per sector for different α values.

users close to Pico-BSs, they are not forced to associate with the Pico-BSs. The rest of the simulation parameters are given in Table 4.2 [24].

Figure 4.3 illustrates the average energy efficiency and the spectral efficiency of the sectors for different α values for five cases. In the first case, users do not have any rate constraints. For the other cases, the following rate constraints are enforced: 8 kbps, 32 kbps, 128 kbps, and 512 kbps. As expected, the average energy efficiency of the network decreases with α

for all cases. When users do not have minimum rate constraint and α is equal to 0, the average energy efficiency of the network reaches its highest point and it becomes 484.83 kbits/Joule. When we increase α for this case, the energy efficiency of the network decreases with α as expected. When α becomes 1 (i.e., the objective becomes maximizing the spectral efficiency of the network), the average energy efficiency drops by 13%. When the parameter α increases, the transmission power of the MBSs increases with α in order to increase the spectral efficiency. For example, the average transmission power of the MBSs increases from 23.94dB to 29.68dB when α increases from 0 to 1. Although this change increases the spectral efficiency of the network by 7%, it also causes the MBSs to work in the energy-inefficient regions. In other words, by increasing α from 0 to 1, 13% energy efficiency sacrifice can be turned into 7% gain in terms of spectral efficiency when users do not have any rate requirements. On the other hand, the average transmission power of Pico-BSs is not affected by α when users do not have minimum rate constraints and they always transmit at the full power. Due to the fact that the power consumptions of Pico-BSs are less than those of the MBSs and the distance between Pico-BSs and the associated users is low, both energy efficiency and spectral efficiency of the Pico-BSs increase with parameter β within the given ranges. In other words, the most energy-efficient state and the most spectrally-efficient state coincide for these base stations. When users have minimum rate constraints, both energy efficiency and spectral efficiency of the network decrease. The cumulative effect of the following reasons cause this drop. First, in order to satisfy the rate requirements of users, MBSs further increase their transmission powers to energy-inefficient levels. This increase elevates the cross-tier interference from MBS to cell-edge Pico-BSs on Subband A and also intercell interference in the network. Second, the frequency assignment algorithm favors users that cannot satisfy their rate requirement. These users usually have worse channel conditions than the other users. Therefore, both energy efficiency and spectral efficiency are harmed by the change in frequency assignment. As a result of all these factors, both energy efficiency and the spectral efficiency of the network decrease with the minimum rate

Table 4.3: The outage probabilities of users for different α values

	Outage probability			
Minimum	$\alpha = 0$		$\alpha = 1$	
GBR (kbps)	MUE	PUE	MUE	PUE
8	0.8%	0%	1.1%	0%
32	1.7%	0%	2.4%	0%
128	3.1%	0.6%	4.3%	0.6%
512	9.6%	2%	12.3%	0.6%

requirements of the users. In addition, when we increase the minimum rate requirements of the users, the effect of the parameter α on energy efficiency and spectral efficiency decreases. For example, as specified earlier, 7% spectral efficiency loss can be turned into 13% energy efficiency gain when users do not have any rate requirements. On the other hand, when the minimum rate requirements of users are 512 kbps, 5% spectral efficiency loss can only be turned into 4% energy efficiency gain. These results show that when users have minimum rate requirements, the proposed algorithm prioritizes satisfying the rate requirements of more users and the effect of parameter α on energy efficiency and spectral efficiency decreases. Note from Figure 4.3 that for the no-rate-constraint-case, improving energy efficiency decreases spectral efficiency and vice versa. Therefore, all points on this curve $(\eta_s(\boldsymbol{\varepsilon}, \boldsymbol{\beta}), \nu_s(\boldsymbol{\varepsilon}, \boldsymbol{\beta}))$ are Pareto optimal for $0 \leq \alpha \leq 1$.

Second, we investigate the relation between the parameter α and outage probabilities. In Table 4.3, we investigate four cases, the minimum rate requirements of users are 8 kbps, 32 kbps, 128 kbps, and 512 kbps. The outage probability is not defined when users do not have a minimum rate requirement. In our network, we have two different type of users: MUEs and PUEs. First, we observe that when we increase the parameter α, the outage probabilities of the MUEs increase with α for all four cases. For example, when the minimum rate requirement of the users is 512 kbps, changing α from 0 to 1 increases the outage probability of MUEs from 9.6% to 12.3%. Similar behavior can also be observed for the other cases. When the parameter α increases, the transmission powers of MBSs and Pico-

BSs increase with this parameter. For example, when we change the parameter α from 0 to 1, the transmission powers of the Pico-BSs increase from 27.7dBm to 28.4dBm for the case that minimum rate requirements of the users are 512 kbps. Although this change increases the average spectral efficiency of the network, cross-tier interference from Pico-BSs to MUEs increases the outage probability of MUEs. In the same manner, the transmission power increase of MBSs elevates the intercell interference and that is another reason of the increased outage probabilities. On the other hand, the outage probabilities of the PUEs only exists when the minimum rate requirements of users are high. However, even for the worst case, only 2% of the PUEs could not satisfy their rate requirements. In the network, PUEs are located close to their associated Pico-BSs and they have significantly better channel conditions than the MUEs. In addition, the number of PUEs that are associated with each Pico-BS is significantly lower. Therefore, more resource blocks are assigned to these users on average. As a result, PUEs can satisfy their rate requirements easier than MUEs.

Figures 4.4(a-d) show the average usage rate of the subbands A by MBSs, subbands A by Pico-BSs, subbands B, C, and D by MBSs, and subbands B, C, and D by Pico-BSs, respectively. First, we observe that when we increase the minimum rate requirements of the users, the usage of the resource blocks by MBSs decreases. The second part of the proposed frequency assignment algorithm decreases the number of assigned resource blocks and transmits on the fewer resource blocks. For example, MBSs use almost all assigned resource blocks for all different α values when users do not have minimum rate requirements. However, when users have minimum rate requirements, MBSs decide not to assign some of the available resource blocks. When the minimum rate requirements of the users increase, intercell interference becomes a more significant problem, due to the fact that base stations increase their transmission power to satisfy the rate requirements of their users. In order to alleviate the interference, base stations do not assign the resource blocks that do not increase the energy efficiency and spectral efficiency while creating significant interference to other base stations. Figure 4.4(b) illustrates that usage rate of subband A by Pico-BSs

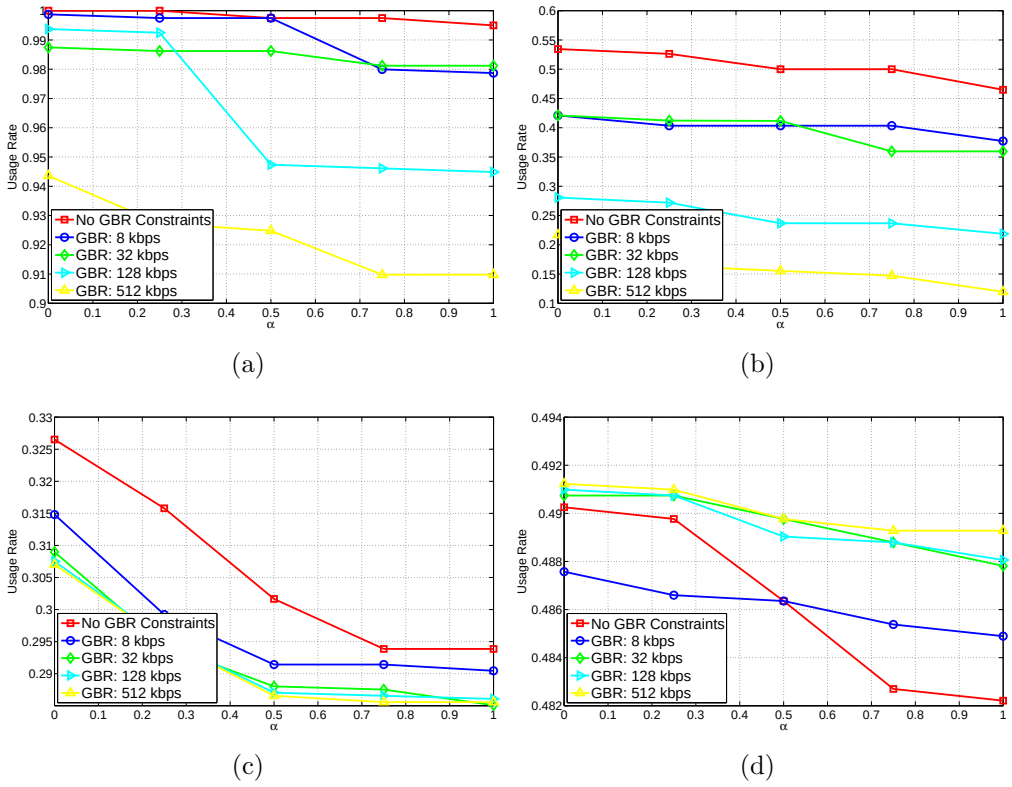

Figure 4.4: Average Usage Rate of Subband A by MBSs (a), Average Usage Rate of Subband A by Pico-BSs (b), Average Usage Rate of Subbands B, C, and D by MBSs (c), Average Usage Rate of Subbands B, C, and D by Pico-BSs (d) for different α values.

significantly decreases when we increase the minimum rate of the users. The reason for this decrease is twofold. First, cell-edge Pico-BSs do not assign some resource blocks on subband A to help satisfy the minimum rate constraints of the cell-center MUEs in the same sector. Second, cell-center radii expand with the minimum rate requirements. Therefore, the number of Pico-BSs that are located in the cell-edge region decreases and fewer Pico-BSs will use subband A. Another important observation is when we increase the parameter α, the usage of the resource blocks further decreases. In order to increase the spectral efficiency of the network, base stations decide to transmit on the resource blocks that have better channel quality and do not assign the others to increase the overall spectral efficiency of the network. Therefore, when we increase α, the subband usage further decreases to improve the spectral efficiency of the network.

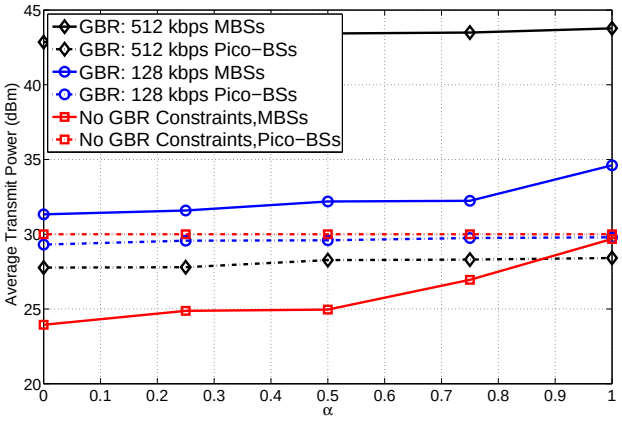

Figure 4.5: The average transmission power of MBSs and Pico-BSs for different α values for different rate requirements.

Figure 4.5 shows the average power consumption of the MBSs and Pico-BSs for the following cases: No rate requirement and rate requirements equal to 128 kbps and 512 kbps. Similar observations can be made for the other rate requirements. As expected, when we increase the minimum rate requirements, the transmission power of the MBSs increases. On the other hand, under the same conditions, the transmission power of the Pico-BSs decreases. The increase of the minimum rate constraints causes outage of the more MUEs. In order to satisfy these users' rate requirements, MBSs increase their transmission power, increase the interference prices, and assign more resource blocks to these users. Elevated interference prices force some of the Pico-BSs to decrease their transmission power to help satisfy the rate requirements of more MUEs. Therefore, the average transmission power of the Pico-BSs decreases with the minimum rate requirements. In addition, the average transmission power of both MBSs and Pico-BSs increases with parameter α to increase the spectral efficiency of the network.

Figure 4.6 compares the performance of the suboptimal and optimal power control algorithms in terms of energy efficiency and spectral efficiency when the minimum rate requirements of users are 128 kbps. The performance of both algorithms is similar. When $\alpha = 0$, the optimal algorithm performs 3.2% better than the suboptimal algorithm. On the other hand, when

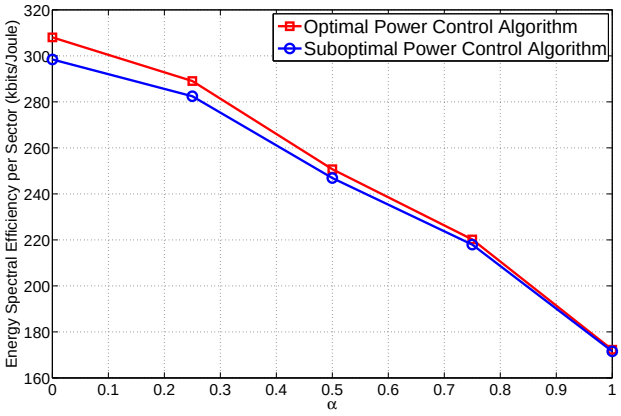

Figure 4.6: The average energy spectral efficiency of network for different α values when minimum rate constraints are 128 kbps.

$\alpha = 1$, the performance difference drops to 0.4%. In the suboptimal power control algorithm, MBS and Pico-BSs update their power control parameters separately. The transmission powers of the base stations increase with the parameter α, therefore the difference between the performance of these algorithms decreases.

4.6 Conclusion

In this chapter, we studied the energy efficiency and spectral efficiency tradeoffs in multi-cell heterogeneous wireless networks. We defined the problem as multi-objective optimization and proposed a cell-center radius selection algorithm, a scheduling algorithm, and a power control algorithm that solve these problems separately. The proposed algorithm also includes the minimum rate requirements of users to the given problem. A dynamic cell-center radius selection algorithm is proposed to determine the available resources to the base stations. In addition, the proposed scheduling mechanism has distributed the resources to users in order to satisfy the minimum rate requirements of them and also to maximize our objective metric. Furthermore, we employed a Levenberg-Marquardt method-based power allocation algorithm to solve the power control problem. Based on our results, first the tradeoff between

energy efficiency and spectral efficiency can be adjusted via the weight of the multi-objective function. We can obtain 13% improvement in terms of energy efficiency by sacrificing 7% spectral efficiency. In addition, our results show that the most energy-efficient state and the most spectral efficient state coincide for the Pico-BSs. Second, while we increase the spectral efficiency of the network, it also increases the outage probabilities of the network due to the increased intercell-interference. Third, we showed that the number of resource blocks that are transmitted can be reduced by increasing the minimum rate constraints or the parameter α. Fourth, we demonstrated that while the transmission powers of the MBSs increase with the minimum rate constraints of the users, the transmission power of Pico-BSs decreases. Last, we studied the optimal and a suboptimal power control algorithms. We showed that these algorithms perform similarly and increasing the parameter α, shrinks the gap between these algorithms.

Chapter 5

Conclusion and Future Works

In this dissertation, we investigated energy efficiency and spectral efficiency in wireless heterogeneous networks. It is discussed that data demand of the users will increase tremendously, therefore the network operators should prepare to meet this demand. First, benefits of deploying more small cell base stations is discussed. Second, the environmental and economical effects of spectral efficiency increase are pointed out and energy-efficient solutions are addressed. Third, deployment of small cell base stations is examined and investigated to solve the problem. In particular, deployment of the small cell base station, energy-efficient resource allocation in heterogeneous networks, and both energy- and spectral-efficient resource allocation in heterogeneous networks are investigated in this dissertation.

In Chapter 2, energy-efficient base station deployment was investigated. Deployment of microcell base stations can increase the throughput and energy efficiency of the network tremendously if they are deployed in the appropriate amount. If they are deployed at too large numbers, they can decrease the energy efficiency of the network. In this dissertation, a greedy base station deployment algorithm was proposed for the base station deployment problem. The proposed algorithm first selects a subset of feasible locations as candidate

locations, and then greedily deploys these base stations to meet the required capacity increase. The proposed algorithm performs better than the constant-factor approximation of the optimum solution. In this dissertation, deployment and operational costs of the base stations are not included into the problem. For example, depending on the terrestrial conditions, the rental cost may vary. Therefore, as a future work, investigating the same problem with including these costs and the total budget constraints would be an interesting and more realistic problem.

In Chapter 3, the energy efficiency aspect of the small cell base station deployment was investigated. The proposed algorithm separates cell-center radius selection, frequency assignment, and power allocation problems and solves them iteratively. First, an iterative cell-center radius selection algorithm is proposed to find the optimum cell-center radius for the FFR algorithm. Second, the frequency resources are assigned to users to maximize the Lagrangian function. Last, optimum transmission power is obtained by a Levenberg-Marquard based-method. It is shown that significant energy savings can be achieved with reduced outage probabilities. In Chapter 3, single antenna transmission is considered only. As a future work, considering multiple antenna transmission can be a new research direction.

Chapter 4 addressed energy efficiency and spectral efficiency tradeoff in multi-cell multi-tier wireless networks. The problem is defined as a multi-objective optimization problem. We defined the objective function as a weighted summation of energy efficiency and spectral efficiency functions. We included the minimum rate requirements of the users in the problem by dual decomposition techniques. We decoupled the problem as the cell-center radius selection problem, a scheduling problem, and a power control problem. We proposed a three-stage algorithm that solves these problems iteratively until convergence. In the first stage, the cell-center radius is determined with a heuristic algorithm. The cell-center radius is updated every iteration. In the second stage, frequency resources are assigned to the users. In the third stage, optimum transmission powers are determined. It is shown that

a Pareto optimum solution exists for energy efficiency and spectral efficiency. Sacrifices in terms of energy efficiency can be transformed to gains in terms of spectral efficiency and vice versa. In Chapter 4, outage probabilities of users are investigated and it is shown that spectral-efficient solutions causes higher outage probabilities. In addition, the relation between resource allocation and minimum rate constraints are addressed. It is shown that fewer resource blocks are assigned to users when the minimum rate constraints increase. Moreover, it is demonstrated that transmission powers of the MBSs increase with the minimum rate constraints while transmission powers of the Pico-BSs decrease.

Appendix A

The Detailed Expressions of the Terms

In what follows, we obtain an exact expression for the pricing function employed. Our goal is to quantify how the utility of a sector s' changes when there is a unit increase in the variables ε and β of sector s. Let us rewrite the utility of sector s' as

$$\begin{aligned}\mathcal{L}(\mathbf{x}_s, \boldsymbol{\lambda}, \nu_s, \tau_s, \rho_s) =& \eta_s(\mathbf{x}_s) - \theta_s(\mathbf{x}_s) - \sum_{k \in \mathcal{K}_{M,s}} \lambda_{l,s}\big(R_{\min,l} - (\boldsymbol{C}^l_{M,s}\boldsymbol{F}^{(l,:)}_{M,s}\boldsymbol{R}^{(:,l)}_1 \\ &+ (1 - \boldsymbol{C}^l_{M,s})\boldsymbol{F}^{(l,:)}_{M,s}\boldsymbol{R}^{(:,l)}_2)\big) - \sum_{k \in \mathcal{K}_{P,s}} \lambda_{l,s}\big(R_{\min,l} - (\boldsymbol{C}^l_{P,s}\boldsymbol{F}^{(l,:)}_{P,s}\boldsymbol{R}^{(:,l)}_3 \\ &+ (1 - \boldsymbol{C}^l_{P,s})\boldsymbol{F}^{(l,:)}_{P,s}\boldsymbol{R}^{(:,l)}_4)\big) + \nu_s\beta_s + \tau_s(1 - \beta_s) + \rho_s\varepsilon_s.\end{aligned} \tag{A.1}$$

where $\mathcal{K}_{M,s'}$ denotes the set of MUEs associated with the MBS m'. The parameter $R_{\min,l}$ is the minimum rate constraint of user l. The region of MUE l whether in cell-center or not is indicated by $\boldsymbol{C}^l_{M,s}$. The region of PUE l whether in cell-center or not is indicated by $\boldsymbol{C}^l_{P,s}$.

Whether the subcarrier n is assigned to MUE l or not is indicated by $\boldsymbol{F}_{M,s}^{(l,n)}$. Whether the subcarrier n is assigned to PUE l or not is indicated by $\boldsymbol{F}_{P,s}^{(l,n)}$. The parameters $\lambda_{l,s'}$, ν'_s, τ'_s, and ρ'_s denote the Lagrange multiplier associated with the rate constraint of user l in sector s', the Lagrange multiplier associated with lower and upper bound on β'_s, and the lower bound on ε'_s, respectively. If we denote the interference incurred by user l on subcarrier n is $I^{(l,n)}$, by using the chain rule, we can write partial derivatives, $\partial\mathcal{L}_{s'}/\partial\varepsilon'_s$ and $\partial\mathcal{L}_{s'}/\partial\beta_s$, as

$$\begin{aligned}\frac{\partial\mathcal{L}_{s'}}{\partial\varepsilon_s} =&\frac{\partial\mathcal{L}_{s'}}{\partial I^{(l,n)}}\cdot\frac{\partial I^{(l,n)}}{\partial p_M^{(n)}}\cdot\frac{\partial p_m^{(n)}}{\partial\varepsilon_s} = -\pi_{k,l}^{(n)}g_{l,m}^{(n)}\cdot\frac{\partial p_M^{(n)}}{\partial\varepsilon_s},\\ \frac{\partial\mathcal{L}_{s'}}{\partial\beta_s} =&\frac{\partial\mathcal{L}_{s'}}{\partial I^{(l,n)}}\cdot\frac{\partial I^{(l,n)}}{\partial p_M^{(n)}}\cdot\frac{\partial p_M^{(n)}}{\partial\beta_s} = -\pi_{k,l}^{(n)}g_{l,m}^{(n)}\cdot\frac{\partial p_m^{(n)}}{\partial\beta_s},\end{aligned} \tag{A.2}$$

where $g_{l,m}^{(n)}$ is the channel gain of the interfering link between MBS M and user l on subcarrier n. This term weights the interference created to the users in other sectors. The interference price from user k in sector s to user l in sector s' on subcarrier n can be expressed as

$$\pi_{k,l}^{(n)} = -\frac{\partial\mathcal{L}_{s'}}{\partial I^{(l,n)}} = (\lambda_{l,s'}+\frac{1}{\psi_{s'}})\cdot\frac{\Delta_n}{\ln(2)}\cdot\frac{\gamma_l}{1+\gamma_l}\cdot\frac{1}{I^{(l,n)}+N_0\Delta_n}, \tag{A.3}$$

where $\gamma_l^{(n)}$ denotes the SINR of user l on subcarrier n. Thus, we can rewrite (4.13) as

$$\theta_s(\varepsilon,\beta) = \sum_{n\in\mathcal{N}_M}\varepsilon_s\sum_{l\neq k,\,l\in\mathcal{K}^{(n)}}\pi_{k,l}^{(n)}g_{l,M}^{(n)}\cdot\frac{\partial p_M^{(n)}}{\partial\varepsilon_s} + \sum_{n\in\mathcal{N}_M}\beta_s\sum_{l\neq k,\,l\in\mathcal{K}^{(n)}}\pi_{k,l}^{(n)}g_{l,M}^{(n)}\cdot\frac{\partial p_M^{(n)}}{\partial\beta_s}. \tag{A.4}$$

Note that the MBS transmit power on subcarrier n depends on the subband. For the FFR scheme in Fig. 4.1, it takes the value $p_M^{(n)} = P_M$ for the subcarriers allocated to the cell-center region, whereas it is $p_M^{(n)} = \varepsilon P_M$ for the subcarriers allocated to the cell-edge region.

Appendix B

Proof of Quasiconcavity

In what follows, we prove that $F_s^{EE-SE} = (1-\alpha)\eta_s(\boldsymbol{\varepsilon}, \boldsymbol{\beta}) + \alpha\frac{W_{tot}}{P_s}\nu_s(\boldsymbol{\varepsilon}, \boldsymbol{\beta})$ is quasiconcave in ε_s and $\boldsymbol{\beta_s}$. We will demonstrate the proof for one Pico-BS case for Sector 1 but it can be extended to multiple Pico-BS case by using the same approach.

First, let's rewrite the F_s^{EE-SE} function

$$\begin{aligned} F_s^{EE-SE} =& (\frac{(1-\alpha)}{\psi_s(\boldsymbol{\beta_s})} + \frac{\alpha\frac{W_{tot}}{P_s}}{W_s})(\sum_{k\in\mathcal{K}_{M,s}} (\boldsymbol{C}_{M,s}^k \boldsymbol{F}_{M,s}^{(k,:)} \boldsymbol{R}_1^{(:,k)} + (1-\boldsymbol{C}_{M,s}^k)\boldsymbol{F}_{M,s}^{(k,:)}\boldsymbol{R}_2^{(:,k)}) \\ &+ \sum_{k\in\mathcal{K}_{P,s}} (\boldsymbol{C}_{P,s}^k \boldsymbol{F}_{P,s}^{(k,:)} \boldsymbol{R}_3^{(:,k)} + (1-\boldsymbol{C}_{P,s}^k)\boldsymbol{F}_{P,s}^{(k,:)}\boldsymbol{R}_4^{(:,k)})). \end{aligned} \tag{B.1}$$

The function F_s^{EE-SE} is a quasiconcave if and only if the following property holds

$$\mathbf{z}_s^T \nabla F_s^{EE-SE} = 0 \text{ and } \mathbf{z}_s^T \nabla^2 F_s^{EE-SE} \mathbf{z}_s \leq 0 \tag{B.2}$$

where $\mathbf{z}_s = [\beta_M \;\; \varepsilon_M \;\; \beta_P]^T$.

First, we introduce new definitions for the proof, and then express the first and second order

derivatives. Let R_s denote the aggregate throughput of sector s which is given by

$$\begin{aligned} R_s = &\sum_{k \in \mathcal{K}_{M,s}} (\boldsymbol{C}^k_{M,s} \boldsymbol{F}^{(k,:)}_{M,s} \boldsymbol{R}^{(:,k)}_1 + (1 - \boldsymbol{C}^k_{M,s}) \boldsymbol{F}^{(k,:)}_{M,s} \boldsymbol{R}^{(:,k)}_2) \\ &+ \sum_{k \in \mathcal{K}_{P,s}} (\boldsymbol{C}^k_{P,s} \boldsymbol{F}^{(k,:)}_{P,s} \boldsymbol{R}^{(:,k)}_3 + (1 - \boldsymbol{C}^k_{P,s}) \boldsymbol{F}^{(k,:)}_{P,s} \boldsymbol{R}^{(:,k)}_4), \end{aligned} \tag{B.3}$$

where

$$\begin{aligned} R^{(n,k)}_1 =& \Delta_n \log\left(1 + \frac{\beta_M a}{b + \varepsilon_M c}\right), \qquad & R^{(n,k)}_2 =& \Delta_n \log\left(1 + \frac{\varepsilon \beta_M a}{b + \varepsilon_M c}\right), \\ R^{(n,k)}_3 =& \Delta_n \log\left(1 + \frac{\beta_P d}{f}\right), & R^{(n,k)}_4 =& \Delta_n \log\left(1 + \frac{\beta_P d}{g}\right), \end{aligned} \tag{B.4}$$

where $a = P_{\max,M} g^{(n)}_{k,M} / I^{(n)}_{k,M}$, $b = N_A$, $c = N_B$, $d = P_{\max,P} g^{(n)}_{k,P} / I^{(n)}_{k,P}$, $f = N_C + N_D$, and $g = N_A + N_C + N_D$. The term $I^{(n)}_{k,M}$ corresponds to $\sum_{\substack{M' \in \mathcal{B}_M \\ M' \neq M}} P^{(n)}_{M'} g^{(n)}_{k,M'} + \sum_{P \in \mathcal{B}_P} P^{(n)}_P g^{(n)}_{k,P} + N_0 \Delta_n$ and $I^{(n)}_{k,P}$ is $\sum_{M' \in \mathcal{B}_M} P^{(n)}_{M'} g^{(n)}_{k,M'} + \sum_{\substack{P' \in \mathcal{B}_P \\ P' \neq P}} P^{(n)}_{P'} g^{(n)}_{k,P'} + N_0 \Delta_n$. Using these definitions, the first derivative of R_s with respect to β_M is

$$\begin{aligned} \frac{\partial R_s}{\partial \beta_M} = &\sum_{k \in \mathcal{K}_{M,s}} (\boldsymbol{C}^k_{M,s} \boldsymbol{F}^{(k,:)}_{M,s} \frac{\partial \boldsymbol{R}^{(:,k)}_1}{\partial \beta_M} + (1 - \boldsymbol{C}^k_{M,s}) \boldsymbol{F}^{(k,:)}_{M,s} \frac{\partial \boldsymbol{R}^{(:,k)}_2}{\partial \beta_M}) \\ &+ \sum_{k \in \mathcal{K}_{P,s}} (\boldsymbol{C}^k_{P,s} \boldsymbol{F}^{(k,:)}_{P,s} \frac{\partial \boldsymbol{R}^{(:,k)}_3}{\partial \beta_M} + (1 - \boldsymbol{C}^k_{P,s}) \boldsymbol{F}^{(k,:)}_{P,s} \frac{\partial \boldsymbol{R}^{(:,k)}_4}{\partial \beta_M}), \end{aligned} \tag{B.5}$$

where

$$\begin{aligned} \frac{\partial R^{(n,k)}_1}{\partial \beta_M} =& \Delta_n \frac{a}{a\beta_M + b + c\varepsilon_M}, \qquad & \frac{\partial R^{(n,k)}_2}{\partial \beta_M} =& \Delta_n \frac{a\varepsilon_M}{b + \varepsilon_M (c + a\beta_M)}, \\ \frac{\partial R^{(n,k)}_3}{\partial \beta_M} =& 0, & \frac{\partial R^{(n,k)}_4}{\partial \beta_M} =& \Delta_n \frac{\beta_P}{\beta_P d + g} \frac{\partial d}{\partial \beta_M}. \end{aligned} \tag{B.6}$$

The second derivative of R_s with respect to β_M is given by

$$\begin{aligned}\frac{\partial^2 R_s}{\partial \beta_M^2} = &\sum_{k\in\mathcal{K}_{M,s}} (\boldsymbol{C}_{M,s}^k \boldsymbol{F}_{M,s}^{(k,:)} \frac{\partial^2 \boldsymbol{R}_1^{(:,k)}}{\partial \beta_M^2} + (1-\boldsymbol{C}_{M,s}^k)\boldsymbol{F}_{M,s}^{(k,:)} \frac{\partial^2 \boldsymbol{R}_2^{(:,k)}}{\partial \beta_M^2}) \\ &+ \sum_{k\in\mathcal{K}_{P,s}} (\boldsymbol{C}_{P,s}^k \boldsymbol{F}_{P,s}^{(k,:)} \frac{\partial^2 \boldsymbol{R}_3^{(:,k)}}{\partial \beta_M^2} + (1-\boldsymbol{C}_{P,s}^k)\boldsymbol{F}_{P,s}^{(k,:)} \frac{\partial^2 \boldsymbol{R}_4^{(:,k)}}{\partial \beta_M^2}),\end{aligned} \tag{B.7}$$

where

$$\begin{aligned}&\frac{\partial^2 R_1^{(n,k)}}{\partial \beta_M^2} = -\Delta_n \frac{a^2}{\left(a\beta_M + b + c\varepsilon_M\right)^2}, \qquad \frac{\partial^2 R_2^{(n,k)}}{\partial \beta_M^2} = -\Delta_n \frac{a^2\varepsilon_M^2}{\left(b + \varepsilon_M\left(c + a\beta_M\right)\right)^2}, \\ &\frac{\partial^2 R_3^{(n,k)}}{\partial \beta_M^2} = 0, \qquad \frac{\partial^2 R_4^{(n,k)}}{\partial \beta_M^2} = -\Delta_n \frac{\beta_P^2}{(\beta_P d + g)^2}\frac{\partial d}{\partial \beta_M} + \Delta_n \frac{\beta_P}{\beta_P d + g}\frac{\partial^2 d}{\partial \beta_M^2}.\end{aligned} \tag{B.8}$$

Similarly, the first derivative of R_s with respect to ε_M can be expressed as

$$\begin{aligned}\frac{\partial R_s}{\partial \varepsilon_M} = &\sum_{k\in\mathcal{K}_{M,s}} (\boldsymbol{C}_{M,s}^k \boldsymbol{F}_{M,s}^{(k,:)} \frac{\partial \boldsymbol{R}_1^{(:,k)}}{\partial \varepsilon_M} + (1-\boldsymbol{C}_{M,s}^k)\boldsymbol{F}_{M,s}^{(k,:)} \frac{\partial \boldsymbol{R}_2^{(:,k)}}{\partial \varepsilon_M}) \\ &+ \sum_{k\in\mathcal{K}_{P,s}} (\boldsymbol{C}_{P,s}^k \boldsymbol{F}_{P,s}^{(k,:)} \frac{\partial \boldsymbol{R}_3^{(:,k)}}{\partial \varepsilon_M} + (1-\boldsymbol{C}_{P,s}^k)\boldsymbol{F}_{P,s}^{(k,:)} \frac{\partial \boldsymbol{R}_4^{(:,k)}}{\partial \varepsilon_M}),\end{aligned} \tag{B.9}$$

where

$$\begin{aligned}&\frac{\partial R_1^{(n,k)}}{\partial \varepsilon_M} = -\Delta_n \frac{ac\beta_M}{\left(b + c\varepsilon_M\right)\left(a\beta_M + b + c\varepsilon_M\right)}, \\ &\frac{\partial R_2^{(n,k)}}{\partial \varepsilon_M} = \Delta_n \frac{ba\beta_M}{\left(b + c\varepsilon_M\right)\left(b + \varepsilon_M\left(c + a\beta_M\right)\right)}, \\ &\frac{\partial R_3^{(n,k)}}{\partial \varepsilon_M} = 0, \qquad \frac{\partial R_4^{(n,k)}}{\partial \varepsilon_M} = \Delta_n \frac{\beta_P}{\beta_P d + g}\frac{\partial d}{\partial \varepsilon_M}.\end{aligned} \tag{B.10}$$

The second derivative of R_s with respect to ε_M is given by

$$\begin{aligned}\frac{\partial^2 R_s}{\partial \varepsilon_M^2} = &\sum_{k\in\mathcal{K}_{M,s}} (\boldsymbol{C}_{M,s}^k \boldsymbol{F}_{M,s}^{(k,:)} \frac{\partial^2 \boldsymbol{R}_1^{(:,k)}}{\partial \varepsilon_M^2} + (1-\boldsymbol{C}_{M,s}^k)\boldsymbol{F}_{M,s}^{(k,:)} \frac{\partial^2 \boldsymbol{R}_2^{(:,k)}}{\partial \varepsilon_M^2}) \\ &+ \sum_{k\in\mathcal{K}_{P,s}} (\boldsymbol{C}_{P,s}^k \boldsymbol{F}_{P,s}^{(k,:)} \frac{\partial^2 \boldsymbol{R}_3^{(:,k)}}{\partial \varepsilon_M^2} + (1-\boldsymbol{C}_{P,s}^k)\boldsymbol{F}_{P,s}^{(k,:)} \frac{\partial^2 \boldsymbol{R}_4^{(:,k)}}{\partial \varepsilon_M^2}),\end{aligned} \tag{B.11}$$

where

$$\begin{aligned}&\frac{\partial^2 R_1^{(n,k)}}{\partial \varepsilon_M^2} = \Delta_n \frac{\beta_M a c^2 \left(a\beta_M + 2\left(b + c\varepsilon_M\right)\right)}{\left(b + c\varepsilon_M\right)^2 \left(a\beta_M + b + c\varepsilon_M\right)^2}, \\ &\frac{\partial^2 R_2^{(n,k)}}{\partial \varepsilon_M^2} = -\Delta_n \frac{ba\beta_M \left(\left(b + c\varepsilon_M\right)\left(2c + d\beta_M\right) + cd\varepsilon_M\beta_M\right)}{\left(b + c\varepsilon_M\right)^2 \left(b + \varepsilon_M\left(c + d\beta_M\right)\right)^2}, \\ &\frac{\partial^2 R_3^{(n,k)}}{\partial \varepsilon_M^2} = 0, \qquad \frac{\partial^2 R_4^{(n,k)}}{\partial \varepsilon_M^2} = -\Delta_n \frac{\beta_P^2}{(\beta_P d + g)^2} \frac{\partial d}{\partial \varepsilon_M} + \Delta_n \frac{\beta_P}{\beta_P d + g} \frac{\partial^2 d}{\partial \varepsilon_M^2}.\end{aligned} \tag{B.12}$$

Similarly, the first derivative of R_s with respect to β_P is

$$\begin{aligned}\frac{\partial R_s}{\partial \beta_P} = &\sum_{k\in\mathcal{K}_{M,s}} (\boldsymbol{C}_{M,s}^k \boldsymbol{F}_{M,s}^{(k,:)} \frac{\partial \boldsymbol{R}_1^{(:,k)}}{\partial \beta_P} + (1-\boldsymbol{C}_{M,s}^k)\boldsymbol{F}_{M,s}^{(k,:)} \frac{\partial \boldsymbol{R}_2^{(:,k)}}{\partial \beta_P}) \\ &+ \sum_{k\in\mathcal{K}_{P,s}} (\boldsymbol{C}_{P,s}^k \boldsymbol{F}_{P,s}^{(k,:)} \frac{\partial \boldsymbol{R}_3^{(:,k)}}{\partial \beta_P} + (1-\boldsymbol{C}_{P,s}^k)\boldsymbol{F}_{P,s}^{(k,:)} \frac{\partial \boldsymbol{R}_4^{(:,k)}}{\partial \beta_P}),\end{aligned} \tag{B.13}$$

where

$$\begin{aligned}&\frac{\partial R_1^{(n,k)}}{\partial \beta_P} = \Delta_n \frac{\beta_M}{\beta_M a + b + c\varepsilon_M} \frac{\partial a}{\partial \beta_P}, && \frac{\partial R_2^{(n,k)}}{\partial \beta_P} = 0, \\ &\frac{\partial R_3^{(n,k)}}{\partial \beta_P} = \Delta_n \frac{d}{d\beta_P + f}, && \frac{\partial R_4^{(n,k)}}{\partial \beta_P} = \Delta_n \frac{d}{d\beta_P + g}.\end{aligned} \tag{B.14}$$

The second derivative of R_s with respect to β_P is given by

$$\begin{aligned}\frac{\partial^2 R_s}{\partial \beta_P^2} = &\sum_{k\in\mathcal{K}_{M,s}} (\boldsymbol{C}^k_{M,s}\boldsymbol{F}^{(k,:)}_{M,s}\frac{\partial^2 \boldsymbol{R}_1^{(:,k)}}{\partial\beta_P^2} + (1-\boldsymbol{C}^k_{M,s})\boldsymbol{F}^{(k,:)}_{M,s}\frac{\partial^2 \boldsymbol{R}_2^{(:,k)}}{\partial\beta_P^2}) \\ &+ \sum_{k\in\mathcal{K}_{P,s}} (\boldsymbol{C}^k_{P,s}\boldsymbol{F}^{(k,:)}_{P,s}\frac{\partial^2 \boldsymbol{R}_3^{(:,k)}}{\partial\beta_P^2} + (1-\boldsymbol{C}^k_{P,s})\boldsymbol{F}^{(k,:)}_{P,s}\frac{\partial^2 \boldsymbol{R}_4^{(:,k)}}{\partial\beta_P^2}),\end{aligned} \tag{B.15}$$

where

$$\begin{aligned}&\frac{\partial^2 R_1^{(n,k)}}{\partial\beta_P^2} = -\Delta_n \frac{\beta_M^2}{(\beta_M a + b + c\varepsilon_M)^2}\frac{\partial a}{\partial\beta_P} + \Delta_n \frac{\beta_M}{\beta_M a + b + c\varepsilon_M}\frac{\partial^2 a}{\partial\beta_P^2}, \qquad \frac{\partial^2 R_2^{(n,k)}}{\partial\beta_P^2} = 0, \\ &\frac{\partial^2 R_3^{(n,k)}}{\partial\beta_P^2} = -\Delta_n \frac{d^2}{(d\beta_P + f)^2}, \qquad \frac{\partial^2 R_4^{(n,k)}}{\partial\beta_P^2} = -\Delta_n \frac{d^2}{(d\beta_P + g)^2}.\end{aligned} \tag{B.16}$$

Similarly, the derivative of R_s with respect to β_M and ε_M is

$$\begin{aligned}\frac{\partial^2 R_s}{\partial\beta_M\partial\varepsilon_M} = &\sum_{k\in\mathcal{K}_{M,s}} (\boldsymbol{C}^k_{M,s}\boldsymbol{F}^{(k,:)}_{M,s}\frac{\partial^2 \boldsymbol{R}_1^{(:,k)}}{\partial\beta_M\partial\varepsilon_M} + (1-\boldsymbol{C}^k_{M,s})\boldsymbol{F}^{(k,:)}_{M,s}\frac{\partial^2 \boldsymbol{R}_2^{(:,k)}}{\partial\beta_M\partial\varepsilon_M}) \\ &+ \sum_{k\in\mathcal{K}_{P,s}} (\boldsymbol{C}^k_{P,s}\boldsymbol{F}^{(k,:)}_{P,s}\frac{\partial^2 \boldsymbol{R}_3^{(:,k)}}{\partial\beta_M\partial\varepsilon_M} + (1-\boldsymbol{C}^k_{P,s})\boldsymbol{F}^{(k,:)}_{P,s}\frac{\partial^2 \boldsymbol{R}_4^{(:,k)}}{\partial\beta_M\partial\varepsilon_M}),\end{aligned} \tag{B.17}$$

where

$$\begin{aligned}&\frac{\partial^2 R_1^{(n,k)}}{\partial\beta_M\partial\varepsilon_M} = -\Delta_n \frac{ac}{(a\beta_M + b + c\varepsilon_M)^2}, \quad \frac{\partial^2 R_2^{(n,k)}}{\partial\beta_M\partial\varepsilon_M} = \Delta_n \frac{ba}{(b + \varepsilon_M(c + a\beta_M))^2}, \\ &\frac{\partial^2 R_3^{(n,k)}}{\partial\beta_M\partial\varepsilon_M} = 0, \quad \frac{\partial^2 R_4^{(n,k)}}{\partial\beta_M\partial\varepsilon_M} = \Delta_n \frac{\beta_P^2}{(\beta_P d + g)^2}\frac{\partial d}{\partial\beta_M}\frac{\partial d}{\partial\varepsilon_M} + \Delta_n \frac{\beta_P}{\beta_P d + g}\frac{\partial^2 d}{\partial\beta_M\partial\varepsilon_M}.\end{aligned} \tag{B.18}$$

Similarly, the derivative of R_s with respect to β_M and β_P is

$$\begin{aligned}\frac{\partial^2 R_s}{\partial\beta_M\partial\beta_P} = &\sum_{k\in\mathcal{K}_{M,s}} (\boldsymbol{C}^k_{M,s}\boldsymbol{F}^{(k,:)}_{M,s}\frac{\partial^2\boldsymbol{R}^{(:,k)}_1}{\partial\beta_M\partial\beta_P} + (1-\boldsymbol{C}^k_{M,s})\boldsymbol{F}^{(k,:)}_{M,s}\frac{\partial^2\boldsymbol{R}^{(:,k)}_2}{\partial\beta_M\partial\beta_P})\\ &+\sum_{k\in\mathcal{K}_{P,s}} (\boldsymbol{C}^k_{P,s}\boldsymbol{F}^{(k,:)}_{P,s}\frac{\partial^2\boldsymbol{R}^{(:,k)}_3}{\partial\beta_M\partial\beta_P} + (1-\boldsymbol{C}^k_{P,s})\boldsymbol{F}^{(k,:)}_{P,s}\frac{\partial^2\boldsymbol{R}^{(:,k)}_4}{\partial\beta_M\partial\beta_P}),\end{aligned} \tag{B.19}$$

where

$$\begin{aligned}&\frac{\partial^2 R^{(n,k)}_1}{\partial\beta_M\partial\beta_P} = -\Delta_n\frac{b+c\varepsilon_M}{(a\beta_M+b+c\varepsilon_M)^2}\frac{\partial a}{\partial\beta_P}, \quad \frac{\partial^2 R^{(n,k)}_2}{\partial\beta_M\partial\beta_P} = 0,\\ &\frac{\partial^2 R^{(n,k)}_3}{\partial\beta_M\partial\beta_P} = 0, \quad \frac{\partial^2 R^{(n,k)}_4}{\partial\beta_M\partial\beta_P} = \Delta_n\frac{g}{(\beta_P d+g)^2}\frac{\partial d}{\partial\beta_M}.\end{aligned} \tag{B.20}$$

Similarly, the derivative of R_s with respect to ε_M and β_P is

$$\begin{aligned}\frac{\partial^2 R_s}{\partial\varepsilon_M\partial\beta_P} = &\sum_{k\in\mathcal{K}_{M,s}} (\boldsymbol{C}^k_{M,s}\boldsymbol{F}^{(k,:)}_{M,s}\frac{\partial^2\boldsymbol{R}^{(:,k)}_1}{\partial\varepsilon_M\partial\beta_P} + (1-\boldsymbol{C}^k_{M,s})\boldsymbol{F}^{(k,:)}_{M,s}\frac{\partial^2\boldsymbol{R}^{(:,k)}_2}{\partial\varepsilon_M\partial\beta_P})\\ &+\sum_{k\in\mathcal{K}_{P,s}} (\boldsymbol{C}^k_{P,s}\boldsymbol{F}^{(k,:)}_{P,s}\frac{\partial^2\boldsymbol{R}^{(:,k)}_3}{\partial\varepsilon_M\partial\beta_P} + (1-\boldsymbol{C}^k_{P,s})\boldsymbol{F}^{(k,:)}_{P,s}\frac{\partial^2\boldsymbol{R}^{(:,k)}_4}{\partial\varepsilon_M\partial\beta_P}),\end{aligned} \tag{B.21}$$

where

$$\begin{aligned}&\frac{\partial^2 R^{(n,k)}_1}{\partial\varepsilon_M\partial\beta_P} = -\Delta_n\frac{c\beta_M}{(a\beta_M+b+c\varepsilon_M)^2}\frac{\partial a}{\partial\beta_P}, \quad \frac{\partial^2 R^{(n,k)}_2}{\partial\varepsilon_M\partial\beta_P} = 0,\\ &\frac{\partial^2 R^{(n,k)}_3}{\partial\varepsilon_M\partial\beta_P} = 0, \quad \frac{\partial^2 R^{(n,k)}_4}{\partial\varepsilon_M\partial\beta_P} = \Delta_n\frac{g}{(\beta_P d+g)^2}\frac{\partial d}{\partial\varepsilon_M}.\end{aligned} \tag{B.22}$$

The gradient of F_s^{EE-SE} can be expressed as

$$\nabla F_s^{EE-SE} = \begin{pmatrix} \dfrac{\partial F_s^{EE-SE}}{\partial \beta_M} \\ \dfrac{\partial F_s^{EE-SE}}{\partial \varepsilon_M} \\ \dfrac{\partial F_s^{EE-SE}}{\partial \beta_P} \end{pmatrix} = \begin{pmatrix} \dfrac{\partial R_s}{\partial \beta_M}\dfrac{1}{\psi(\boldsymbol{\beta_s})} - \dfrac{R_s}{\psi(\boldsymbol{\beta_s})^2}\dfrac{\partial \psi(\boldsymbol{\beta_s})}{\partial \beta_M} \\ \dfrac{\partial R_s}{\partial \varepsilon}\dfrac{1}{\psi(\boldsymbol{\beta_s})} \\ \dfrac{\partial R_s}{\partial \beta_P}\dfrac{1}{\psi(\boldsymbol{\beta_s})} - \dfrac{R_s}{\psi(\boldsymbol{\beta_s})^2}\dfrac{\partial \psi(\boldsymbol{\beta_s})}{\partial \beta_P} \end{pmatrix}. \tag{B.23}$$

Consider that $z^T \nabla F_s^{EE-SE} = 0$, if we use (B.23), we will obtain

$$\frac{\partial R_s}{\partial \beta_M} z_1 + \frac{\partial R_s}{\partial \varepsilon_M} z_2 + \frac{\partial R_s}{\partial \beta_P} z_3 = \frac{\partial \psi(\boldsymbol{\beta_s})}{\partial \beta_M}\frac{1}{\psi(\boldsymbol{\beta_s})} R_s z_1 + \frac{\partial \psi(\boldsymbol{\beta_s})}{\partial \beta_P}\frac{1}{\psi(\boldsymbol{\beta_s})} R_s z_3. \tag{B.24}$$

Then we can write the $\nabla^2 F_s^{EE-SE}$ is given by

$$\nabla^2 F_s^{EE-SE} = \begin{pmatrix} \dfrac{\partial^2 F_s^{EE-SE}}{\partial \beta_M^2} & \dfrac{\partial^2 R_s}{\partial \varepsilon_M \partial \beta}\dfrac{1}{\psi(\boldsymbol{\beta_s})} - \dfrac{\partial R_s}{\partial \varepsilon_M}\dfrac{\partial \psi(\boldsymbol{\beta_s})}{\partial \beta_M}\dfrac{1}{\psi(\boldsymbol{\beta_s})^2} & \dfrac{\partial^2 F_s^{EE-SE}}{\partial \beta_M \partial \beta_P} \\ \dfrac{\partial^2 R_s}{\partial \varepsilon_M \partial \beta_M}\dfrac{1}{\psi(\boldsymbol{\beta_s})} - \dfrac{\partial R_s}{\partial \varepsilon_M}\dfrac{\partial \psi(\boldsymbol{\beta_s})}{\partial \beta_M}\dfrac{1}{\psi(\boldsymbol{\beta_s})^2} & \dfrac{\partial^2 R_s}{\partial \varepsilon^2}\dfrac{1}{\psi(\boldsymbol{\beta_s})} & \dfrac{\partial^2 R_s}{\partial \varepsilon_M \partial \beta_P}\dfrac{1}{\psi(\boldsymbol{\beta_s})} - \dfrac{\partial R_s}{\partial \varepsilon_M}\dfrac{\partial \psi(\boldsymbol{\beta_s})}{\partial \beta_P}\dfrac{1}{\psi(\boldsymbol{\beta_s})^2} \\ \dfrac{\partial^2 F_s^{EE-SE}}{\partial \beta_M \partial \beta_P} & \dfrac{\partial^2 R_s}{\partial \varepsilon_M \partial \beta_P}\dfrac{1}{\psi(\boldsymbol{\beta_s})} - \dfrac{\partial R_s}{\partial \varepsilon_M}\dfrac{\partial \psi(\boldsymbol{\beta_s})}{\partial \beta_P}\dfrac{1}{\psi(\boldsymbol{\beta_s})^2} & \dfrac{\partial^2 F_s^{EE-SE}}{\partial \beta_P^2} \end{pmatrix}, \tag{B.25}$$

where

$$\begin{aligned} \frac{\partial^2 F_s^{EE-SE}}{\partial \beta_M^2} &= \frac{\partial^2 R_s}{\partial \beta_M^2}\frac{1}{\psi(\boldsymbol{\beta_s})} - \frac{2}{\psi(\boldsymbol{\beta_s})^2}\frac{\partial R_s}{\partial \beta_M}\frac{\partial \psi(\boldsymbol{\beta_s})}{\partial \beta_M} - \frac{R_s}{\psi(\boldsymbol{\beta_s})^2}\left(\frac{\partial^2 \psi(\boldsymbol{\beta_s})}{\partial \beta_M^2}\right) + 2\frac{R_s}{\psi(\boldsymbol{\beta_s})^3}\left(\frac{\partial \psi(\boldsymbol{\beta_s})}{\partial \beta_M}\right)^2 \\ \frac{\partial^2 F_s^{EE-SE}}{\partial \beta_M \partial \beta_P} &= \frac{\partial^2 R_s}{\partial \beta_M \partial \beta_P}\frac{1}{\psi(\boldsymbol{\beta_s})} - \frac{1}{\psi(\boldsymbol{\beta_s})^2}\frac{\partial R_s}{\partial \beta_M}\frac{\partial \psi(\boldsymbol{\beta_s})}{\partial \beta_P} - \frac{1}{\psi(\boldsymbol{\beta_s})^2}\frac{\partial R_s}{\partial \beta_P}\frac{\partial \psi(\boldsymbol{\beta_s})}{\partial \beta_M} - \frac{R_s}{\psi(\boldsymbol{\beta_s})^2}\left(\frac{\partial^2 \psi(\boldsymbol{\beta_s})}{\partial \beta_M \partial \beta_P}\right) \\ &\quad + 2\frac{R_s}{\psi(\boldsymbol{\beta_s})^3}\left(\frac{\partial \psi(\boldsymbol{\beta_s})}{\partial \beta_M}\right)\left(\frac{\partial \psi(\boldsymbol{\beta_s})}{\partial \beta_P}\right) \\ \frac{\partial^2 F_s^{EE-SE}}{\partial \beta_P^2} &= \frac{\partial^2 R_s}{\partial \beta_P^2}\frac{1}{\psi(\boldsymbol{\beta_s})} - \frac{2}{\psi(\boldsymbol{\beta_s})^2}\frac{\partial R_s}{\partial \beta_P}\frac{\partial \psi(\boldsymbol{\beta_s})}{\partial \beta_P} - \frac{R_s}{\psi(\boldsymbol{\beta_s})^2}\left(\frac{\partial^2 \psi(\boldsymbol{\beta_s})}{\partial \beta_P^2}\right) + 2\frac{R_s}{\psi(\boldsymbol{\beta_s})^3}\left(\frac{\partial \psi(\boldsymbol{\beta_s})}{\partial \beta_P}\right)^2 \end{aligned} \tag{B.26}$$

When we expand the terms, we get

$$\begin{aligned}\mathbf{z}_s^T \nabla^2 F_s^{EE-SE} \mathbf{z}_s = z_1^2 \frac{\partial^2 F_s^{EE-SE}}{\partial \beta_M^2} + 2z_1 z_2 \frac{\partial^2 R_s}{\partial \varepsilon_M \partial \beta} \frac{1}{\psi(\boldsymbol{\beta_s})} - \frac{\partial R_s}{\partial \varepsilon_M} \frac{\partial \psi(\boldsymbol{\beta_s})}{\partial \beta_M} \frac{1}{\psi(\boldsymbol{\beta_s})^2} \\ + 2z_1 z_3 \frac{\partial^2 F_s^{EE-SE}}{\partial \beta_M \partial \beta_P} + z_2^2 \frac{\partial^2 R_s}{\partial \varepsilon^2} \frac{1}{\psi(\boldsymbol{\beta_s})} \\ + 2z_2 z_3 \frac{\partial^2 R_s}{\partial \varepsilon_M \partial \beta_P} \frac{1}{\psi(\boldsymbol{\beta_s})} - \frac{\partial R_s}{\partial \varepsilon_M} \frac{\partial \psi(\boldsymbol{\beta_s})}{\partial \beta_P} \frac{1}{\psi(\boldsymbol{\beta_s})^2} + z_3^2 \frac{\partial^2 F_s^{EE-SE}}{\partial \beta_P^2}.\end{aligned} \tag{B.27}$$

In our extensive simulations, we have observed that $\mathbf{z}_s^T \nabla^2 F_s^{EE-SE} \mathbf{z}_s \leq 0$ is always satisfied. Therefore, we conclude that F_s^{EE-SE} is quasiconcave in β_M, ε_M, and β_P.

Bibliography

[1] Cisco Systems, Inc., "Cisco Visual Networking Index: Global mobile data traffic forecast update, 2016-2021," White Paper, Feb. 2017.

[2] "Rising to meet the 1000x mobile data challenge," White Paper, Qualcomm, June 2012.

[3] W. V. Heddeghem, S. Lambert, B. Lannoo, D. Colle, M. Pickavet, and P. Demeester, "Trends in worldwide ICT electricity consumption from 2007 to 2012," *Computer Communications*, vol. 50, pp. 64 – 76, 2014, Green Networking. [Online]. Available: http://www.sciencedirect.com/science/article/pii/S0140366414000619

[4] [B. Metz, O.R. Davidson, P.R. Bosch, R. Dave, L.A. Meyer, *Climate Change 2007: Mitigation. Contribution of Working Group III to the Fourth Assessment Report of the Intergovernmental Panel on Climate Change.* Cambridge University Press, 2007.

[5] A. Ghosh, N. Mangalvedhe, R. Ratasuk, B. Mondal, M. Cudak, E. Visotsky, T. Thomas, J. Andrews, P. Xia, H. Jo, H. Dhillon, and T. Novlan, "Heterogeneous cellular networks: From theory to practice," *IEEE Commun. Mag.*, vol. 50, no. 6, pp. 54–64, Jun. 2012.

[6] K. Davaslioglu and E. Ayanoglu, "Quantifying potential energy efficiency gain in green cellular wireless networks," *IEEE Commun. Surveys Tuts.*, vol. 16, no. 4, pp. 2065–2091, Fourth Quarter 2014.

[7] S. Yunas, M. Valkama, and J. Niemelä, "Spectral and energy efficiency of ultra-dense networks under different deployment strategies," *IEEE Commun. Mag.*, vol. 53, no. 1, pp. 90–100, January 2015.

[8] H. Holma and A. Toskala, *LTE-Advanced: 3GPP Solution for IMT-Advanced.* John Wiley & Sons, Ltd, 2012.

[9] G. Boudreau, J. Panicker, N. Guo, R. Chang, N. Wang, and S. Vrzic, "Interference coordination and cancellation for 4G networks," *IEEE Commun. Mag.*, vol. 47, no. 4, pp. 74–81, April 2009.

[10] A. Damnjanovic, J. Montojo, Y. Wei, T. Ji, T. Luo, M. Vajapeyam, T. Yoo, O. Song, and D. Malladi, "A survey on 3GPP heterogeneous networks," *IEEE Wireless Communications*, vol. 18, no. 3, pp. 10–21, June 2011.

[11] A. Ghosh and R. Ratasuk, *Essentials of LTE and LTE-A*. Cambridge University Press, 2011.

[12] Z. Hasan, H. Boostanimehr, and V. Bhargava, "Green cellular networks: A survey, some research issues and challenges," *IEEE Commun. Surveys Tuts.*, vol. 13, no. 4, pp. 524–540, Fourth 2011.

[13] A. Bianzino, C. Chaudet, D. Rossi, and J. Rougier, "A survey of green networking research," *IEEE Commun. Surveys Tuts.*, vol. 14, no. 1, pp. 3–20, First 2012.

[14] D. Feng, C. Jiang, G. Lim, J. Cimini, L.J., G. Feng, and G. Li, "A survey of energy-efficient wireless communications," *IEEE Commun. Surveys Tuts.*, vol. 15, no. 1, pp. 167–178, First 2013.

[15] Y. Chen, S. Zhang, S. Xu, and G. Li, "Fundamental trade-offs on green wireless networks," *IEEE Commun. Mag.*, vol. 49, no. 6, pp. 30–37, June 2011.

[16] K. Johansson, "Cost effective deployment strategies for heterogenous wireless networks," Ph.D. dissertation, KTH Info. and Commun. Tech., Stockholm, Sweden, Nov. 2007.

[17] A. Fehske, G. Fettweis, J. Malmodin, and G. Biczok, "The global footprint of mobile communications: The ecological and economic perspective," *IEEE Commun. Mag.*, vol. 49, no. 8, pp. 55–62, August 2011.

[18] D. Lopez-Perez, I. Guvenc, G. de la Roche, M. Kountouris, T. Quek, and J. Zhang, "Enhanced intercell interference coordination challenges in heterogeneous networks," *IEEE Wireless Communications*, vol. 18, no. 3, pp. 22–30, June 2011.

[19] C. wei Tan, "Optimal power control in rayleigh-fading heterogeneous networks," in *2011 Proceedings IEEE INFOCOM*, April 2011, pp. 2552–2560.

[20] J. Gora, K. Pedersen, A. Szufarska, and F. Frederiksen, "Cell-specific uplink power control for heterogeneous networks in LTE," in *2010 IEEE 72nd Veh. Technol. Conf. Fall (VTC 2010-Fall)*, Sept 2010, pp. 1–5.

[21] K. Son, E. Oh, and B. Krishnamachari, "Energy-aware hierarchical cell configuration: From deployment to operation," in *2011 IEEE Conf. on Computer Commun. Workshops (INFOCOM WKSHPS)*, April 2011, pp. 289–294.

[22] L. Hu, I. Kovacs, P. Mogensen, O. Klein, and W. Stormer, "Optimal new site deployment algorithm for heterogeneous cellular networks," in *2011 IEEE Veh. Technol. Conf. (VTC 2011-Fall)*, Sept 2011, pp. 1–5.

[23] F. Richter, A. Fehske, and G. Fettweis, "Energy efficiency aspects of base station deployment strategies for cellular networks," in *2009 IEEE 70th Veh. Technol. Conf. Fall (VTC 2009-Fall)*, Sept 2009, pp. 1–5.

[24] 3GPP, TR 36.814, "Further advancements for E-UTRA physical layer aspects (Release 9)," 3GPP, Tech. Rep., Mar. 2010.

[25] A. Fehske, F. Richter, and G. Fettweis, "Energy efficiency improvements through micro sites in cellular mobile radio networks," in *2009 IEEE GLOBECOM Workshops*, Nov. 2009, pp. 1–5.

[26] H. Holtkamp, G. Auer, V. Giannini, and H. Haas, "A parameterized base station power model," *IEEE Commun. Letters*, vol. 17, no. 11, pp. 2033–2035, Nov. 2013.

[27] O. Arnold, F. Richter, G. Fettweis, and O. Blume, "Power consumption modeling of different base station types in heterogeneous cellular networks," in *2010 Future Network and Mobile Summit*, June 2010, pp. 1–8.

[28] E. Oh, B. Krishnamachari, X. Liu, and Z. Niu, "Toward dynamic energy-efficient operation of cellular network infrastructure," *IEEE Commun. Mag.*, vol. 49, no. 6, pp. 56–61, June 2011.

[29] R. K. Ahuja, T. L. Magnanti, and J. B. Orlin, *Network Flows: Theory, Algorithms, and Applications*. Prentice Hall, Feb. 1993.

[30] G. Nemhauser, L. Wolsey, and M. Fisher, "An analysis of the approximations for maximizing submodular set functions-I," *Mathematical Programming*, vol. 14, no. 1, pp. 265–294, Dec. 1978.

[31] C. C. Coskun and E. Ayanoglu, "Energy-efficient base station deployment in heterogeneous networks," *IEEE Wireless Commun. Letters*, vol. 3, no. 6, pp. 593–596, Dec 2014.

[32] ——, "A greedy algorithm for energy-efficient base station deployment in heterogeneous networks," in *Proc. IEEE Int. Conf. Commun. (ICC)*, June 2015, pp. 7–12.

[33] Cisco Systems, Inc., "Cisco Visual Networking Index: Global mobile data traffic forecast update, 2015-2020," White Paper, Feb. 2016.

[34] Z. Han, D. Niyato, W. Saad, T. Başar, and A. Hjørungnes, *Game Theory in Wireless and Communication Networks: Theory, Models, and Applications*. Cambridge Univ. Press, 2012.

[35] J. Huang, R. Berry, and M. Honig, "Distributed interference compensation for wireless networks," *IEEE J. Sel. Areas Commun.*, vol. 24, no. 5, pp. 1074–1084, May 2006.

[36] C. Shi, R. Berry, and M. Honig, "Distributed interference pricing for OFDM wireless networks with non-separable utilities," in *Proc. Annu. Conf. Inform. Sciences and Systems (CISS)*, Mar. 2008, pp. 755–760.

[37] ——, "Monotonic convergence of distributed interference pricing in wireless networks," in *Proc. IEEE Int. Symp. Information Theory (ISIT)*, June 2009, pp. 1619–1623.

[38] C. Saraydar, N. B. Mandayam, and D. Goodman, "Pricing and power control in a multicell wireless data network," *IEEE J. Sel. Areas Commun.*, vol. 19, no. 10, pp. 1883–1892, Oct. 2001.

[39] ——, "Efficient power control via pricing in wireless data networks," *IEEE Trans. Commun.*, vol. 50, no. 2, pp. 291–303, Feb. 2002.

[40] C. Xiong, G. Y. Li, S. Zhang, Y. Chen, and S. Xu, "Energy-efficient resource allocation in OFDMA networks," *IEEE Trans. Commun.*, vol. 60, no. 12, pp. 3767–3778, December 2012.

[41] Z. Zheng, L. Dan, S. Gong, and S. Li, "Energy-efficient resource allocation for downlink OFDMA systems," in *2013 IEEE International Conference on Communications Workshops (ICC)*, June 2013, pp. 391–395.

[42] X. Xiao, X. Tao, and J. Lu, "QoS-aware energy-efficient radio resource scheduling in multi-user OFDMA systems," *IEEE Commun. Letters*, vol. 17, no. 1, pp. 75–78, January 2013.

[43] R. S. Prabhu and B. Daneshrad, "An energy-efficient water-filling algorithm for OFDM systems," in *Proc. IEEE Int. Conf. Commun. (ICC)*, May 2010, pp. 1–5.

[44] G. Miao, N. Himayat, and G. Li, "Energy-efficient link adaptation in frequency-selective channels," *IEEE Trans. Commun.*, vol. 58, no. 2, pp. 545–554, Feb. 2010.

[45] G. Miao, N. Himayat, G. Li, and S. Talwar, "Distributed interference-aware energy-efficient power optimization," *IEEE Trans. Wireless Commun.*, vol. 10, no. 4, pp. 1323–1333, Apr. 2011.

[46] D. W. K. Ng, E. S. Lo, and R. Schober, "Energy-efficient resource allocation in multicell OFDMA systems with limited backhaul capacity," *IEEE Trans. Wireless Commun.*, vol. 11, no. 10, pp. 3618–3631, October 2012.

[47] L. Venturino, A. Zappone, C. Risi, and S. Buzzi, "Energy-efficient scheduling and power allocation in downlink OFDMA networks with base station coordination," *IEEE Trans. Wireless Commun.*, vol. PP, no. 99, pp. 1–1, 2014.

[48] E. Hossain, V. K. Bhargava, and G. P. Fettweis, *Green Radio Communication Networks*. Cambridge Univ. Press, 2012.

[49] C. Isheden, Z. Chong, E. Jorswieck, and G. Fettweis, "Framework for link-level energy efficiency optimization with informed transmitter," *IEEE Trans. Wireless Commun.*, vol. 11, no. 8, pp. 2946–2957, Aug. 2012.

[50] M. Assaad, "Optimal fractional frequency reuse (FFR) in multicellular OFDMA system," in *Proc. IEEE Veh. Technol. Conf. (VTC)*, Sep. 2008, pp. 1–5.

[51] Z. Xu, G. Li, C. Yang, and X. Zhu, "Throughput and optimal threshold for FFR schemes in OFDMA cellular networks," *IEEE Trans. Wireless Commun.*, vol. 11, no. 8, pp. 2776–2785, Aug. 2012.

[52] M. Peng, K. Zhang, J. Jiang, J. Wang, and W. Wang, "Energy-efficient resource assignment and power allocation in heterogeneous cloud radio access networks," *IEEE Trans. Veh. Technol.*, vol. 64, no. 11, pp. 5275–5287, Nov 2015.

[53] K. M. S. Huq, S. Mumtaz, and J. Rodriguez, "QoS aware energy-efficient resource scheduling for HetNet CoMP," in *2015 IEEE International Conference on Communications (ICC)*, June 2015, pp. 5954–5960.

[54] P. Lee, T. Lee, J. Jeong, and J. Shin, "Interference management in LTE femtocell systems using fractional frequency reuse," in *Proc. Int. Conf. Adv. Comm. Techno. (ICACT)*, vol. 2, Feb. 2010, pp. 1047–1051.

[55] N. Saquib, E. Hossain, and D. I. Kim, "Fractional frequency reuse for interference management in LTE-Advanced HetNets," *IEEE Wireless Commun.*, vol. 20, no. 2, pp. 113–122, Apr. 2013.

[56] M. Heath and A. Brydon, "Wireless network traffic 2008–2015: Forecasts and analysis," London, U.K., 2008.

[57] K. Davaslioglu, C. Coskun, and E. Ayanoglu, "Energy-efficient resource allocation for fractional frequency reuse in heterogeneous networks," *IEEE Trans. Wireless Commun.*, vol. 14, no. 10, pp. 5484–5497, Oct 2015.

[58] C. Raman, G. J. Foschini, R. A. Valenzuela, R. D. Yates, and N. B. Mandayam, "Power savings from half-duplex relaying in downlink cellular systems," in *Proc. Allerton Conf. Commun. Control Comput.*, Sept. 2009, pp. 748–753.

[59] S. Sesia, I. Toufik, and M. Baker, *LTE - The UMTS Long Term Evolution: From Theory to Practice*. Wiley, 2009.

[60] D. Gesbert, S. Hanly, H. Huang, S. Shamai Shitz, O. Simeone, and W. Yu, "Multi-cell MIMO cooperative networks: A new look at interference," *IEEE J. Sel. Areas Commun.*, vol. 28, no. 9, pp. 1380–1408, December 2010.

[61] C. Isheden and G. P. Fettweis, "Energy-efficient multi-carrier link adaptation with sum rate-dependent circuit power," in *2010 IEEE Global Telecommunications Conference (GLOBECOM 2010)*, Dec 2010, pp. 1–6.

[62] D. W. K. Ng, E. S. Lo, and R. Schober, "Energy-efficient resource allocation for secure OFDMA systems," *IEEE Trans. Veh. Technol.*, vol. 61, no. 6, pp. 2572–2585, July 2012.

[63] F. Richter, A. Fehske, and G. Fettweis, "Energy efficiency aspects of base station deployment strategies for cellular networks," in *Proc. IEEE Veh. Technol. Conf.*, Sep. 2009, pp. 1–5.

[64] G. Auer *et al.*, "How much energy is needed to run a wireless network?" *IEEE Wireless Commun.*, vol. 18, no. 5, pp. 40–49, Oct. 2011.

[65] L. Hoo, B. Halder, J. Tellado, and J. Cioffi, "Multiuser transmit optimization for multicarrier broadcast channels: Asymptotic FDMA capacity region and algorithms," *IEEE Trans. Commun.*, vol. 52, no. 6, pp. 922–930, Jun. 2004.

[66] W. Yu, "Multiuser water-filling in the presence of crosstalk," in *Proc. Inform. Theory and Appl. (ITA) Workshop*, Jan 2007, pp. 414–420.

[67] A. Najjar, N. Hamdi, and A. Bouallegue, "Efficient frequency reuse scheme for multi-cell OFDMA systems," in *Proc. IEEE Symp. Computers and Commun. (ISCC)*, July 2009, pp. 261–265.

[68] K. Davaslioglu and E. Ayanoglu, "Interference-based cell selection in heterogeneous networks," in *Proc. Inform. Theory and Appl. (ITA) Workshop*, San Diego, CA, Feb. 2013, pp. 1–6.

[69] T. Yang, F. Heliot, and C. H. Foh, "A survey of green scheduling schemes for homogeneous and heterogeneous cellular networks," *IEEE Commun. Mag.*, vol. 53, no. 11, pp. 175–181, November 2015.

[70] W. Rhee and J. Cioffi, "Increase in capacity of multiuser OFDM system using dynamic subchannel allocation," in *Proc. IEEE Veh. Technol. Conf. (VTC)*, vol. 2, May 2000, pp. 1085–1089.

[71] M. S. Bazaraa, H. D. Sherali, and C. M. Shetty, *Nonlinear Programming: Theory and Algorithms*. John Wiley & Sons, Ltd, 1993.

[72] P. M. Pardalos and M. G. C. Resende, Eds., *Handbook of Applied Optimization*. Oxford Univ. Press, 2002.

[73] S. Boyd and L. Vanderberghe, *Convex Optimization*. Cambridge Univ. Press, 2012.

[74] C. C. Coskun, K. Davaslioglu, and E. Ayanoglu, "An energy-efficient resource allocation algorithm with QoS constraints for heterogeneous networks," in *2015 IEEE Global Communications Conference (GLOBECOM)*, Dec 2015, pp. 1–7.

[75] ——, "Three-stage resource allocation algorithm for energy-efficient heterogeneous networks," 2017, to appear in *IEEE Trans. Veh. Technol.*, available on IEEEXplore.

[76] D. Tsilimantos, J. Gorce, and K. Jaffrès-Runser, "Spectral and energy efficiency trade-off with joint power-bandwidth allocation in OFDMA networks," *CoRR*, vol. abs/1311.7302, 2013.

[77] Y. Li, M. Sheng, C. Yang, and X. Wang, "Energy efficiency and spectral efficiency tradeoff in interference-limited wireless networks," *IEEE Commun. Letters*, vol. 17, no. 10, pp. 1924–1927, October 2013.

[78] R. Marler and J. Arora, "Survey of multi-objective optimization methods for engineering," *Structural and Multidisciplinary Optimization*, vol. 26, no. 6, pp. 369–395, 2004.

[79] L. Deng, Y. Rui, P. Cheng, J. Zhang, Q. Zhang, and M. Li, "A unified energy efficiency and spectral efficiency tradeoff metric in wireless networks," *IEEE Commun. Letters*, vol. 17, no. 1, pp. 55–58, January 2013.

[80] J. Rao and A. Fapojuwo, "On the tradeoff between spectral efficiency and energy efficiency of homogeneous cellular networks with outage constraint," *IEEE Trans. Veh. Technol.*, vol. 62, no. 4, pp. 1801–1814, May 2013.

[81] W. Jing, Z. Lu, X. Wen, Z. Hu, and S. Yang, "Flexible resource allocation for joint optimization of energy and spectral efficiency in OFDMA multi-cell networks," *IEEE Commun. Letters*, vol. 19, no. 3, pp. 451–454, March 2015.

[82] C. He, B. Sheng, P. Zhu, X. You, and G. Li, "Energy- and spectral-efficiency tradeoff for distributed antenna systems with proportional fairness," *IEEE J. Sel. Areas Commun.*, vol. 31, no. 5, pp. 894–902, May 2013.

[83] J. Tang, D. So, E. Alsusa, and K. Hamdi, "Resource efficiency: A new paradigm on energy efficiency and spectral efficiency tradeoff," *IEEE Trans. Wireless Commun.*, vol. 13, no. 8, pp. 4656–4669, Aug 2014.

[84] C. Yang, J. Li, A. Anpalagan, and M. Guizani, "Joint power coordination for spectral-and-energy efficiency in heterogeneous small cell networks: A bargaining game-theoretic perspective," *IEEE Trans. Wireless Commun.*, vol. 15, no. 2, pp. 1364–1376, Feb 2016.

[85] C. C. Coskun and E. Ayanoglu, "Energy-spectral efficiency tradeoff for heterogeneous networks with QoS constraints," accepted to appear in *Proc. IEEE Int. Conf. Commun. (ICC)*, May 2017.